FINAL TECHNICAL REPORT
GTRI PROJECT A-5676

Systems Analyses of Pneumatic Technology for High Speed Civil Transport Aircraft

SUMMARY OF RESEARCH, FINAL REPORT

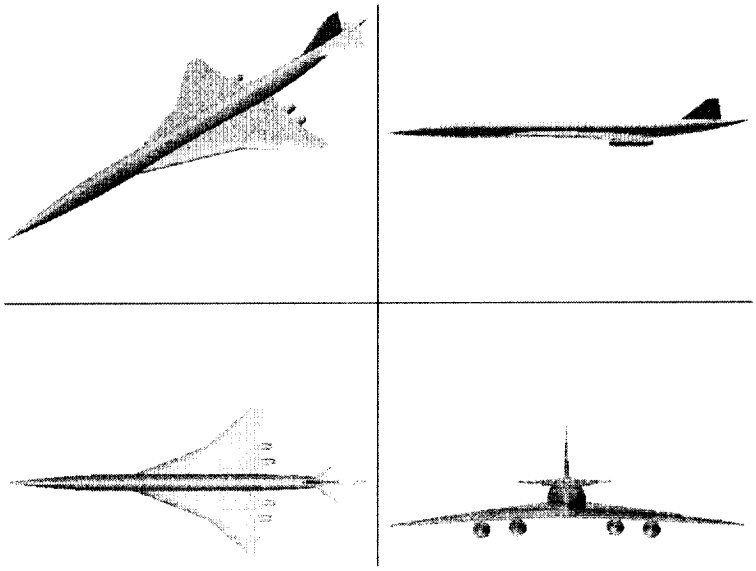

Submitted to:
NASA Langley Research Center
Grants Officer, MS 126
Hampton, VA 23681-2199

Grant Number: NAG-1-2051

by
Dimitri N. Mavris, Academic Principal Investigator and Professor
Jimmy C. Tai, Research Engineer II and Manager
Michelle M. Kirby and Bryce A. Roth, Graduate Research Assistants

Aerospace Systems Design Laboratory
School of Aerospace Engineering
Georgia Institute of Technology
Atlanta GA 30332-0844

Period Covered: April 6, 1998 to July 5, 1999

October 3, 1999

Executive Summary

The primary aspiration of this study was to objectively assess the feasibility of the application of a low speed pneumatic technology, in particular CC, to an HSCT concept. Circulation Control has been chosen as an enabling technology to be applied on a generic High Speed Civil Transport (HSCT) under the NASA Grant NAG-1-1517. This technology has been proven for various subsonic vehicles including flight tests on a Navy A-6 and computational application on a Boeing 737. Yet, CC has not been widely accepted for general commercial fixed-wing use but its potential has been extensively investigated for decades in wind tunnels across the globe for application to rotorcraft. More recently, an experimental investigation was performed at GTRI with application to an HSCT-type configuration. The data from those experiments was to be applied to a full-scale vehicle to assess the impact from a system level point of view. Hence, this study attempted to quantitatively assess the impact of this technology to an HSCT. The study objective was achieved in three primary steps.

1. Defining the need for CC technology
2. Wind tunnel data reduction
3. Detailed takeoff/landing performance assessment

Defining the need for the CC technology application to an HSCT encompassed a preliminary system level analysis. This was accomplished through the utilization of recent developments in modern aircraft design theory at ASDL. These developments include the creation of techniques and methods needed for the identification of technical feasibility show stoppers. These techniques and methods allow the designer to rapidly assess a design space and disciplinary metric enhancements to enlarge or improve the design space. The takeoff and landing field lengths were identified as the concept "show-stoppers".

Once the need for CC was established, the actual application of data and trends was assessed. This assessment entailed a reduction of the wind tunnel data from the experiments performed by Mr. Bob Englar at the GTRI. Relevant data was identified and manipulated based on the required format of the analysis tools utilized. Propulsive, aerodynamic, duct sizing, and vehicle sizing investigations were performed and information supplied to a detailed takeoff and landing tool. From the assessments, CC was shown to improve the low speed performance metrics, which were previously not satisfied. An HSCT with CC augmentation *does show* potential for full-scale application. Yet, an economic assessment of an HSCT with and without CC showed that a moderate penalty was incurred from the increased RDT&E costs associated with developing the CC technology and slight increases in empty weight.

Acknowledgments

The Aerospace Systems Design Laboratory would like to thank many individuals who contributed to this research. In particular, we would like to thank the following:

Aerospace Systems Design Laboratory

Michelle R. Kirby
Dr. Jae Moon Lee
Songtao Qiu
Bryce Roth
Dr. Jimmy Tai

Georgia Tech Research Institute

Bob Englar

Table of Contents

List of Figures

List of Tables

List of Acronyms

$/RPM	Average Required Yield Per Revenue Passenger Mile
AEO	All Engines Operating
ALCCA	Aircraft Life Cycle Cost Analysis
AOA	Angle Of Attack
APU	Auxiliary Propulsion Unit
AR	Aspect Ratio
ASDL	Aerospace Systems Design Laboratory
BDAP	Boeing Design and Analysis Program
BPR	Bypass Pressure Ratio
CC	Circulation Control
CDF	Cumulative Probability Distribution Function
CDP	Compressor Discharge Pressure
CDT	Compressor Discharge Temperature
DOC	Direct Operating Costs
DoE	Design of Experiments
ELAPS	Equivalent LAminates Plate Solution
ENGGEN	ENGine GENeration program
EPNL	Estimated Perceived Noise Level
FAA	Federal Aviation Administration
FAR	Federal Aviation Regulations
FADEC	Full Authority Digital Engine Control
FI	Flight Idle
FLOPS	FLight OPtimization System
FoM	Figure of Merit
FON	Fly-Over Noise
FPI	Fast Probability Integration
FPR	Fan Pressure Ratio
GTRI	Georgia Tech Research Institute
HP	High Pressure
HSCT	High Speed Civil Transport
HT	Horizontal Tail
IGE	In-Ground Effect
LDGFL	Landing Field Length
LE	Leading Edge
LP	Low Pressure
LSF	Limit State Function
MFTF	Mixed Flow Turbo Fan
MPP	Most Probable Point
MTBF	Mean Time Between Failures
MTTR	Mean Time To Repair
NASP	National AeroSpace Plane
NEPP	Navy/NASA Engine Performance Program
OEI	One Engine Inoperative
OGE	Out-of-Ground Effect
OPR	Overall Pressure Ratio
P	Pressure
RAM	Rapid Aircraft Modeler
RSE	Response Surface Equation
RSM	Response Surface Methodology
SFC	Specific Fuel Consumption
SLN	Side Line Noise
SLS	Sea Level Static
STOL	Short Takeoff and Landing

T	Temperature
T1	First Unit Cost
TE	Trailing Edge
T4	Turbine Inlet Temperature
TOFL	Takeoff Field Length
TOGW	Takeoff Gross Weight
TTL	Transistor-Transistor Logic
Vapp	Approach Speed
Vlof	Lift-off Speed
Vrot	Rotation Speed
VORLAX	Vortex Lattice Method code
VORVIEW	VORLAX graphical interface
VT	Vertical Tail
WINGDES	Wing Design program
WT	Wind Tunnel

Nomenclature

α	Angle of Attack
α_{rot}	Angle of Attack at Rotation
C_μ	Blowing Momentum Coefficient
C_D	Total Drag Coefficient
C_L	Lift Coefficient
C_{Lmax}	Maximum Lift Coefficient
C_μ	Moment Coefficient
δ_{flap}	Flap Deflection
ΔC_D	Change in Total Drag Coefficient
ΔC_L	Change in Lift Coefficient
ft/min	Feet per Minute
ft/s	Feet per Second
γ	Ratio of Specific Heats
G	Acceleration Force/gravitational force
h/c	Slot Height to Local Chord Ratio
lb	Pounds force
lbm	Pound mass
L/D	Lift-to-Drag ratio
M	Mach number
$\dot{m}$	Mass flow rate
NO_X	Nitrous Oxide
P_∞	Freestream pressure
P_o	Stagnation pressure
psia	Pounds per square inch absolute
psf	Pounds per square foot
psi	Pounds per square inch
q	Dynamic pressure
°R	Degrees Rankine
S_G	Ground roll distance
S_{ref}	Wing reference area
t/c	wing thickness-to-chord ratio
T_{amb}	Ambient Temperature
T_o	Stagnation temperature
T/W	Thrust-to-Weight ratio
V_j	Jet exit velocity
V_{LO}	Lift-off Velocity
V_{obs}	Velocity at 35 ft obstacle

1. Introduction/Background

Travelers have always welcomed the idea of reaching distant destinations in less time without having to spend a great deal of money. Over the last 60 years, this has driven the need for commercial aircraft that can fly farther and faster than those of previous generations. Passenger travel started with the Ford Tri-motor, progressed through propeller driven aircraft, such as the C-47, to turbojet powered aircraft such as the Boeing 707. Today, commercial aircraft are powered with high-bypass turbofan engines such as those on the MD-11. However, with the exception of the Concorde, the speed of commercial aircraft has not significantly increased over the last 20 years because of the enormous technical difficulties associated with faster-than-sound travel. However, in recent times, the technology to achieve faster-than-sound commercial travel in an economically viable manner has matured to the point that full-scale application is possible.

During the late 1960's, an attempt to create a supersonic commercial transport aircraft resulted in the Concorde. Although the Concorde was a technological triumph, it was something less than an economic success. Only 20 were ever produced and 14 delivered to airlines. The ticket fare (approximately $6,500.00 for New York to London [1]) is as much as eight times higher than current commercial subsonic transports. In fact, the aircraft has not generated a significant profit for the operators or owners. In addition, these aircraft are nearing the end of their usable life and will need to be replaced by newer aircraft capable of fulfilling the same mission but subjected to today's more stringent environmental regulations. A High Speed Civil Transport (HSCT) in the United States and the Second Generation Supersonic Transport Initiative in Europe are the only current, active candidates to replace the aging Concorde.

1.1 Importance of an HSCT

The Concorde is expected to reach its life-cycle limit within the next ten to fifteen years. This has initiated interest among many commercial aircraft operators to find a successor. The Concorde, at the time of its inception, represented an innovative solution to one of the most challenging commercial transport endeavors, that of supersonic transportation. However, this supersonic transport had many shortcomings: poor reliability, high specific fuel consumption (SFC), and low payload capacity [2]. Furthermore, the Concorde does not adhere to any of the environmental restrictions imposed in recent years, such as NO_X emission and FAR 36 Stage III noise requirements. In fact, an amendment was made to exclude this aircraft from abiding to the noise restrictions imposed on other commercial transports.

From a manufacturer's point of view, the Concorde was a challenging task full of technological unknowns that forced a move into uncharted territories. This led to over-designing in order to avoid unexpected surprises for which added to the weight and cost of the aircraft. Consequently, the Concorde received a weak response from commercial airlines. The airlines were reluctant to accept the high acquisition price, narrow or non-existent profitability, and market studies which indicated that the required ticket fare for this aircraft was too high for most passengers to pay (average yield per Revenue Passenger Mile, $/RPM $\approx$ 0.8). In addition, the program had chronic financial difficulties and would not have been completed had it not been heavily subsidized by the French and

British governments. The engine's poor reliability record has also contributed to the poor operational performance. Since these engines were developed in the 1960's, their reliability record (1,000 hrs Mean Time Between Failures, MTBF) cannot compete with current subsonic commercial aircraft engines (10-15,000 hrs MTBF).

In recent times, recognition of the environmental impact of high flying aircraft to the upper atmospheric ozone concentration has resulted in de-facto limitations on the emission of certain compounds, most notably, NO_X. At the time of the Concorde's inception, this upper atmospheric concern was not an issue; therefore, it was not designed to meet any type of emissions standard. Also, the Concorde is powered by turbojet engines, which are inherently noisy. Most airports have been forced to ban the Concorde due to noise complaints from surrounding residential neighborhoods. In the United States the Concorde flies only out of Miami, JFK, Washington, D.C., and most recently, Atlanta.

Since the introduction of the Concorde in 1975, many changes have occurred in both technology and the international air travel market. Current technology has now reached a stage where it will soon be possible to build a commercially viable supersonic aircraft. In addition, the number of people traveling abroad has increased steadily in recent years [3]. These changes warrant a very serious re-examination of the market and the technological potential for a second-generation supersonic transport [4].

An HSCT is the United States' response to this growing need for a next-generation supersonic aircraft. The most evident benefit that an HSCT brings to the traveling community is the travel time reduction that results from flying at high supersonic speeds. The travel time for a passenger on a typical New York to Paris flight can be reduced by as much as 65% and a Los Angeles to Tokyo reduction from 10 hour to 4 hours [5]. Such time savings will have a strong appeal to the business executive who has limited time to spend away from the office, and the number of days required for business trips would be substantially reduced. This would result in a rise in business efficiency in the form of higher sales for the same work load. The increase in international flights for business interactions will help to promote the "door-to-door" policy [6] that seems to be dwindling in an era of e-mail, faxes, and modems. Current forecasts predict the strongest growth in international air travel will occur in the Pacific Basin region [7, 8]. Growth in air travel for such city-pairs as Tokyo-Los Angeles could cause an increase of roughly 1% in Gross National Product for the respective countries [9]. An HSCT concept could also have an enormous impact for the country that produces the aircraft. The United States, if it were to produce this vehicle, could ensure that aerospace technical superiority remains within the U.S. and provide an estimated 140,000 jobs [10, 11] for a $200 billion HSCT market to stimulate the aerospace industry.

The greatest challenge facing an HSCT is the necessity to go farther with a greater payload capacity than the Concorde at an operating cost for the airline comparable to that of current subsonic transports. This translates to an increase in vehicle range and passenger capacity while minimizing the fuel cost per trip. Furthermore, recent research studies have revealed that the success of an HSCT will require significant technological advances in order to provide the needed environmental compatibility and economic viability [12].

Based on the current NASA High Speed Research program effort, an HSCT is a Mach 2.4, 300 passenger aircraft with a 5,000 nm range [11] and four mixed-flow turbofan (MFTF) engines [13]. The aircraft is restricted to subsonic flight over land due to the impact of sonic boom and must abide by all FAA regulations. Previous studies

have shown that an HSCT is not technically feasible or economically viable with conventional technologies [14, 15, 16]; where feasibility and viability are measured by compliance with noise levels, takeoff and landing field length requirements, gross weight limitations, and affordability goals. Various technologies have been proposed to address these issues including composite materials to reduce weights [14, 17], advanced engines to reduce SFC [13, 14, 15], laminar flow devices to reduce cruise drag [14], and circulation control to improve low speed characteristics [18]. The application of circulation control to an HSCT will be the focus of this study. The CC technology is briefly described below.

1.2 Circulation Control

Circulation Control (CC) is considered one of the most efficient methods for lift augmentation at low speed flight [19]. CC augments an airfoil's lift capability by tangentially ejecting a thin jet of high momentum air over a rounded trailing edge, as shown in Figure 1 [20]. The jet sheet, if its velocity is greater than the local outer flow, will remain attached over the curved surface by means of the Coanda effect. This behavior arises from the low-pressure region created by the jet, which energizes the boundary layer across the mixing boundary. The suction created by the low-pressure region is sufficient to overcome the centrifugal forces and remain attached well onto the lower surface of the airfoil. The trailing edge stagnation point moves to the lower surface, thereby increasing the airfoil circulation, and hence, the lift [21]. The characteristic of a wall jet remaining attached to a curved surface dates back to 1800 when Young first described the phenomena [22] and later to Henri Coanda in 1910 [23, 24].

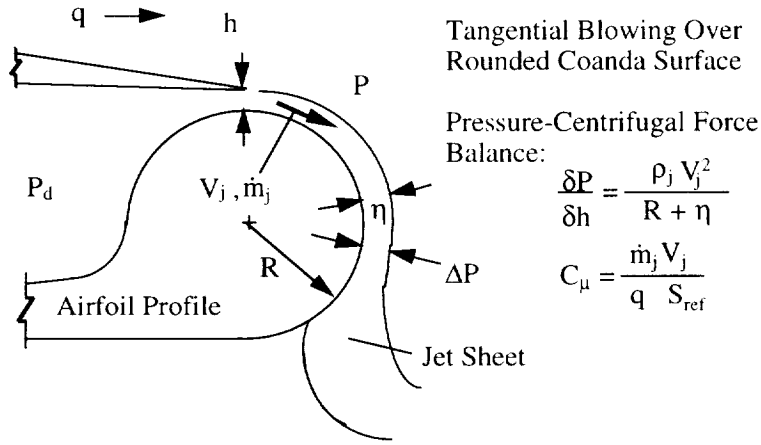

FIGURE 1: CIRCULATION CONTROL AERODYNAMIC FEATURES

The CC concept was not seriously investigated until the early 1960's by Dunham [25] and later Cheeseman [26], both of the National Gas Turbine Establishment in England. Dunham focused on application of CC to circular cylinders and Cheeseman on the development of CC airfoils for rotorcraft. In the late 1960's, work first began in the United States at the David Taylor Model Basin [27, 28]. Most CC research efforts have focused on the application to rotorcraft and/or short takeoff and landing (STOL) vehicles where an elliptical, or rounded trailing edge, airfoil was used.

The CC concept was first demonstrated at West Virginia University in April 1974 on the WVU CC Technology Demonstrator STOL [29], and five years later in March 1979 on a modified Navy A-6A [30, 31]. The purpose of these flight tests was to demonstrate the advantages which had been proposed by the application of CC, in particular, reduction in landing velocities, increased aircraft payload and wing loading, high drag generation on approach, reduced landing and takeoff distances, and improved pilot visibility [20]. Both of these demonstrators had rounded trailing edge sections to maximize the Coanda effect. Yet, the blunt trailing edges tended to negatively affect other characteristics of the flight and performance of the aircraft. For example, the blunt trailing edges increased the drag during cruise due to premature flow separation, parasitic drag increase due to energy requirements to provide the blowing, and large negative pitching moments resulting from large suction peaks on the upper surface trailing edge regions [32]. These problems could be overcome by applying a sharp trailing edge [33], a splitter plate [32], or a dual-radius circulation control concept [34] to relieve the high drag associated with the mixing of the blown air and freestream and the separation of the blown air on the lower surface [33]. The development of the dual-radius CC airfoil has been a primary focus of recent experimental investigations. The dual-radius CC airfoil was initially applied on a computational model of a modified Boeing 737-200 [34]. More recently, this CC airfoil was applied to an HSCT-type aircraft [35]. The wind tunnel data from these experiments will be utilized for this study on a full size HSCT.

2. Methodology

The objective of this study is to objectively assess the system level benefit/degradation of the application of CC to an HSCT. This is accomplished in three primary steps:

1. Defining the need for CC technology
2. Wind tunnel data reduction
3. Detailed takeoff/landing performance assessment

Defining the need for the CC technology application to an HSCT encompasses a preliminary system level analysis. This is accomplished through the utilization of recent developments in modern aircraft design theory at ASDL. These developments include the creation of techniques and methods that are needed for the identification of technical feasibility show stoppers. These techniques and methods allow the designer to rapidly assess a design space and disciplinary metric enhancements to enlarge or improve the design space. Once the need for CC is established, the actual application of data and trends must be assessed. This assessment entailed a reduction of the wind tunnel data from the experiments performed by Mr. Bob Englar at the Georgia Tech Research Institute (GTRI). Relevant data was identified and manipulated based on the required format of the analysis tools utilized. Propulsive, aerodynamic, duct sizing, and vehicle sizing investigations were performed and information supplied to the detailed takeoff and landing tools. From the assessments, conclusions will be drawn as to the benefit/degradation of adding CC to the technical feasibility and economic viability of an HSCT. Each of these steps is described in detail below.

2.1 Defining the Need for CC

The first step of this study is to prove that an HSCT with conventional technology is not technically feasible. Furthermore, feasibility can be obtained through the addition of CC. This demonstration facilitates new aspects in aircraft design theory, recently developed by researchers at ASDL, and includes advances in probabilistic approaches for assessing technical feasibility and economic viability of a vehicle and is described below.

2.1.1 Fast Probability Integration

Recent developments in modern aircraft design theory at Georgia Tech's ASDL, form the basis for the approach described here. The design theory is based on the paradigm shift from design-for-performance to design-for-affordability. Aircraft design is inherently a multi-disciplinary, multi-attribute, and multi-constrained problem; methods such as response surfaces, genetic algorithms, and multidisciplinary optimization techniques have not been completely efficient or accurate in these situations. An alternative method, based on the Fast Probability Integration (FPI) technique, is proposed. This technique provides *valuable* information in an efficient manner so as to perform system tradeoffs in a more realistic fashion. A brief description of FPI is given below and the reader is referred to References [36, 37, 38] for more information of the theory and application of FPI.

The FPI computer program [39] was developed by researchers at the Southwest Research Institute for the NASA Lewis Research Center. FPI is a probability analysis code based on the determination of a Most Probable Point (MPP); a concept frequently used in structural reliability analysis. The MPP analysis utilizes a response function, $Z(\mathbf{X})$, that is a function of several random variable distributions. Each point in the design space spanned by the $\mathbf{X}_i$'s has a specific probability of occurrence according to their joint probability distribution function. Thus, each point in the design space corresponds to one specific response value $Z(\mathbf{X})$ which has a given probability of occurrence.

In cost analysis and other disciplines involving random variables, it is often desirable to find the probability of achieving response values below a critical value of interest, z_0. This critical value can be used to form a limit-state function (LSF), $g(\mathbf{X}) = Z(\mathbf{X}) - z_0$, where values of $g(\mathbf{X}) \geq 0$ are undesirable. The MPP analysis calculates the cumulative probability of all points that yield $g(\mathbf{X}) \leq 0$ for the given z_0 (Figure 2). Since the LSF "cuts off" a section of the joint probability distribution (Figure 3), a point with maximal probability of occurrence can be identified on that LSF. This point is called the Most Probable Point. It is found most conveniently in a transformed space (Figure 3) in which all random variables are normally distributed. Once the MPP for a given probability is identified, the process can be repeated for several z_0 values, mapping each probability over the normalized distribution space to get a cumulative probability distribution function (CDF).

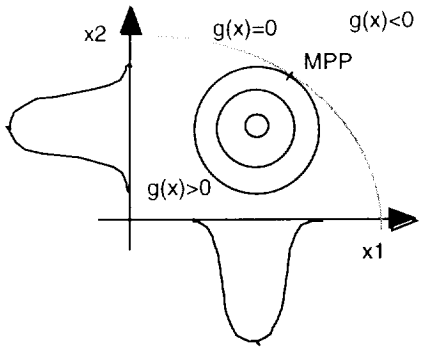

FIGURE 2: MOST PROBABLE POINT (MPP) LOCATION

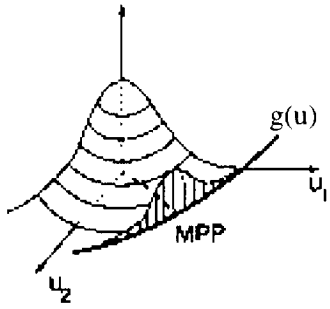

FIGURE 3: VISUALIZATION OF MPP

The FPI code offers several very efficient techniques that eliminate the need for an expensive Monte Carlo Simulation. FPI wraps around a synthesis/sizing code and controls the variation of inputs in accordance with the assigned probability distributions. The code is executed, pertinent output tabulated, and the next combination of input settings prepared to repeat the process. This continues until the CDF for the specified response is established. This process eliminates the need for a metamodel, such as Response Surface Equations.

2.1.2 General System Level Approach

The FPI technique described above can be applied to any vehicle design problem via the methodology depicted in Figure 4. To summarize, the technical feasibility and economic viability is assessed in six primary steps:

1. Define the problem
2. Determine system feasibility
3. Determine economic viability (if feasible space exists)
4. Evaluate the probability of obtaining a feasible and viable design space
5. Infuse new technologies if these probabilities prove unsatisfactory (repeat 1-4)
6. Examine design solutions and robustness

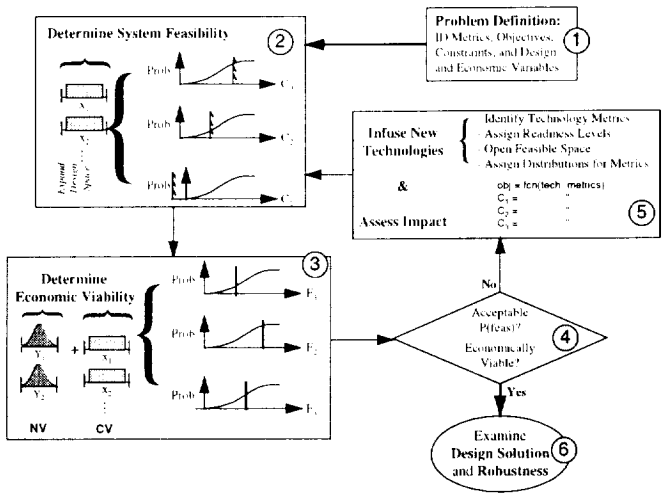

FIGURE 4: SYSTEM LEVEL EVALUATION METHODOLOGY

2.1.2.1 Define the Problem

A primary aspiration of any commercial vehicle is to be competitive with existing commercial aircraft with respect to $/RPM, acquisition price, and direct operating cost (DOC) per trip. Additional objectives arise from the following: maintain comparative performance characteristics (approach and cruise speeds), remain compatible with existing airport infrastructures (constrained takeoff gross weights and takeoff and landing field lengths), and comply with FAA regulations (community noise and emission levels). Hence, the problem requires the definition of objectives or metrics that capture the needs of the airframe manufacturer, airlines, airports, and passengers. "Metrics" are figures of merit which characterize various disciplines involved in a system's development, including $/RPM, DOC, acquisition price, takeoff gross weight, takeoff field length, approach speed, and landing field length. The target and constraint values are identified for each objective as established from experience, previous work, current airport infrastructures, and/or FAA regulations. The constraints are "rigid' limits placed on the performance and economic objectives of the vehicle, while targets are simply goals whereby achievement is strongly desirable. The metrics identified for this study are summarized in Table 1.

Performance metrics are defined in terms of key design variables for specified ranges. These design variables are often referred to as "control" factors; that is, the variables in a design problem within the designer's control. Examples include wing aspect ratio (AR), reference areas (S_{ref}), maximum thickness-to-chord (t/c) ratios, quarter-chord sweeps, horizontal (HT S_{ref}) and vertical tail (VT S_{ref}) areas, and thrust-to-weight ratio (T/W). The variables identified as pertinent to the design should be based on the objectives of the designer. From previous ASDL studies, the design variables identified as important for the current study are listed in Table 2.

TABLE 1: OBJECTIVES AND TARGETS/CONSTRAINTS

Objective	Target	Constraint
Performance		
Takeoff Gross Weight (TOGW)	*minimize*	< 1,000,000 lbs
Takeoff Field Length (TOFL)	*minimize*	< 11,000 ft
Landing Field Length (LDGFL)	*minimize*	< 11,000 ft
Approach Speed (V_{app})	*minimize*	< 155 kts
Fly Over Noise (FON)	110 EPNL	*minimize*
Sideline Noise (SLN)	110 EPNL	*minimize*
Economic		
$/RPM	$0.14	*minimize*
DOC per Trip	$76,000	*minimize*

TABLE 2: DESIGN VARIABLES

Variable	Minimum	Maximum
Wing LE kink x-location*	1.54	1.69
Wing LE kink y-location*	0.44	0.58
Wing LE tip x-location*	2.1	2.36
Wing TE tip x-location*	2.4	2.58
Wing TE kink x-location*	2.19	2.36
Wing TE kink y-location*	0.44	0.58
Wing TE root x-location*	2.19	2.5
Wing t/c	0.03	0.05
Wing reference area (S_{ref})	7,000 ft^2	9,500 ft^2
Design C_L	0.08	0.12
HT LE tip x-location**	0.95	1.73
HT S_{ref} / Wing S_{ref}	0.045	0.09
VT S_{ref} / Wing S_{ref}	0.045	0.07
Nacelle Scaling	0.9	1.1
Wing apex from fuselage nose	22 %	28 %
flap chord length / wing local chord	0.25	0.35
Overall Pressure Ratio (OPR)	18.0	22.0
Fan Pressure Ratio (FPR)	3.5	4.5
Turbine Inlet Temperature (T_4)	3,000.0 °R	3,300.0 °R
Thrust-to-weight ratio (T/W)	0.26	0.32

* values non-dimensionalized by the wing semi-span

** values non-dimensionalized by the HT semi-span

The economic metrics are primarily functions of "noise" factors, or variables beyond the designer's grasp that affect the fulfillment of the system objectives. For example, the cost of fuel will directly affect the operating costs of an aircraft, yet the designer cannot "design for" a given fuel cost. The economic variables of relevance are based on the operational environment of the vehicle and current economic issues. All remaining noise variables are fixed to their most likely values. For this study, all economic parameters will remain at the most likely values. The economic metrics will only be a function of control, or geometric, parameters and will be tracked, not used as a constraint to the design space. The identification of the feasible design space is a primary objective in this study, and the impact of CC on the economics of an HSCT will be considered from a deterministic point of view, not subject to economic uncertainty.

2.1.2.2 Feasibility and Viability

As stated previously, the FPI technique provides a CDF for the defined objectives based on the variables listed in Table 2. The CDF can be compared to the appropriate target and the probability of a feasible or viable design space can be assessed through system optimization. An example of the feasibility assessment is shown in Figure 5. The probability of success is determined by placing the objective target on the CDF and reading the corresponding probability value. Any probability of achieving a solution is favorable since it represents the outcome of design variables. Yet, the decision-maker strives for alternatives that maximize the feasible and viable design space that can be explored for robust configurations.

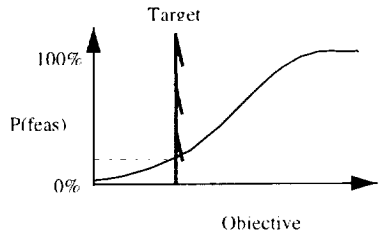

FIGURE 5: FEASIBILITY OR VIABILITY EVALUATION

2.1.2.3 Determine Technical Feasibility and Economic Viability

Technical feasibility is a measure of the system's ability to meet the imposed performance targets and to satisfy all constraints. Referring to Table 1, all performance objectives are constrained, specifically by aviation regulations, airport compatibility, and customer requirements, except for the noise limits that will be considered as goals. Therefore, in order to be successful, an HSCT must satisfy each constraint with a sufficiently high probability value where the exact value is determined by the designer or decision-maker. In other words, the larger the magnitude of the probability, the larger the feasible design space, i.e. more alternatives, in which robust solutions may exist. For the technical feasibility assessment, only the control variables are allowed to vary in the manner described previously. These variables vary in FPI between the minimum and maximum values using uniform distributions. This allows all possible values within the ranges specified to become equally likely. The result is a CDF (similar to Figure 5) for the different performance metrics which allows for quick assessment of technical feasibility and identification of concept "show-stoppers".

Economic viability is a measure of the system's ability to achieve specified cost and profitability goals as well as satisfy any imposed constraints. In the most general application of an economic viability assessment, control and noise variables are varied in FPI between the minimum and maximum values using uniform and normal distributions, respectively. Yet, as stated previously, only the control variables are considered in this study. Thus, FPI generates a CDF for the economic objectives that are valid for the design space under consideration. The viability assessment is performed in the same manner as feasibility with the CDF target.

2.1.2.4 Evaluate the Probability of Feasibility and Viability

The evaluation of feasibility and viability of a vehicle is based on the value of the probability of a given objective for the specified target value. For example, if an objective has an 80% chance of achieving the target, the decision-maker may assume that this objective is no longer a constraint and does not warrant further investigation. Yet, a low probability value (or small chance) of achieving a solution that satisfies the constraints implies that a means of improvement must be identified; perhaps infusion of new technology. This process of evaluation must be performed for each objective and constraint.

2.1.2.5 New Technology Infusion

The infusion of new technologies can be considered in the aircraft design process when the feasibility and economic viability probability space for a given configuration design space are not within acceptable limits to the decision-makers. The need for the infusion of a technology is required when the manipulation of the variable ranges has been exhausted, optimization is ineffective, constraints are relaxed to a minimum, and the maximum performance attainable from a given level of technology is achieved. The maximum level of a given technology is essentially the natural limit of the benefit, displayed in Figure 6 [40], and implies that the maturation variation with time is constant. When this limit is reached, there is *no other alternative* but to infuse a new technology.

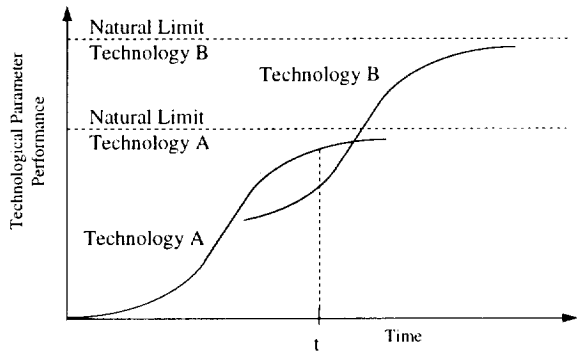

FIGURE 6: NEED FOR NEW TECHNOLOGY

2.1.2.6 Technology Impact Assessment

The infusion of new technologies for a given configuration must be considered when all other alternatives (optimization, opening design space, etc.) have been explored. Unfortunately, advanced technologies are difficult to assess. Sizing/synthesis tools are typically based on regressed historical data, limiting or removing their applicability to exotic concepts or technologies. Furthermore, higher fidelity tools, such as finite element methods and computational fluid dynamics can not always capture the physics associated with a new technology, nor do these tools allow for rapid parametric assessments of a design space. However, the impact of a technology can be qualitatively assessed with technology metric "k" factors. These "k" factors modify technical metrics, such as specific fuel consumption (SFC), lift to drag ratio (L/D), and component weights, that result from some analysis or sizing tool. The modification is essentially a change in the technical metric, either enhancement or degradation. In effect, the "k" factors simulate the discontinuity in benefits or penalties associated with the addition of a new technology.

The impact of "k" factors on the system objectives and constraints can be assessed qualitatively through a linear or higher order sensitivity analysis depending on the level of detailed desired. The analysis can be performed with the prediction profile feature of the JMP statistical package [41], such as the example depicted in Figure 7. The metric in this example is L/D. One can assume that the L/D can be improved by some *generic* technique, say laminar flow control. This technology supplies, not only benefit, but a penalty or degradation in the system associated with that technology. For laminar flow control, this penalty comes through increased SFC, reduced utilization, etc. The SFC is increased due to engine bleeding and power extraction needed for the suction effect over the wing upper surface. This degradation is shown in Figure 7. As the "k" factor increases towards "+1", the benefit of improved L/D increases, yet, the penalty of the increasing SFC, towards "+1", reduces the benefits. Utilization is also affected through increased maintenance efforts, increased component weight due to required ducting, and higher maintenance man hours per flight hour.

$$OBJ = \left[k_{m_1}(\text{metric}_1) + k_{m_2}(\text{metric}_2) + \ldots\right] + \left[k_{p_1}(\text{penalty}_1) + k_{p_2}(\text{penalty}_2) + \ldots\right]$$

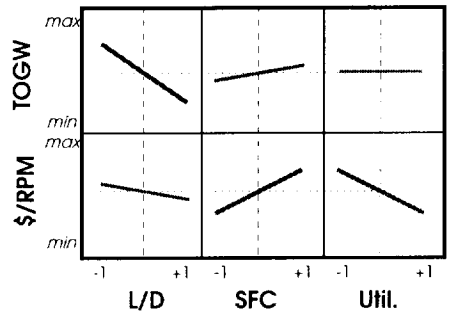

FIGURE 7: EXAMPLE "K" FACTOR PREDICTION PROFILE

However, if a "k" factor for a given technological metric is shown to improve the system objectives and constraints with minimal penalties, that technology impact can be identified as worthy of further investigation. A specific technology must be identified which can provide the "k" factor projections. This method is essentially forecasting the impact of a technology. This technique provides a very efficient means of identifying design alternatives around concept "show-stoppers". Therefore, technologies capable of counteracting the showstoppers aid in the correct allocation of resources for further research and development of the project.

2.1.2.7 Examine Design Solutions and Robustness

Once technological metrics are identified which can provide the given performance improvement, the FPI technique can be applied again to assess improvements in feasibility or viability. This is done by comparing the CDF of the conventional baseline to the enhanced configuration with respect to the target value (Figure 8). This method can be applied to each objective and constraint that did not satisfy the specified targets within an acceptable limit so as to yield a first estimate to the benefit of a technology.

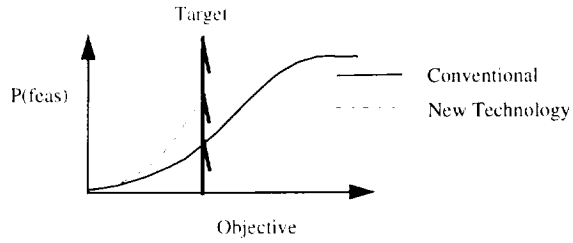

FIGURE 8: NEW TECHNOLOGY IMPROVEMENT

Once the CDFs for the objectives are obtained, the feasibility and viability can be evaluated. Overall improvements may or may not exist requiring quantification of the extent to which the system satisfies or violates objectives. The decision-maker may then elect to continue allocation of resources for further research or terminate the efforts. The definitive decisions are subjective based on the probability levels obtained for each objective. If the probability levels for a feasible or viable configuration are on the order of 20-70%, the risk associated with technologies, uncertainty, and scheduling must be addressed.

2.1.3 HSCT Sizing Tool

All aircraft synthesis/sizing tasks for this study utilized the FLight OPtimization System, FLOPS, a multidisciplinary system of computer programs used for the conceptual and preliminary design and analysis of aircraft configurations [42]. This tool was developed by the NASA Langley Research Center. FLOPS was linked to the Aircraft Life Cycle Cost Analysis, ALCCA, program used for the prediction of all life-cycle costs associated with commercial aircraft and was developed by NASA Ames and further enhanced by ASDL [43]. The direct link of FLOPS and ALCCA provided the capability to create a conceptual aircraft design with immediate evaluation of life cycle cost elements.

2.2 Wind Tunnel Data Reduction

Data regarding the effects of CC on the aerodynamics of an HSCT-type aircraft were provided by the GTRI Aerodynamics Laboratory. In the reduction of the supplied data, the goal was to apply the effects of blowing, as determined experimentally for the GTRI wind tunnel model, to full scale HSCT vehicles. This involved excluding as much of the configuration dependent effects from the WT data to isolate the effects of blowing on the lift and drag of a representative HSCT wing/body. Yet, as will be described, the experimental model and data was not completely representative of current government/industry concepts. Hence, a few modifications and assumptions were made.

2.2.1 Wind Tunnel Model

The test model was an existing GTRI half-span model and the wing planform was representative of a generic HSCT as seen in Figure 9. The fuselage was a recent NASA model and shaped based on volume requirements and aerodynamic tailoring. The wing planform was a low aspect ratio double-delta with leading edge sweeps of 75° and 54°. The wing sections employed a quarter inch flat plate with a sharply-beveled leading edge and a dual radius trailing edge flap (CCW flap) as shown in Figure 10 [44].

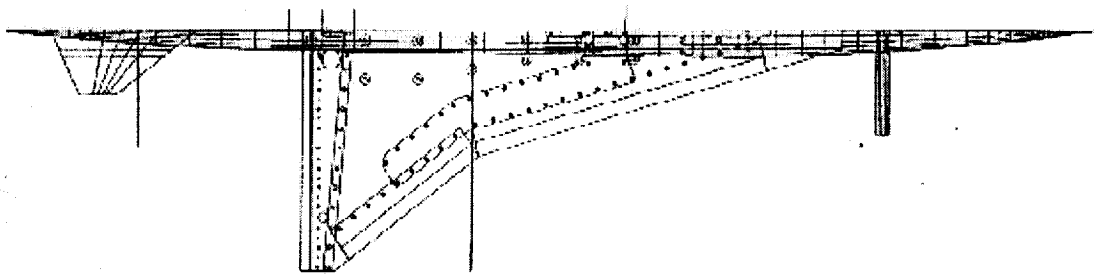

FIGURE 9: GTRI WIND TUNNEL MODEL

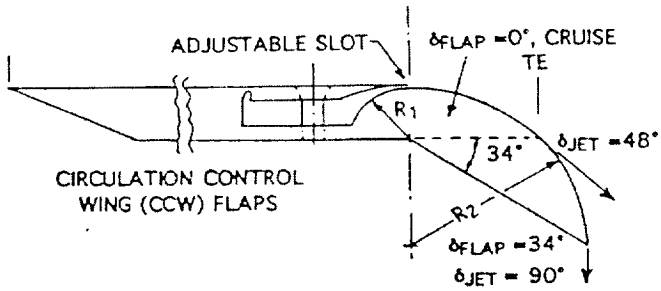

FIGURE 10: GTRI WIND MODEL WING SECTION

2.2.2 Relevant Data

Varieties of experiments were performed on the GTRI model. These experiments include with and without canards, with and without horizontal tail, various blowing levels, angle of attack (AOA) sweeps, various flaps (CC flap and blown jet flap) and flap settings, different slot heights, etc. One aspect of this study was to identify which experiments/runs were relevant. Wind tunnel runs with the horizontal tail and canards were neglected. The rationale behind this decision was threefold. First, the primary performance metrics which are inhibiting technical feasibility are the takeoff and landing field lengths and the approach speed. Hence, if the addition of CC does not show significant benefit to these metrics, then the stability or handling characteristics of the vehicle are not of importance. Therefore, the effects of CC on the wing/body were isolated through consideration of only those pertinent experiments. Second, if the horizontal tail utilized in the WT experiments were scaled to full-size, the area would be on the order of 1,000 ft^2. This is an extremely large area which may be needed for stability and handling issues, which leads to the third issue. Third, the ability to quantitatively assess the stability characteristics of the vehicle are not to the point of maturity. Based on these considerations, 21 runs were considered for further application. These runs are summarized in Table 3 and Table 4. These runs did not have canards or HT. As stated previously, the desire was to isolate the effects of CC on the wing-body. GTRI provided the force coefficients for the runs described in Table 3 and Table 4 for angle of attack sweeps of approximately –5° to 34° for all cases. The experimental runs with the plain flap were of interest. A CCW flap employed on a wing section adds curvature and can increase the lift of a wing section even without blowing in comparison to the plain flap.

As shown below, the dynamic pressure varied between 15 psf and 20 psf. The 20 psf value translated to a Reynolds number of 1.423 x 10^6/ft based on a mean aerodynamic chord of 1.7165 ft and velocity of 129.7 ft/s at sea

level conditions. For a typical HSCT, the operating speeds for takeoff and landing are on the order of 200 kts and 155 kts, respectively. Hence, a full-scale model has a takeoff Reynolds number of 2.166 x 10^8 /ft. This value is based on a mean aerodynamic chord of 101.9 ft and velocity of 335.22 ft/s at sea level conditions; and 1.679 x 10^7/ft for landing at a velocity of 259.92 ft/s. The WT model Reynolds number is one to two orders of magnitude lower than the full-scale model and the dynamic similarity of the flows is in question.

TABLE 3: GTRI EXPERIMENTAL RUNS UTILIZED WITH PLAIN FLAP

Run #	Plain δ_{flap}	C_μ	q_∞ (psf)	Slot Height (in)
517	0°	0.0	20	0.015
530	0°	0.1	20	0.015
531	0°	0.2	20	0.015
535	0°	0.315	15	0.015
544	20°	0.0	20	0.015
550	20°	0.1	20	0.015
551	20°	0.308	15	0.015

TABLE 4: GTRI EXPERIMENTAL RUNS UTILIZED WITH CCW FLAP

Run #	CCW δ_{flap}	C_μ	q_∞ (psf)	Slot Height (in)
645	0°	0.0	20	0.01
647	0°	0.082	20	0.01
648	0°	0.328	15	0.01
658	10°	0.0	20	0.01
659	10°	0.082	20	0.01
660	10°	0.328	15	0.01
625	34°	0.0	20	0.01
630	34°	0.01	20	0.01
631	34°	0.02	20	0.01
632	34°	0.03	20	0.01
626	34°	0.041	20	0.01
627	34°	0.082	20	0.01
628	34°	0.164	20	0.01
629	34°	0.328	15	0.01

2.3 Detailed Takeoff and Landing Analysis

The performance assessment of an HSCT utilizing the CC technology was performed in three steps. First, a reference point was established for the low-speed metrics (takeoff field length, rotation speed, etc.) of a configuration which utilized only conventional high-lift systems, such as leading edge (LE) slats and trailing edge (TE) plain flaps. The reference point was based on the WT model that was scaled up based on an 8,500 ft^2 wing area. A parametric investigation of the LE and TE slats and flaps of the conventional configuration was conducted to determine the optimal settings that would minimized the TOFL, LDGFL, and Vapp. The LE slats and TE flaps varied between 0° and 30° in increments of 10° which translated into 16 different configurations. Second, the incremental changes in force coefficients (lift and drag) were applied to the 16 configurations. CC was applied at all operating speeds. The results obtained from the application of CC were then compared to the conventional configurations and the improvements/degradations quantified. Both step one and two assume the vehicle is at the maximum takeoff gross weight. The final step in the performance analysis includes a deviation from this point. A parametric investigation is performed for different operating conditions, that is, not fully loaded, and procedures (in the form of allowable AOA) with a comparison of the different configurations with and without CC. At this point, the impact of CC is determined.

2.3.1 Performance Analysis Program

The takeoff and landing quantitative performance assessments utilizes the NASA Langley developed program, TAKEOFF Version 2.0.[45] TAKEOFF is a stand-alone version of the FLight OPtimization System [42] (FLOPS) takeoff and landing module. The TAKEOFF program is based on an analysis of a commercial vehicle's low speed performance such that all applicable FAR 25 regulations are met. All FAR requirements are determined including second-segment climb gradient, missed approach climb gradient, constrained speeds for all engines operating (AEO) and one engine inoperative (OEI) conditions, etc. Furthermore, the balanced field length is calculated. Flowcharts of the calculation procedures for takeoff and landing are shown in Figure 11 and Figure 12, respectively. These algorithms are typical for most performance assessment programs. The TAKEOFF program requires, at a minimum, the following input parameters to determine the low speed performance metrics: takeoff gross weight, landing weight, wing area, atmospheric temperature, altitude, engine performance characteristics, maximum C_L for takeoff and landing, and arrays of C_L and C_D, both as functions of α, for takeoff and landing. All performance assessments assumed in-ground-effect.

It should be noted that the takeoff and landing modules each use just a single C_L- and C_D- versus-alpha curve. This is rather impractical for an aircraft utilizing CC because it requires a different C_L- and C_D- versus-alpha curve for each velocity or operating dynamic pressure. This requirement stems from the definition of the blowing coefficient, C_μ, shown in Eq. (1). This additional C_μ parameter is used to describe the aerodynamic performance of the wing. It is proportional to the ejected mass flux ($\dot{m}$) and jet velocity (V_j) and inversely proportional to the freestream dynamic pressure (q_∞) and the wing reference area (S_{ref}). This definition results in variability of mass flow with flight speed, q_∞.

$$C_{\mu} = \frac{\dot{m}V_j}{q_{\infty}S_{ref}} \tag{1}$$

To properly capture this effect, the TAKEOFF program was modified to accept a matrix of incremental changes in lift and drag as a function of speed and angle of attack. Hence, within the program at each temporal step, the effects of CC were added to the "clean" force coefficients through a two-dimensional table look up. This step is more clearly described in the implementation section. Furthermore, the value of ejected mass flux and jet velocity is determined via an off line internal ducting analysis and an assessment of the available energy from the engines at takeoff and landing. The OEI condition was of primary importance for the current investigation since the application of the CC technology is dependent upon the ejected mass flux that was supplied from the engines. Hence, if the OEI condition occurs, not only does the thrust reduce, but the freestream dynamic pressure reduces *and* the amount of bleed flow reduces. Therefore, in addition to the low speed metrics, an issue to be addressed was the low speed performance degradation due to OEI or possible engine oversizing. The propulsive issues will be addressed in later sections. The low speed metrics of interest are defined in Table 5.

TABLE 5: LOW SPEED METRICS

Metric	Constraint/Objective Value
Takeoff Field Length (TOFL)	≤ 11,000 ft
Landing Field Length (LdgFL)	≤ 11,000 ft
Approach Speed (Vapp)	≤ 155 kts
One Engine Inoperative Lift-off speed (OEI_Vlof)	*minimize*
One Engine Inoperative Rotation speed (OEI_Vrot)	*minimize*
All Engine Operative Lift-off speed (AEO_Vlof)	*minimize*
All Engine Operative Rotation speed (AEO_Vrot)	*minimize*
Stall Speed Landing (Vstall_Ldg)	*minimize*
Stall Speed Takeoff (Vstall_TO)	*minimize*

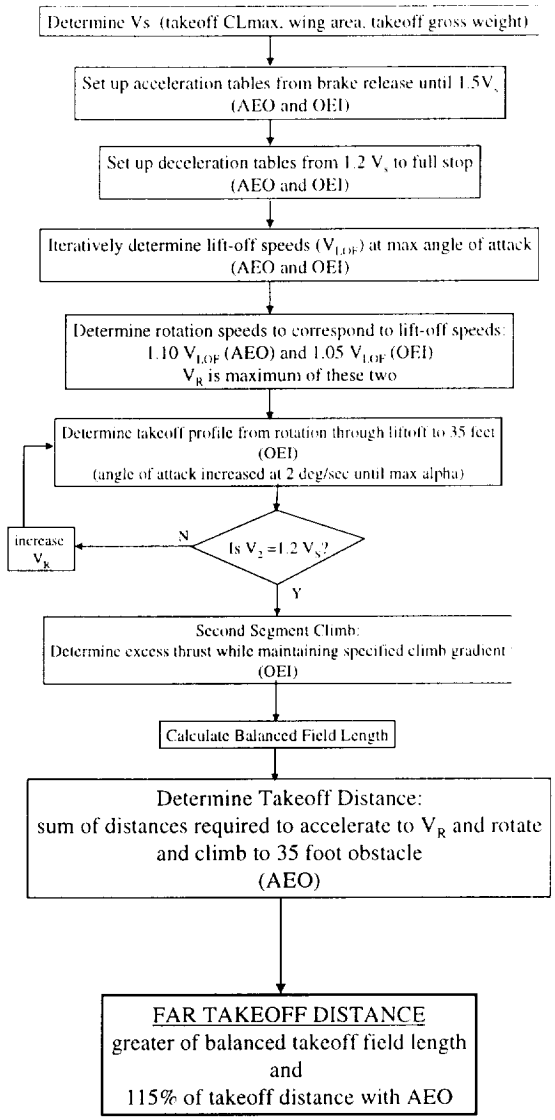

FIGURE 11 TAKEOFF PROGRAM FLOW CHART FOR TAKEOFF CONDITION

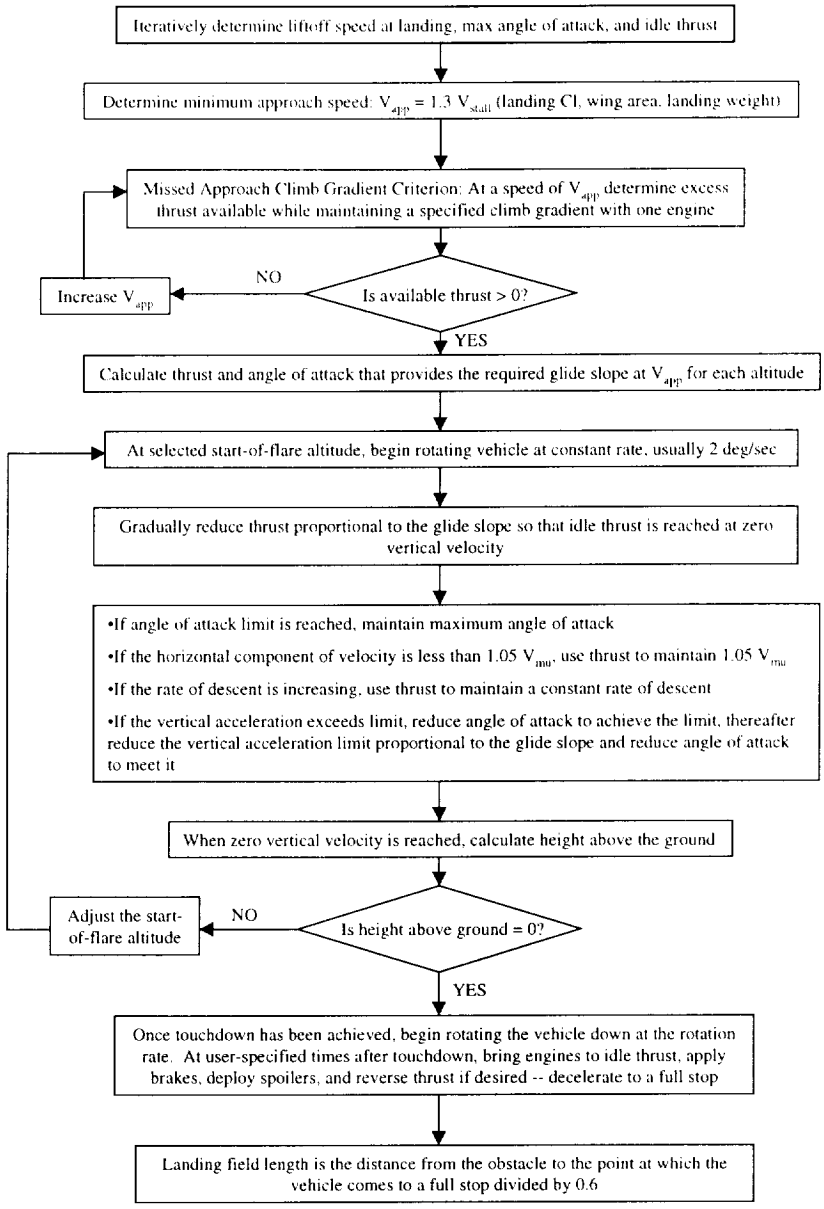

FIGURE 12 TAKEOFF PROGRAM FLOW CHART FOR LANDING CONDITION

2.3.2 CC Duct Sizing

Now that the required jet momentum is calculated, additional analysis needs to be done to ensure that the required blowing levels could be met. To perform this C_μ available analysis, an ASDL developed code called CCDUCT was used to determine the necessary size of the internal ducting to deliver the available mass flow from the engine and is depicted in Figure 13. The inputs to this program include the desired flight condition (e.g. altitude, and speed), number of engines, maximum engine bleed flow available per engine, total pressure and total temperature at the engine bleed point, wing area, and a ducting layout (from bleed point to the CC devices). CCDUCT iterates to a converged slot height which can deliver the available engine bleed flow. The program algorithm is described in more detail below.

The main constraint made in CC duct sizing program, CCDUCT, is that the Mach number within the ducting system remains below 0.4 in order to ensure proper CC system performance. Based on the given total pressure and temperature at the engine bleed point as well as the available CC mass flow from each engine, the mass flow parameter is calculated which dictates the CC duct area. This area is taken to be the upper bound of the CC ducting coming out the engine and the ducting supplying the mass flow to be ejected. This program is specifically tailored to calculate the ducting size for an HSCT since it calculates the CC slot area based on the specified starting value of h/c (slot height to chord ratio) and on the wing planform. Since the CC ducting system was arranged in such a fashion that each engine supplies the CC blowing momentum for a section of the wing, CCDUCT makes an assumption that the available CC slot area is divided evenly among each engine. This assumption is consistent with the fact that only one quarter (4 engines) of the total available engine bleed is being passed through this CC slot area.

The program then takes the flow condition at the engine bleed exit, and calculates the pressure loss due to the flow being piped from the engine to the CC devices at the trailing edge of the HSCT. The pressure loss calculated is based on the ducting system information (such as duct length, number of turns, etc.) that the user specifies. Another assumption made here is that the flow from the engine to the CC device is undergoing a isentropic expansion process. Therefore, based on the pressure and temperature and the CC slot area, a strip theory approach is taken to calculate the mass flow that can be ejected at each wing span station. The total mass flow is then summed and compared to the available bleed flow. CCDUCT then adjust h/c, and the program recalculates the CC slot area based on the new h/c. This iteration continues until a converged h/c is reached which can deliver the available engine bleed flow. Other output from CCDUCT include CC jet velocity (also calculated using isentropic equations) and available C_μ. The methodology steps and programs described in this section are extensively used to perform a detailed analysis of the impact of CC technology to an HSCT. Specifically, one of the main objectives of this study is to assess the impact on takeoff and landing performance of an HSCT due to the infusion of this new technology. The next section of the report will discuss the implementation details of the methodology as well as the computer simulation programs discussed above.

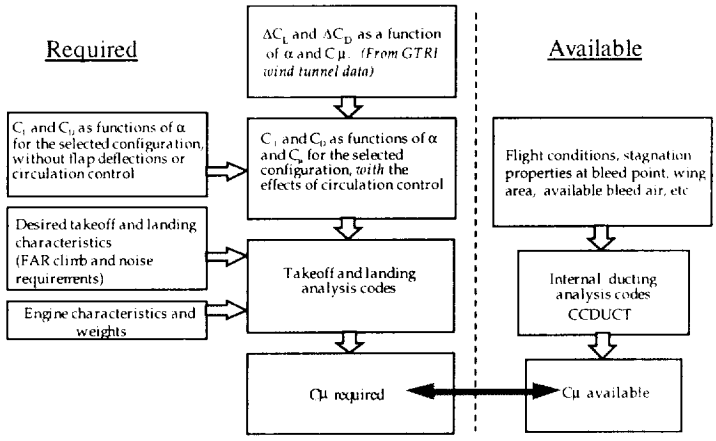

FIGURE 13: CONVERGENCE OF REQUIRED AND AVAILABLE LEVELS OF BLOWING

3. Implementation

The primary objective of this study was to objectively assess the feasibility of a low speed pneumatic technology, in particular CC, application to an HSCT concept. This technology has been proven for various subsonic vehicles including a Navy A6 and a Boeing 737. Yet, CC has not been widely accepted for commercial fixed-wing use but its potential has been extensively investigated for decades in wind tunnels across the globe for application to rotorcraft. More recently, an experimental investigation was performed at GTRI with application to an HSCT-type configuration. The data from those experiments was to be applied to a full-scale vehicle to assess the impact from a system level point of view. Hence, this study attempted to quantitatively assess the impact of this technology to an HSCT. The study objective was achieved in three primary steps.

First, a preliminary system level analysis was performed to establish that a need exists for a low speed technology on an HSCT. This was accomplished through the implementation of new developments in modern aircraft design theory developed at ASDL which included identification of probabilistic methods which facilitate rapid, parametric assessments of a design space so as to identify technical feasibility "show-stoppers". Specifically, the Fast Probability Integration technique was utilized to analyze a typical HSCT parametric design space. From the application of this technique, the takeoff field length was identified as the most critical performance constraint. Furthermore, a new method, called Technology Impact Forecasting, was applied to identify system level metrics that would create a region of feasible designs from technology metric "k" factors. From this investigation, improvements in low speed system level metrics, lift-to-drag ratio and C_{Lmax}, were identified as having the most influence on the infeasible design space.

Based on these results, the second goal of this study was considered. Once the need for an enabling technology for an HSCT was established, the identification of the specific technology which could possibly deliver the benefits assumed was defined as Circulation Control. Wind tunnel experiments were performed by GTRI on an HSCT-type configuration and this data was to be applied to a system level analysis to quantify the impact, including benefit and degradation, on an HSCT with actual data. The application of the wind tunnel data was not straightforward and approximation techniques were utilized to remove as much of the model and experimental condition dependencies as possible. This was necessary due to the flat-plate wing utilized in the experiments. The flat-plate, along with the beveled leading edge, created a significant amount of vortex-lift which would not exist on an operational vehicle. Typically, an operational vehicle would have a sharp leading edge on the outboard wing secion, but a finite leading-edge radius in the inboard section. Hence, not as much flow separation and vortex generation would be created. This last aspect was performed through second-order regressed polynomials of selected wind tunnel data as a function of angle of attack for a fixed blowing coefficient. This would allow for simulating the effects of CC to the aerodynamics of a full sized vehicle by adding the increment in lift and drag for a given alpha and blowing coefficient (or freestream velocity).

The final goal of the study was to quantitatively assess the impact of CC on the takeoff and landing performance of an HSCT as compared to a configuration with traditional high-lift systems. A detailed performance analysis was conducted with a modified version of the NASA Langley takeoff and landing program, TAKEOFF. Off-line detailed aerodynamic, propulsive, and ducting assessments were conducted to supply the code with as

accurate input information as possible. A more representative configuration was adapted for this purpose. This configuration was sized for an 80-20 split subsonic-supersonic mission. The aircraft takeoff gross weight was then included into the analysis code and the low speed performance analyzed. A parametric investigation was performed for various flap settings to establish the best configuration for reducing the low speed performance metrics. For the conventional configuration, a leading edge and trailing edge deflection of 10° and 30°, respectively, minimized the takeoff field length. The flap deflection for the landing field length and approach speed were 20°. The incremental changes in force coefficients were then added to the conventional configuration and the performance compared. The CC augmented configuration was shown to reduce all metrics by as much as 20% for various flap settings. Furthermore, an operational environment variation was conducted to quantify off-design point performance. The CC augmented configurations does show improvement and potential for full-scale application. Yet, an economic assessment of an HSCT with and without CC showed that a moderate penalty was incurred from the increased RDT&E costs associated with developing the CC technology and slight increases in empty weight.

These results were determined from three primary steps: identification of the need of CC, wind tunnel data reduction, and detailed takeoff and landing performance analysis. The implementation of each of these steps is described in detail below.

3.1 Establishing the Need for CC

Due to the non-conventional nature of an HSCT configuration, the historically based, regressed equations within FLOPS are not valid, nor accurate. Previous work performed by researchers at ASDL has corrected some of these inadequacies, in particular, the aerodynamics and wing weight calculations. These capabilities were enhanced with metamodels, which approximated more sophisticated aerodynamic and structural analysis tools. These metamodels, in the form of Response Surface Equations (RSE) [37], were inserted into the FLOPS source code and utilized for the preliminary system level study. The reader is referred to [46] for more detailed information on the structural enhancements, to [47, 48] for the aerodynamics, and [49, 50] for the general description of the methodology for the RSE generation. Specifically for this study, Equivalent Laminates Plate Solution, ELAPS [51, 52, 53] is used to model the wing and provide the weight, and the drag polars are generated using VORLAX, a linearized-potential flow solver. This information is then provided to FLOPS as weights in the case of structures and as tables of profile and induced drag coefficients in the case of aerodynamics.

The configurations analyzed in this study are sized for a 5,000 nautical mile mission with the primary cruise altitude of 67,000 ft at Mach 2.4. A subsonic cruise portion precedes the primary cruise segment at an altitude of 35,000 ft at Mach 0.9. The mission profile is shown in Figure 14. The payload of the aircraft is assumed to be 300 passengers with baggage and with a flight crew of two. The engine provided to FLOPS is a mixed flow turbofan and is modeled as a rubberized engine. A typical HSCT configuration is shown in Figure 15.

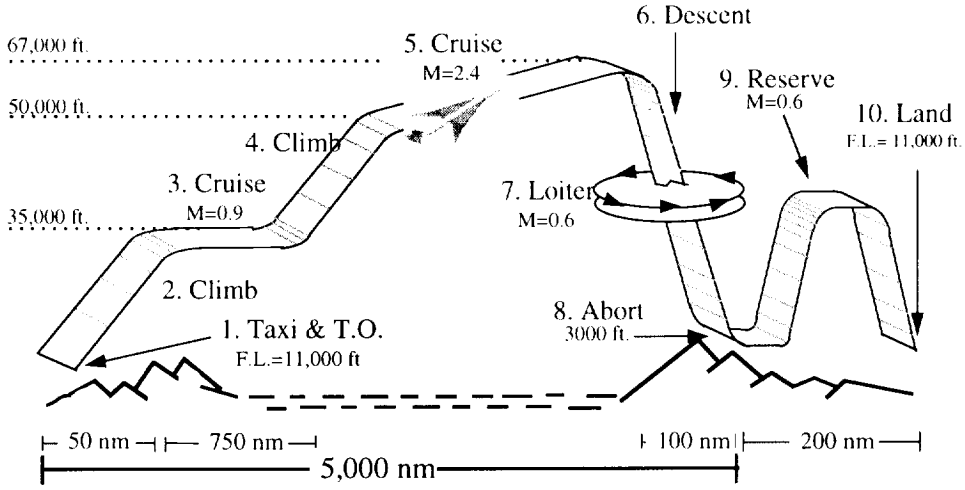

FIGURE 14: TYPICAL HSCT MISSION PROFILE

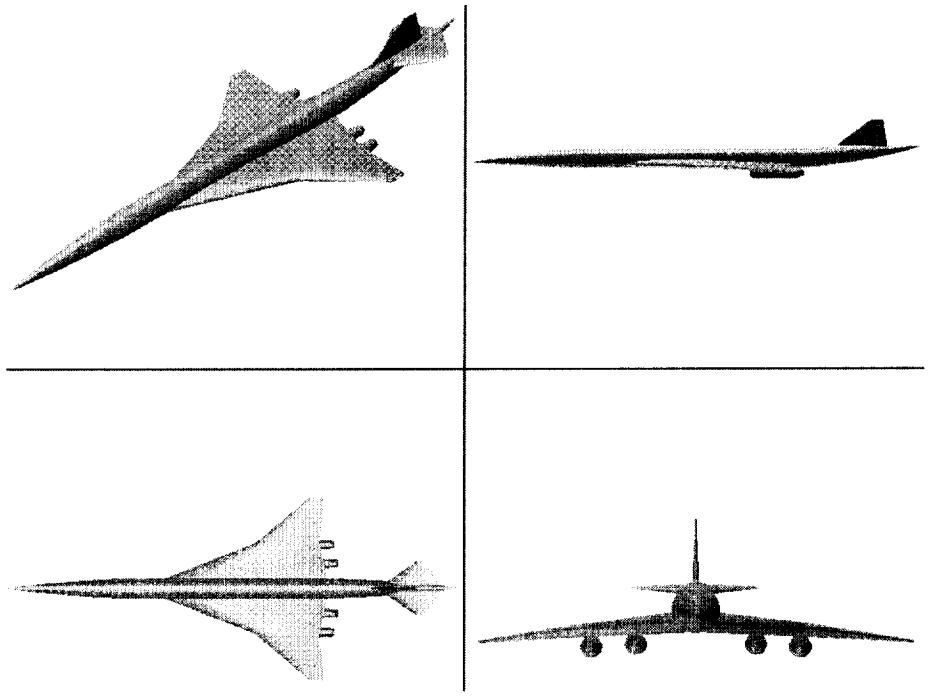

FIGURE 15: TYPICAL HSCT CONFIGURATION

Although takeoff and landing do no directly impact the sizing of the aircraft in FLOPS, the program does provide a detailed analysis of both segments. Information such as the maximum lift coefficient, the drag due to landing gear, and a drag polar of the aircraft with high lift devices activated or deployed must be provided to FLOPS in order to complete this analysis. FLOPS will then calculate balanced field length, obstacle times, velocities, and lift to drag ratios, as well as landing field length and approach speed.

3.1.1 Feasibility and Viability Assessment

Executing the first three steps of the approach, the conventional baseline aircraft failed to demonstrate an acceptable level of technical feasibility. If any of the objectives are not satisfied, then the solution is considered unattainable. The TOGW constraint was satisfied with a 11% probable design space. This result is seen in Figure 16, where the CDF curve for TOGW lies largely on the unfeasible side of the constraint (represented by the vertical line). Furthermore, none of the design space could achieve a TOFL under 11,000 ft (Figure 17) and is thereby the "show-stopper" of this concept. Only 12% of the space could satisfy the V_{app} (Figure 18). The other performance objectives included the landing field length at 100% satisfaction, and fly-over noise and sideline noise, both of which had no feasible space, i.e. 0% probability. Yet, the noise objectives are only considered as goals not hard constraints. Since three of the performance objectives could not satisfy the constraints with an acceptable level of probability, the viability assessment is bypassed completely and infusion of technology is required.

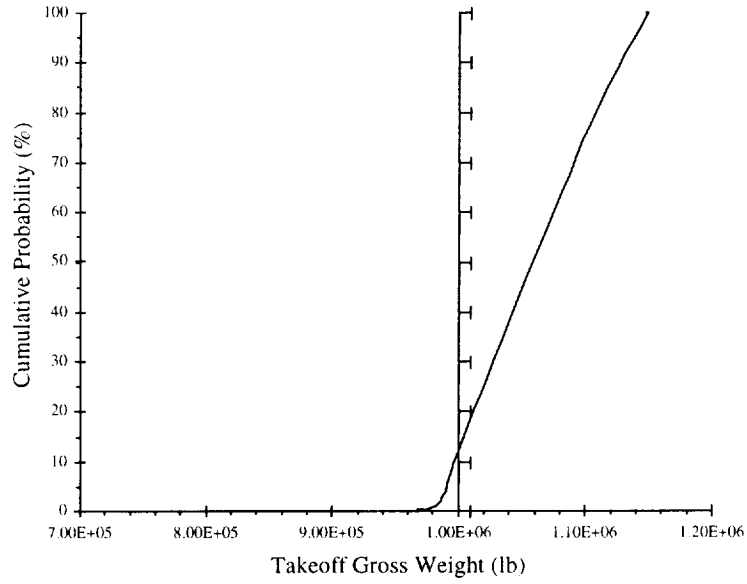

FIGURE 16: TECHNICAL FEASIBILITY ASSESSMENT (TOGW)

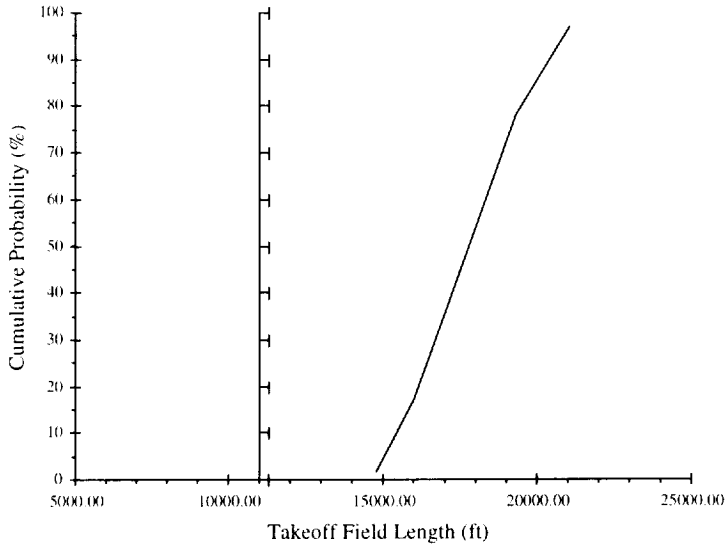

FIGURE 17: TECHNICAL FEASIBILITY ASSESSMENT (TOFL)

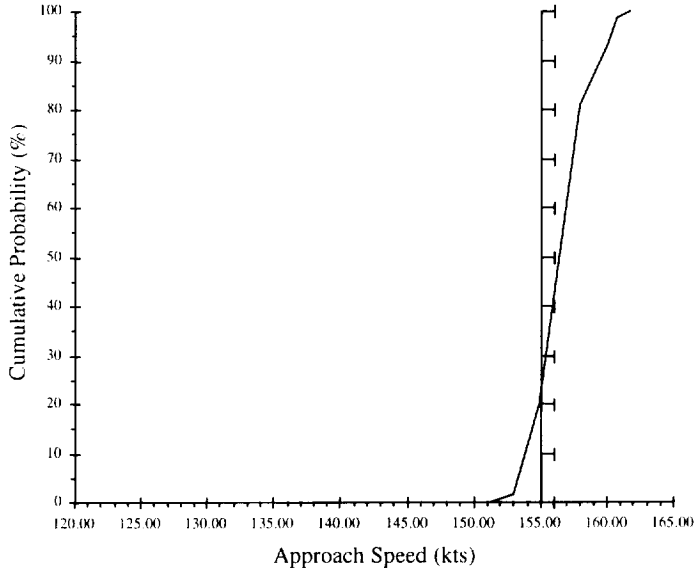

FIGURE 18: TECHNICAL FEASIBILITY ASSESSMENT (V_{APP})

3.1.2 Technology Infusion

The baseline HSCT resulted in a design space of technically unfeasible solutions in the initial investigation. Since the control parameter ranges were based on maximizing the probability of feasible design, the HSCT design space must be infused with new technologies. As described previously, a guideline to the technologies worth investigating can be facilitated through the qualitative manipulation of the technology metric "k" factors. Various technological benefits were considered including SFC and drag reduction in both cruise segments, L/D

improvements at takeoff, C_{Lmax} improvements at takeoff and landing, and first unit cost (T1), MTBF, and MTTR reductions. No penalties were assumed for this investigation. The assumed benefits of various technologies are shown in Table 6. The metrics should be as general as possible to allow for any technological infusion, as long as appropriate values for the factors are justified.

TABLE 6: TECHNOLOGY "K" FACTORS AND PENALTIES

"k" factors	Symbol	Impact range (%)
Drag reduction for supersonic cruise	k_CDsup	-10 to 0
L/D improvement at takeoff	k_L_Dto	0 to 20
C_{Lmax} improvement at landing	k_CLmax	0 to 20
SFC reduction in subsonic cruise	k_SFCsub	-10 to 0
SFC reduction in supersonic cruise	k_SFCsup	-10 to 0
First unit cost reduction	k_T1	0 to -50
MTBF reduction	k_MTBF	-50 to 50
MTTR reduction	k_MTTR	-50 to 50
Drag reduction for subsonic cruise	k_CDsub	-10 to 0

A face-centered Central Composite Design of Experiments (DoE) was performed using the above factors with the addition of thrust-to-weight (T/W) ratio and wing area (S_{ref}) which allowed for vehicle scaling. The DoE technique is described in References [49, 54, and 55]. An effects screening test was performed with a quadratic model to assess the impact of each "k" factor. The results from the DoE were analyzed with the JMP statistical package and a prediction profile was generated to quantify the effect of each parameter [41]. The prediction profile, shown in Figure 19, is evaluated based on the magnitude and direction of the slope. The larger the slope, the greater the influence of a given parameter. If a parameter, listed on the abscissa, does not contribute significantly to the response listed on the left, the slope is approximately zero. The sign of the slope, either positive or negative, depicts the direction of influence of the parameter on the response. For example, increasing the L/D at takeoff reduces the TOFL due to the negative slope.

All performance metrics list in Table 1 violated the constraints with a high probability except for the LDGFL which was satisfied by 100% of the designs. The remaining six objectives can be improved by observing which of the "k" factors most positively influences a given objective. For example, the TOFL can be dramatically improved by increasing the S_{ref}, C_{Lmax}, or L/D at takeoff; the V_{app} can be improved by increased S_{ref} or C_{Lmax}. Furthermore, the TOGW can be decreased by reducing both drag and SFC at the supersonic cruise condition.

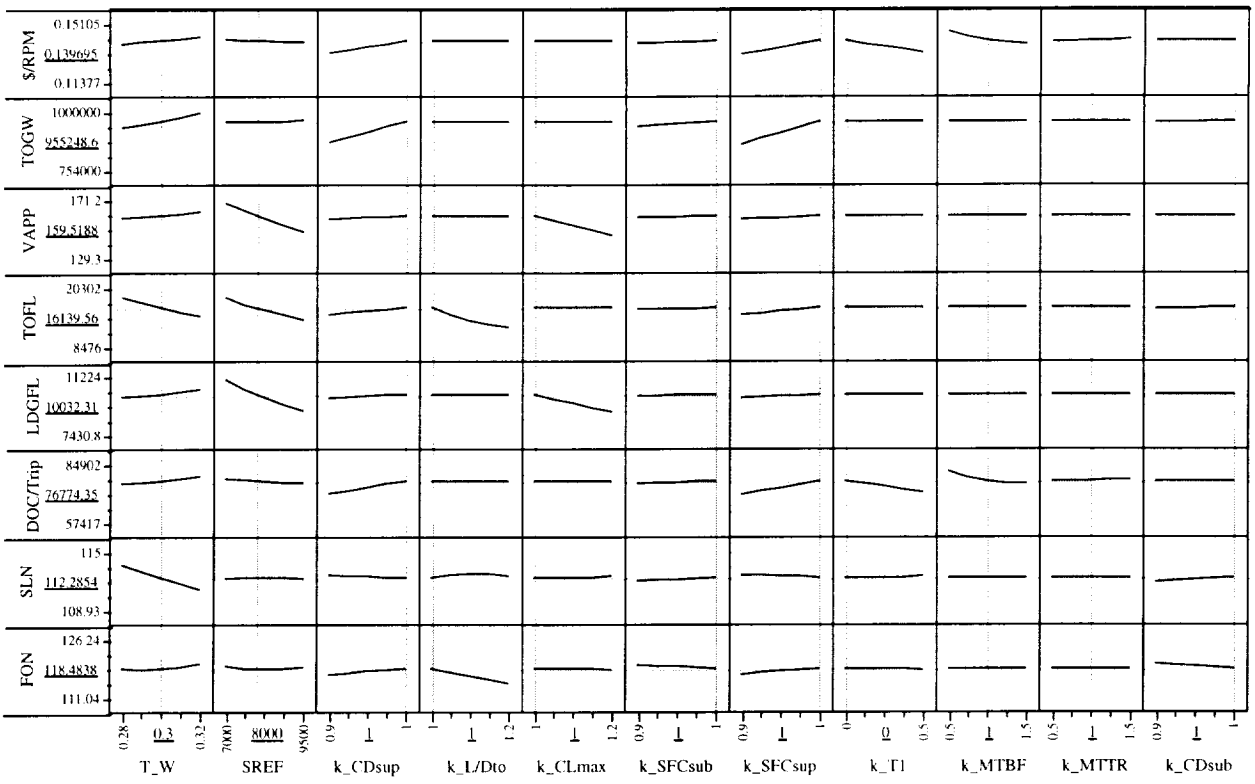

FIGURE 19: PREDICTION PROFILES FOR THE TECHNOLOGY "K" FACTORS

3.1.3 Examination of Design Solutions

The impact of the most significant technological "k" factor metrics on the performance objectives can be assessed through the re-application of the FPI technique. For this study, four "k" factors were considered significant: SFC and C_D reduction at the supersonic cruise condition, L/D increases at takeoff, and increases in C_{Lmax}. These factors were applied to the design space and the resulting CDFs for the violated objectives are depicted in Figure 20 through Figure 22. As is evident, the application of the above stated "k" factors results in a dramatic increase in the design space feasibility. In particular, the TOGW feasibility space for a conventional vehicle design space was 12% and was improved to 100% with the addition of new technologies. Similarly, the TOFL increased from 0% to 92.5%; the V_{app} from 12% to 100%; and the LDGFL maintained at 100%. It should be noted that the relative penalty of the improvement of a given technology application was not quantified since the impact of new technologies on the originally non-feasible design space was desired. Hence, only a point of view of benefit was assumed. The dramatic increase in feasibility space shows that the "show-stoppers", particularly the TOFL, can be overcome with the infusion of new technologies. The tremendous increase in the probability of feasible designs provides the decision-makers a larger number of alternatives to be investigated further.

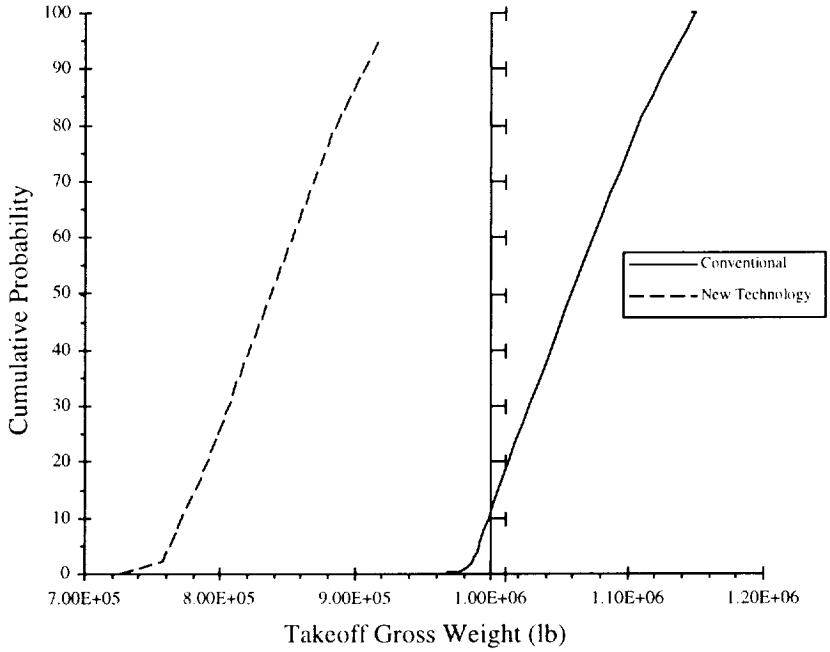

FIGURE 20: TOGW TECHNICAL FEASIBILITY IMPROVEMENT

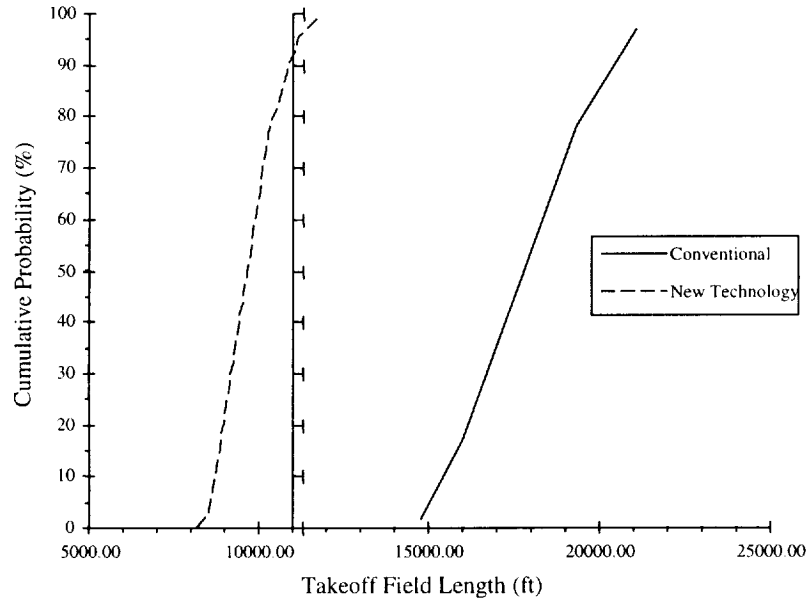

FIGURE 21: TOFL TECHNICAL FEASIBILITY IMPROVEMENT

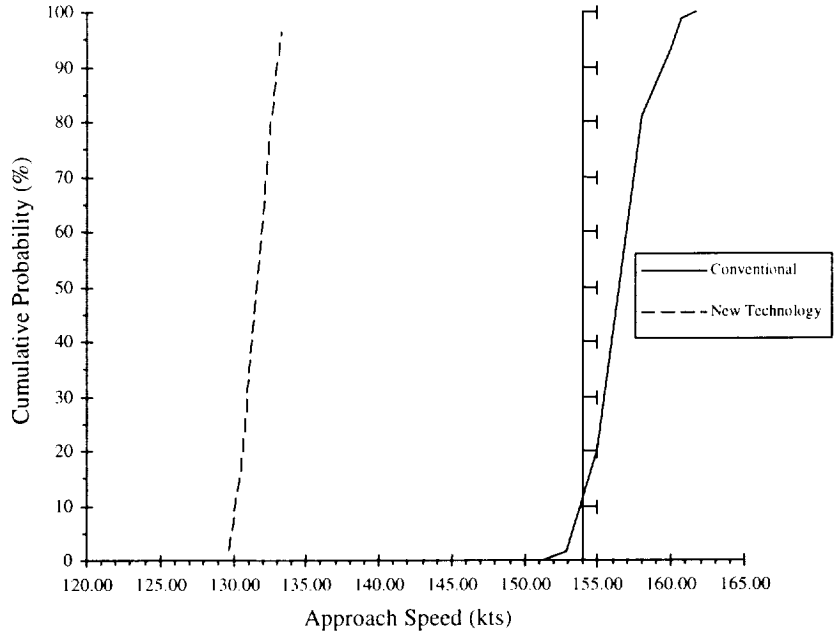

FIGURE 22: V_{APP} TECHNICAL FEASIBILITY IMPROVEMENT

The improvements in feasibility (Figure 20 through Figure 22) for the performance objectives is substantial. Yet, it is unclear which "k" factor setting had the largest impact for a given objective. Therefore, further investigation of the design space is necessary. In fact, the evolution of a design space, if improvements in certain metrics can be attained, is depicted in Figure 23 through Figure 26. The design space with all traditional technologies is depicted in Figure 23. As is evident, there exists no feasible design space (shown as a white space in the figures) which indicates that this concept cannot be built with conventional technologies to meet the constraints of TOGW, V_{app}, and TOFL. The active constraint is the TOFL as expected from Figure 17. Note, in the design space plots to follow, the contours that have underlined labels are merely goals, not hard/rigid constraints. Furthermore, the hash marks on each contour are on the side of increasing value.

The "k" factor settings needed for opening the design space can quickly be determined from the prediction profile in Figure 19. For example, the effect on the design space, if a 10% increase in L/D at takeoff can be achieved, is shown in Figure 24. The white space in the upper right hand corner indicates a feasible design space would be created with such an increase in L/D. The active constraint is still TOFL. This space is small and allows the decision-maker very little deviation for parametric studies.

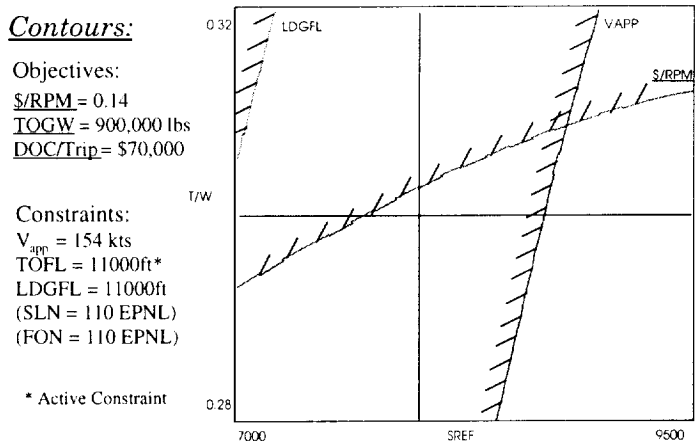

FIGURE 23: NO DESIGN SPACE

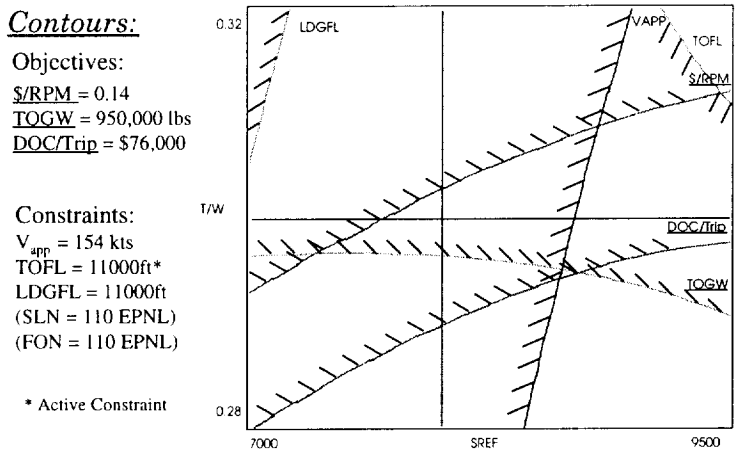

FIGURE 24: DESIGN SPACE WITH AN IMPROVED L/D TAKEOFF OF 10%

However, it is not enough to have a feasible design space. The feasible space must be maximized to allow for permutations without constraint violations. The amount of design space in Figure 24 is not adequate so the prediction profiles are referred to so as to determine where improvements need to be made; in particular, the value of L/D at takeoff. The impact of a 20% increase in L/D at takeoff is illustrated in Figure 25. This impact is dramatic compared to the 10% increase in Figure 24. At this point, V_{app} also becomes an active constraint in the top right corner. To increase the design space even further and deactivate the V_{app} constraint, a 5% increase for C_{Lmax} is modeled in Figure 26. The design space is sufficiently large for the decision-maker to continue with the aircraft design since a large region of feasible configurations exists.

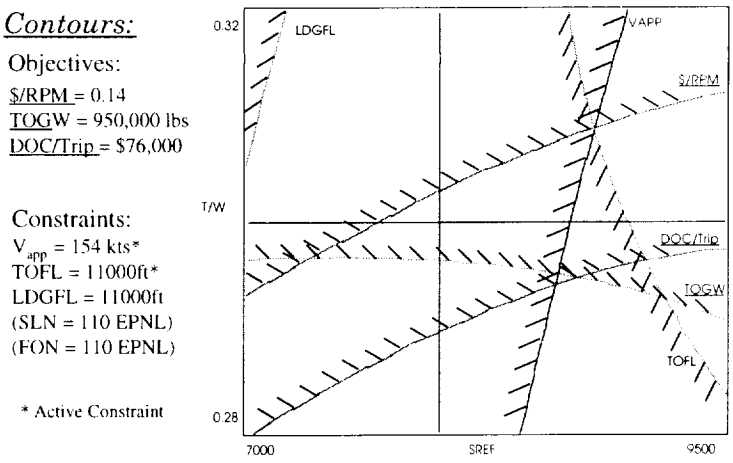

FIGURE 25: 20% INCREASE FOR L/D TAKEOFF

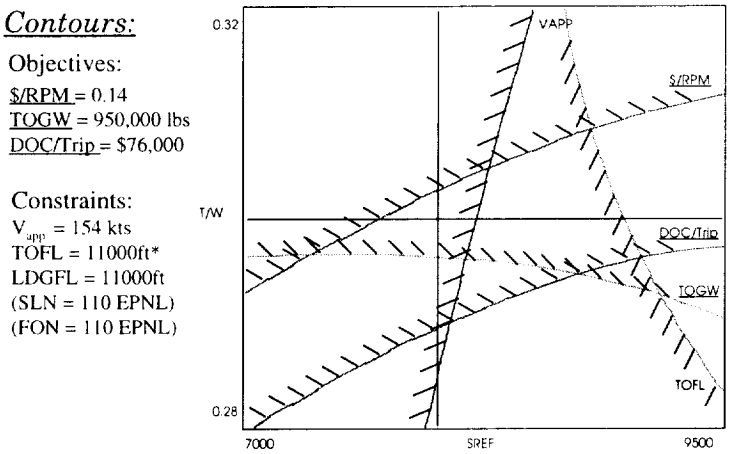

FIGURE 26: 20% INCREASE IN L/D TAKEOFF AND 5% INCREASE IN C_{LMAX}

With these results, the preliminary study at the system level is complete. Through the application of new techniques developed at ASDL, the need for the infusion of low speed technologies on an HSCT has been established. Hence, an actual technology, in particular CC, will now be applied and the impact quantified. In particular, the takeoff condition is critical, in fact, the "show-stopper" to this configuration. Hence, the impact of CC on the takeoff performance of an HSCT will be a primary focus for the detailed analysis.

3.2 Wind Tunnel Data Reduction

The reduction of the WT data was focused on removing as much WT dependent effects as possible as stated previously. The incremental changes in the force coefficients on a wing/body configuration were desired. These changes were due to the addition of a CCW flap in lieu of a plain flap, various levels of blowing, different flap settings, and AOA. The following describes how these effects were captured into a functional form which was utilized in the analysis program. First, a few preliminary checks were performed to ensure that the WT data would be applicable.

3.2.1 Dynamic Pressure Investigation

Prior to reducing the relevant WT data to functional forms for the analysis program, preliminary research was performed to investigate phenomena, which was of concern. As stated previously, the freestream dynamic pressure for the experimental runs was a concern. Typical dynamic pressures for a full scale HSCT operating at takeoff (200 kts) and landing (155 kts) is 135.5 psf and 81.4 psf, respectively. Research has indicated that the lift augmentation capability is sensitive to the ratio of the local freestream velocity to the jet velocity [56]. For the WT model, if a jet velocity of 1,700 ft/s is assumed, then the ratio of the freestream to local jet velocity is 13.1. Yet, for the full-scale model with the same jet velocity, this ratio reduces to 6.5 for landing and 5.04 for takeoff. Based on this fact, an investigation was conducted which considered the effects of dynamic pressure on the model force coefficients before the actual data manipulation or any vehicle specific modeling. The investigation included consideration of the lift and drag coefficients for the CCW flap and the plain flap at different deflections. For the CCW flap at 10°, a q_∞ sweep was performed in Runs 582 (10 psf), 583 (15 psf), and 584 (20 psf). The lift and drag coefficients for these runs are shown in Figure 27 and Figure 28, respectively. As is evident, there is little influence on the lift and drag due to q_∞ until high AOA are achieved. There was insufficient experimental data to compare the *blown* CCW flaps with q_∞, since a constant value of C_μ for an AOA sweep at different q_∞ and flap setting were not preformed. Hence, the plain flap was considered. For no flap deflection and a C_μ of 0.2, two experimental runs were identified, Run 531 (q_∞ =20 psf) and Run 534 (q_∞ =15 psf) and shown in Figure 29 and Figure 30. As can be seen, there is no influence of the augmentation ability due to q_∞. Hence, it was assumed for this study, that the influence of q_∞ to the local jet velocity would not be sufficient enough to prohibit direct application of the WT experiment trends. That is, dynamic similarity was assumed *not* an issue. It is suggested that much higher dynamic pressures should be investigated to completely remove this concern.

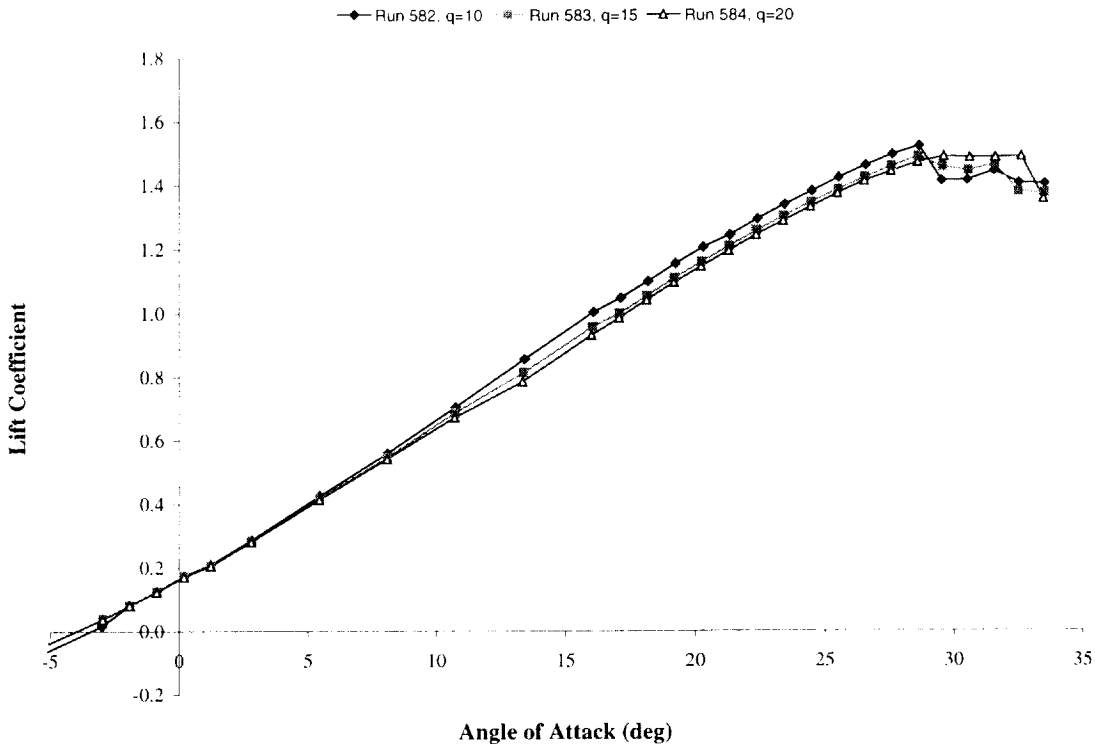

FIGURE 27: DYNAMIC PRESSURE VARIATION FOR LIFT: CCW FLAP, δ=10°

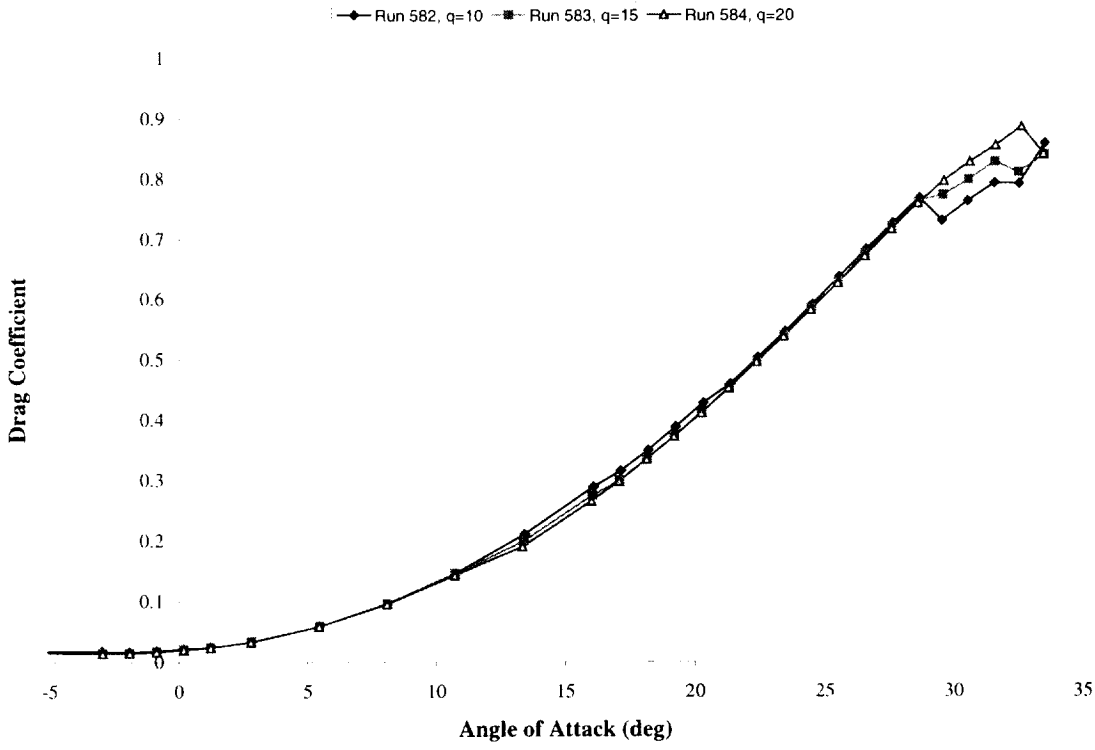

FIGURE 28: DYNAMIC PRESSURE VARIATION FOR DRAG: CCW FLAP, δ=10°

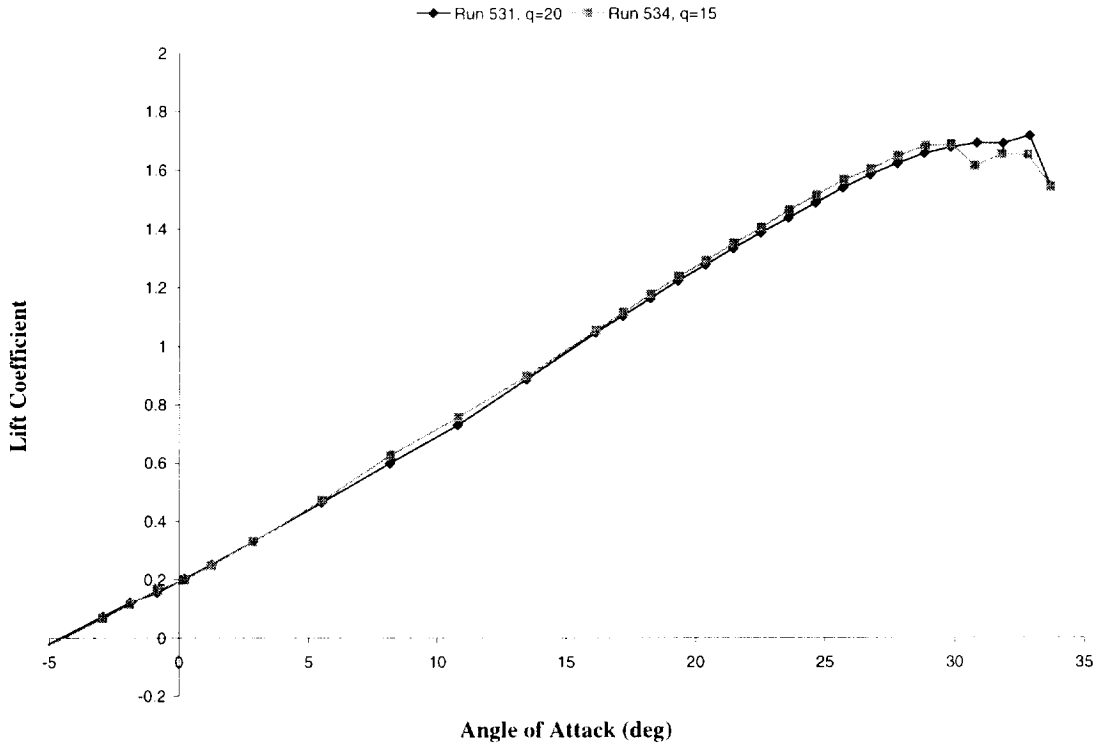

FIGURE 29: DYNAMIC PRESSURE VARIATION FOR LIFT: PLAIN FLAP, $\delta=0°$, $C_\mu=0.2$

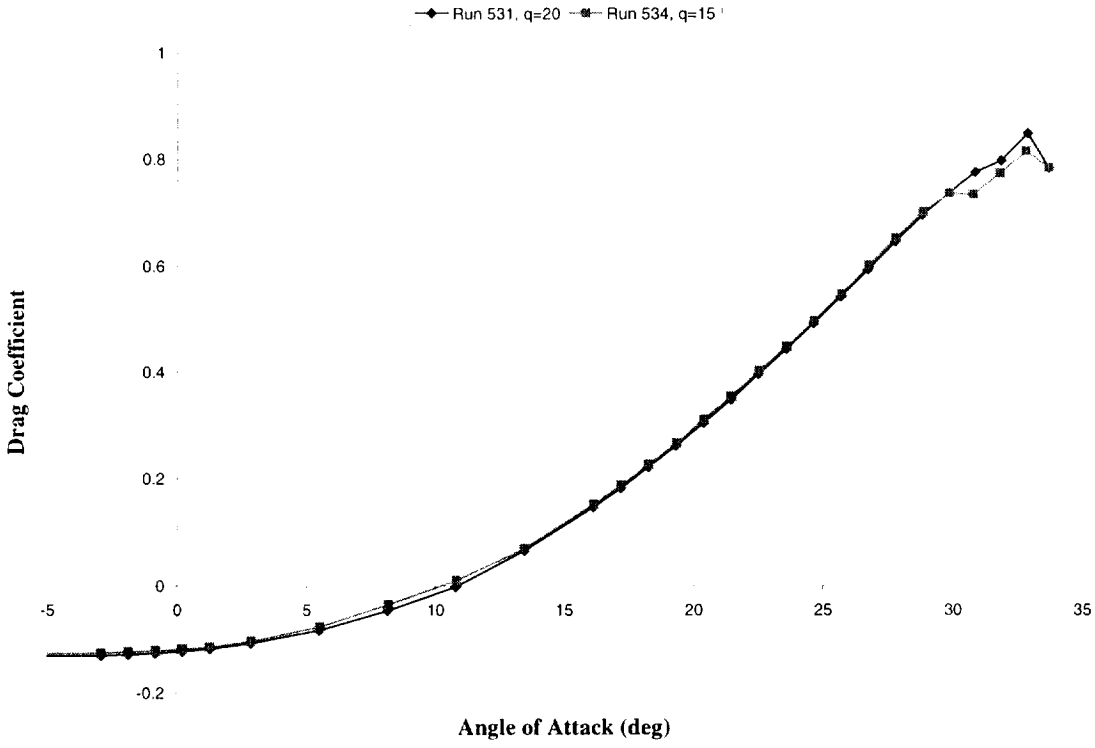

FIGURE 30: DYNAMIC PRESSURE VARIATION FOR DRAG: PLAIN FLAP, $\delta=0°$, $C_\mu=0.2$

3.2.2 Functional Form of WT Data

To analyze the impact of CC on an HSCT, all of the CC specific physical phenomena had to be captured. These effects include changes due to the addition of a CCW flap in lieu of a plain flap, various levels of blowing, different flap settings, and AOA. Furthermore, the effects needed to be put into a functional form for use in the analysis program. The selected WT data was transformed based on the input format needed for the analysis program. Specifically, the data needed to be transformed into incremental changes in lift and drag as a function of AOA and freestream velocity (i.e., q_∞) for a fixed flap deflection. The method utilized to derive the functional forms is described below and a flow chart depicted in Figure 31. In this figure, the lift coefficient is shown as a representative case for a given C_μ and flap deflection. This method was followed for each C_μ, flap deflection, flap type, and force coefficient.

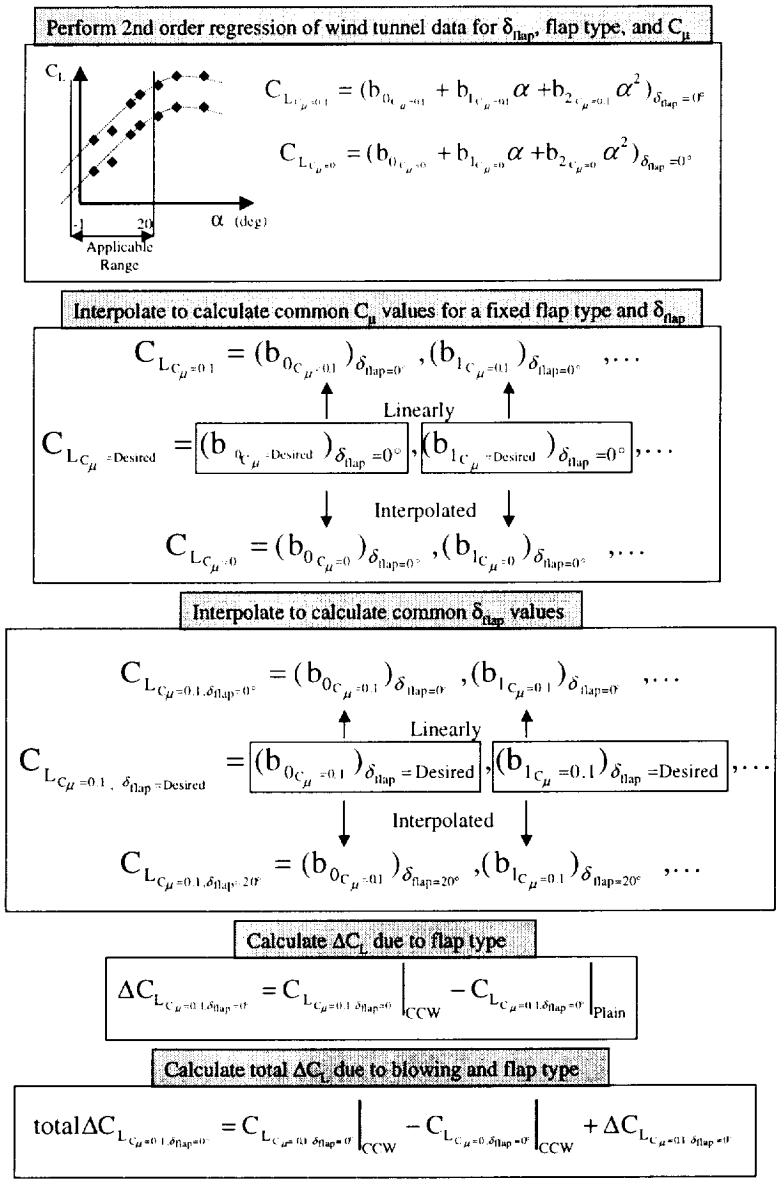

FIGURE 31: FLOW CHART FOR WT DATA REDUCTION

First, a least squares linear regression was performed on the identified data in Table 3 and Table 4 to obtain equations of the form of Eq. 2 for a fixed flap setting (δ), blowing coefficient (C_μ), and flap type.

$$C_L = b_0 + b_1\alpha + b_2\alpha^2$$
$$C_D = b_0 + b_1\alpha + b_2\alpha^2 \quad (2)$$

The regression was performed with the aid of the statistical package, JMP [41]. The data used for the regression was limited to an AOA range of $-1°$ to $20°$ since the operating AOA of a full scale HSCT will not surpass this range due to FAR regulations. Furthermore, the data curves were smoother and allowed for a better fit. A Summary of Fit, such as R^2, analysis was employed to ensure that the model fit was acceptable. As a general rule of thumb, an R^2 value greater than 90% represents a good model fit [57]. An R^2 value greater than 99.9% was achieved for all regressed equations and the equations were assumed to properly model the WT data. A comparison was performed with each equation to the original WT data and a maximum error band of ±5% was achieved.

TABLE 7: PLAIN FLAP REGRESSION COEFFICIENTS FOR LIFT

Run #	Plain δ_{flap} Deflection	C_μ	b_0	b_1	b_2
517	0°	0.0	-0.00533	0.0475006	0.0000895
530	0°	0.1	0.1352077	0.0470895	0.0001774
531	0°	0.2	0.1921267	0.0480686	0.0002606
535	0°	0.315	0.2455052	0.0532457	0.0001702
544	20°	0.0	0.0685051	0.0481474	0.0001184
550	20°	0.1	0.3732497	0.0441111	0.000261
551	20°	0.308	0.5651464	0.0532816	0.0000955

TABLE 8: PLAIN FLAP REGRESSION COEFFICIENTS FOR DRAG

Run #	Plain δ_{flap} Deflection	C_μ	b_0	b_1	b_2
517	0°	0.0	0.0096817	-0.000159	0.000841
530	0°	0.1	-0.050302	0.0007575	0.0008972
531	0°	0.2	-0.121274	0.0010147	0.0009725
535	0°	0.315	-0.197568	0.0021661	0.0009915
544	20°	0.0	0.0139022	0.0009963	0.0008404
550	20°	0.1	-0.022359	0.0035038	0.000937
551	20°	0.308	-0.131646	0.006777	0.0010202

TABLE 9: CCW FLAP REGRESSION COEFFICIENTS FOR LIFT

Run #	CCW δ_{flap} Deflection	C_μ	b_o	b_1	b_2
645	0°	0.0	0.0751519	0.0459198	0.0001101
647	0°	0.082	0.4615598	0.0437492	0.000213
648	0°	0.328	0.7882343	0.0573787	-0.000103
658	10°	0.0	0.1581686	0.0459559	0.0001407
659	10°	0.082	0.5603348	0.0439177	0.0001256
660	10°	0.328	0.9625107	0.0586818	-0.000284
625	34°	0.0	0.3408518	0.0460524	0.000147
630	34°	0.01	0.4412224	0.0452786	0.0001442
631	34°	0.02	0.5731664	0.0441174	0.0001277
632	34°	0.03	0.6551197	0.0477422	-0.000054
626	34°	0.041	0.7503041	0.0478338	-0.000104
627	34°	0.082	0.984632	0.0523358	-0.000373
628	34°	0.164	1.2292546	0.0596137	-0.000634
629	34°	0.328	1.5529575	0.0656343	-0.00075

TABLE 10: CCW FLAP REGRESSION COEFFICIENTS FOR DRAG

Run #	CCW δ_{flap} Deflection	C_μ	b_o	b_1	b_2
645	0°	0.0	0.0104273	0.0010653	0.0008164
647	0°	0.082	-0.002003	0.0046278	0.0009337
648	0°	0.328	-0.116462	0.0111642	0.000991
658	10°	0.0	0.0202953	0.0016695	0.0008653
659	10°	0.082	0.040139	0.0058438	0.0009204
660	10°	0.328	-0.011555	0.0149993	0.000891
625	34°	0.0	0.0510683	0.0041152	0.0009127
630	34°	0.01	0.0560238	0.005349	0.0009124
631	34°	0.02	0.0769356	0.0066923	0.0009158
632	34°	0.03	0.0932079	0.0087108	0.0008716
626	34°	0.041	0.1197227	0.0095743	0.0008673
627	34°	0.082	0.1833519	0.0135822	0.0007958
628	34°	0.164	0.2387824	0.0209468	0.0006672
629	34°	0.328	0.2913709	0.02892	0.0006244

Next, for a given flap type (i.e., plain or CCW) and a fixed flap deflection, a linear interpolation of the coefficients from step 1 was performed for different C_μ values. In particular, the blowing coefficient values listed in Table 11 as calculated from Eq (1). The corresponding velocities that are listed are based on a mass flow rate in the duct of 200 lbm/sec, jet velocity of 1,700 ft/s, and a wing reference area of 8,500 ft^2. As will be shown, the four mixed flow turbofans can each supply 50 lbm/sec bleed mass flow rate without significant degradation in performance and the jet velocity was determined from the internal duct sizing program, CCDUCT. Hence, for each regressed coefficient (b_0, b_1, and b_2), an interpolation was performed for a given flap type and deflection for a different C_μ value. Whenever WT data existed for a given C_μ value or near a desired C_μ value, the actual regressed coefficients were used and not interpolated. This allowed for an increased confidence of data.

TABLE 11: LINEARLY INTERPOLATED BLOWING COEFFICIENTS

Blowing Coefficient Values	Corresponding Speed* (kts)
0	N/A
0.005	270.9
0.007	229.0
0.009	201.9
0.01	191.6
0.015	156.4
0.02	135.5
0.03	110.6
0.04	95.8
0.05	85.7
0.1	60.6

Third, for a given C_μ, another linear interpolation was performed between the coefficients obtained in step 2 to acquire regressed coefficients for flap settings of 0°, 10°, 20°, 30°, and 34° for both flap types. For the plain flap, the coefficients for 30° were determined from an extrapolation of the data since the maximum δ_{flap} was 20°. The 34° deflection was not used. The extrapolation assumption was made since the effect of increasing flap deflection is linear for the blown and unblown experimental runs. For completeness, larger flap deflections should have been performed to obtain more accurate data interpolation. The results of the interpolation for the plain flap and CCW flap are listed in Appendix A. Again, each coefficient was independently interpolated.

The next step in the creation of the incremental forces coefficients included quantifying the effects of the use of CCW flaps in lieu of the plain flaps. This effect was captured by subtracting the plain flap coefficient (b_0, b_1, and b_2) from the corresponding CCW flap coefficient as shown in Figure 31 for each blowing level and flap setting. Finally, the total incremental change due to CC was determined through the addition of the change due to the flap type and the difference of lift or drag at a given blowing level from the unblown condition, also shown in Figure 31. These results are listing in Table 12 through Table 19 for the different flap settings (0° to 30°).

TABLE 12: ΔC_L FOR $\delta_{FLAP} = 0°$

AOA (deg)	C_μ 0.005	C_μ 0.007	C_μ 0.009	C_μ 0.01	C_μ 0.015	C_μ 0.02	C_μ 0.03	C_μ 0.04	C_μ 0.05	C_μ 0.1
-2	0.1243	0.1406	0.1568	0.1650	0.2056	0.2462	0.3274	0.4087	0.4899	0.7680
0	0.1206	0.1366	0.1527	0.1607	0.2008	0.2409	0.3211	0.4013	0.4814	0.7606
2	0.1170	0.1329	0.1488	0.1567	0.1963	0.2360	0.3152	0.3945	0.4738	0.7539
4	0.1137	0.1294	0.1451	0.1530	0.1922	0.2315	0.3100	0.3885	0.4670	0.7480
6	0.1107	0.1262	0.1418	0.1496	0.1885	0.2274	0.3053	0.3831	0.4610	0.7428
8	0.1078	0.1233	0.1388	0.1465	0.1851	0.2238	0.3011	0.3785	0.4558	0.7383
12	0.1028	0.1182	0.1335	0.1412	0.1795	0.2178	0.2945	0.3712	0.4479	0.7317
14	0.1007	0.1160	0.1313	0.1389	0.1772	0.2155	0.2920	0.3686	0.4451	0.7294
17	0.0979	0.1132	0.1285	0.1362	0.1745	0.2128	0.2894	0.3660	0.4426	0.7275
20	0.0956	0.1110	0.1264	0.1341	0.1725	0.2110	0.2880	0.3649	0.4419	0.7271

TABLE 13: ΔC_L FOR $\delta_{FLAP} = 10°$

AOA (deg)	C_μ 0.005	C_μ 0.007	C_μ 0.009	C_μ 0.01	C_μ 0.015	C_μ 0.02	C_μ 0.03	C_μ 0.04	C_μ 0.05	C_μ 0.1
-2	0.1686	0.1839	0.1991	0.2068	0.2449	0.2831	0.3594	0.4357	0.5120	0.7696
0	0.1645	0.1797	0.1948	0.2024	0.2403	0.2782	0.3541	0.4299	0.5057	0.7671
2	0.1606	0.1756	0.1907	0.1982	0.2358	0.2734	0.3486	0.4239	0.4991	0.7633
4	0.1569	0.1718	0.1867	0.1942	0.2314	0.2687	0.3431	0.4176	0.4921	0.7582
6	0.1535	0.1682	0.1830	0.1903	0.2271	0.2640	0.3376	0.4112	0.4848	0.7517
8	0.1503	0.1648	0.1794	0.1866	0.2230	0.2593	0.3319	0.4046	0.4773	0.7439
12	0.1446	0.1587	0.1728	0.1798	0.2150	0.2501	0.3205	0.3908	0.4611	0.7241
14	0.1421	0.1559	0.1697	0.1766	0.2111	0.2456	0.3146	0.3836	0.4526	0.7122
17	0.1388	0.1522	0.1655	0.1722	0.2056	0.2390	0.3057	0.3725	0.4392	0.6919
20	0.1360	0.1489	0.1617	0.1682	0.2003	0.2324	0.2967	0.3609	0.4252	0.6685

TABLE 14: ΔC_L FOR $\delta_{FLAP} = 20°$

AOA (deg)	C_μ 0.005	C_μ 0.007	C_μ 0.009	C_μ 0.01	C_μ 0.015	C_μ 0.02	C_μ 0.03	C_μ 0.04	C_μ 0.05	C_μ 0.1
-2	0.2259	0.2481	0.2704	0.2816	0.3507	0.4198	0.5079	0.6062	0.6675	0.8809
0	0.2210	0.2431	0.2651	0.2762	0.3445	0.4129	0.5079	0.6068	0.6699	0.8972
2	0.2162	0.2381	0.2599	0.2708	0.3383	0.4057	0.5063	0.6053	0.6700	0.9088
4	0.2116	0.2331	0.2547	0.2655	0.3319	0.3983	0.5032	0.6019	0.6676	0.9156
6	0.2070	0.2283	0.2496	0.2603	0.3255	0.3908	0.4986	0.5966	0.6629	0.9177
8	0.2026	0.2236	0.2446	0.2551	0.3191	0.3830	0.4924	0.5893	0.6558	0.9151
12	0.1942	0.2145	0.2347	0.2449	0.3059	0.3670	0.4755	0.5687	0.6344	0.8956
14	0.1902	0.2100	0.2299	0.2398	0.2992	0.3587	0.4647	0.5555	0.6201	0.8788
17	0.1844	0.2036	0.2228	0.2324	0.2891	0.3458	0.4456	0.5319	0.5942	0.8447
20	0.1789	0.1973	0.2158	0.2250	0.2788	0.3325	0.4231	0.5039	0.5629	0.7999

TABLE 15: ΔC_L FOR $\delta_{FLAP} = 30°$

AOA (deg)	C_μ 0.005	C_μ 0.007	C_μ 0.009	C_μ 0.01	C_μ 0.015	C_μ 0.02	C_μ 0.03	C_μ 0.04	C_μ 0.05	C_μ 0.1
-2	0.2831	0.3124	0.3417	0.3563	0.4565	0.5566	0.6565	0.7767	0.8229	0.9923
0	0.2775	0.3064	0.3354	0.3499	0.4487	0.5475	0.6618	0.7836	0.8341	1.0273
2	0.2718	0.3005	0.3291	0.3434	0.4407	0.5380	0.6640	0.7868	0.8409	1.0542
4	0.2662	0.2945	0.3228	0.3369	0.4325	0.5280	0.6633	0.7863	0.8431	1.0730
6	0.2606	0.2884	0.3163	0.3303	0.4239	0.5176	0.6596	0.7820	0.8409	1.0837
8	0.2550	0.2824	0.3098	0.3236	0.4152	0.5068	0.6529	0.7739	0.8343	1.0863
12	0.2438	0.2703	0.2967	0.3099	0.3969	0.4838	0.6304	0.7466	0.8076	1.0671
14	0.2382	0.2642	0.2901	0.3030	0.3874	0.4717	0.6147	0.7273	0.7875	1.0453
17	0.2299	0.2550	0.2800	0.2925	0.3726	0.4527	0.5856	0.6913	0.7491	0.9975
20	0.2217	0.2457	0.2698	0.2818	0.3572	0.4327	0.5496	0.6470	0.7006	0.9314

TABLE 16: ΔC_D FOR $\delta_{FLAP} = 0°$

AOA (deg)	C_μ 0.005	C_μ 0.007	C_μ 0.009	C_μ 0.01	C_μ 0.015	C_μ 0.02	C_μ 0.03	C_μ 0.04	C_μ 0.05	C_μ 0.1
-2	-0.0010	-0.0007	-0.0004	-0.0003	0.0005	0.0012	0.0027	0.0042	0.0057	0.0030
0	0.0022	0.0028	0.0034	0.0037	0.0052	0.0067	0.0096	0.0126	0.0156	0.0191
2	0.0054	0.0063	0.0072	0.0077	0.0100	0.0123	0.0169	0.0215	0.0262	0.0365
4	0.0085	0.0098	0.0110	0.0117	0.0149	0.0181	0.0246	0.0310	0.0375	0.0553
6	0.0114	0.0131	0.0148	0.0157	0.0199	0.0241	0.0326	0.0410	0.0495	0.0753
8	0.0143	0.0164	0.0186	0.0196	0.0249	0.0303	0.0409	0.0516	0.0622	0.0966
12	0.0197	0.0228	0.0259	0.0275	0.0353	0.0431	0.0587	0.0743	0.0899	0.1431
14	0.0222	0.0259	0.0296	0.0314	0.0406	0.0498	0.0681	0.0865	0.1048	0.1684
17	0.0259	0.0304	0.0350	0.0373	0.0487	0.0601	0.0829	0.1057	0.1286	0.2086
20	0.0292	0.0348	0.0403	0.0431	0.0570	0.0708	0.0985	0.1262	0.1539	0.2518

TABLE 17: ΔC_D FOR $\delta_{FLAP} = 10°$

AOA (deg)	C_μ 0.005	C_μ 0.007	C_μ 0.009	C_μ 0.01	C_μ 0.015	C_μ 0.02	C_μ 0.03	C_μ 0.04	C_μ 0.05	C_μ 0.1
-2	0.0101	0.0117	0.0133	0.0141	0.0181	0.0221	0.0300	0.0380	0.0460	0.0705
0	0.0133	0.0153	0.0172	0.0182	0.0230	0.0278	0.0375	0.0471	0.0568	0.0887
2	0.0168	0.0191	0.0213	0.0225	0.0282	0.0338	0.0452	0.0566	0.0679	0.1074
4	0.0205	0.0231	0.0257	0.0270	0.0336	0.0402	0.0533	0.0664	0.0796	0.1265
6	0.0244	0.0274	0.0303	0.0318	0.0393	0.0468	0.0617	0.0767	0.0916	0.1461
8	0.0285	0.0318	0.0352	0.0369	0.0453	0.0537	0.0705	0.0873	0.1041	0.1660
12	0.0374	0.0415	0.0456	0.0477	0.0580	0.0684	0.0890	0.1097	0.1303	0.2073
14	0.0422	0.0467	0.0512	0.0535	0.0648	0.0761	0.0988	0.1214	0.1441	0.2285
17	0.0497	0.0549	0.0600	0.0626	0.0755	0.0883	0.1141	0.1398	0.1655	0.2612
20	0.0578	0.0636	0.0694	0.0723	0.0867	0.1012	0.1301	0.1590	0.1879	0.2949

TABLE 18: ΔC_D FOR $\delta_{FLAP} = 20°$

AOA (deg)	C_μ 0.005	C_μ 0.007	C_μ 0.009	C_μ 0.01	C_μ 0.015	C_μ 0.02	C_μ 0.03	C_μ 0.04	C_μ 0.05	C_μ 0.1
-2	0.0199	0.0215	0.0231	0.0238	0.0343	0.0448	0.0606	0.0851	0.0986	0.1507
0	0.0245	0.0266	0.0287	0.0298	0.0417	0.0537	0.0737	0.1002	0.1159	0.1790
2	0.0294	0.0321	0.0348	0.0361	0.0495	0.0629	0.0868	0.1153	0.1332	0.2064
4	0.0347	0.0379	0.0411	0.0427	0.0576	0.0725	0.1000	0.1304	0.1503	0.2330
6	0.0403	0.0441	0.0478	0.0497	0.0661	0.0824	0.1132	0.1455	0.1673	0.2587
8	0.0463	0.0506	0.0549	0.0570	0.0748	0.0927	0.1264	0.1606	0.1842	0.2836
12	0.0593	0.0647	0.0700	0.0727	0.0935	0.1143	0.1530	0.1908	0.2177	0.3306
14	0.0663	0.0722	0.0781	0.0810	0.1033	0.1256	0.1664	0.2059	0.2342	0.3529
17	0.0775	0.0842	0.0909	0.0942	0.1187	0.1432	0.1865	0.2285	0.2588	0.3846
20	0.0895	0.0969	0.1044	0.1081	0.1349	0.1616	0.2067	0.2511	0.2832	0.4144

TABLE 19: ΔC_D FOR $\delta_{FLAP} = 30°$

AOA (deg)	C_μ 0.005	C_μ 0.007	C_μ 0.009	C_μ 0.01	C_μ 0.015	C_μ 0.02	C_μ 0.03	C_μ 0.04	C_μ 0.05	C_μ 0.1
-2	0.0298	0.0313	0.0328	0.0336	0.0506	0.0675	0.0911	0.1322	0.1511	0.2309
0	0.0357	0.0380	0.0403	0.0414	0.0605	0.0795	0.1099	0.1533	0.1751	0.2693
2	0.0421	0.0451	0.0482	0.0497	0.0708	0.0920	0.1284	0.1740	0.1984	0.3055
4	0.0490	0.0527	0.0565	0.0584	0.0816	0.1048	0.1466	0.1944	0.2210	0.3395
6	0.0563	0.0608	0.0653	0.0676	0.0928	0.1180	0.1646	0.2143	0.2430	0.3714
8	0.0642	0.0694	0.0746	0.0772	0.1044	0.1317	0.1823	0.2339	0.2643	0.4011
12	0.0813	0.0878	0.0944	0.0977	0.1289	0.1602	0.2170	0.2719	0.3050	0.4540
14	0.0905	0.0977	0.1050	0.1086	0.1418	0.1750	0.2340	0.2903	0.3243	0.4773
17	0.1053	0.1135	0.1217	0.1258	0.1619	0.1981	0.2589	0.3172	0.3521	0.5080
20	0.1212	0.1303	0.1394	0.1439	0.1830	0.2221	0.2833	0.3433	0.3784	0.5340

3.3 Detailed Takeoff and Landing Assessment

Up to this point, the need for an advanced technology in the low speed flight regime for an HSCT has been established. New methods in modern aircraft design theory were applied to an HSCT design space. This application identified that configurations with conventional technologies are not feasible due to TOFL constraint violations. Furthermore, qualitative technology impact forecasting identified that improvements in low speed flight could greatly enhance the feasibility space of an HSCT concept. Once this forecasting was completed, an actual technology could be applied to the design space and enhancements or degradation to the system could be quantitatively assessed. For this study, CC was identified as an enabling technology.

The application of actual CC data to a full-scale model was to be used for system level performance studies. WT data was manipulated to remove as much of the WT model geometry and test condition dependencies as possible and second order equations for ΔC_L and ΔC_D were created as described in the previous section. In this section, the incremental changes in lift and drag will be applied to a full-scale vehicle to assess the impact on the low speed performance.

As stated previously, TAKEOFF program requires inputs of C_L and C_D characteristics with and without blowing, aircraft wing area, gross takeoff and landing weight, and an engine deck. These requirements lead to off-line assessments of configuration aerodynamics, vehicle sizing, and the propulsion system. In addition, an investigation was performed to determine the optimal source of bleed air supply for the ejected mass flux; specifically an Auxiliary Power Unit or the engines. Each one of these assessments will be described and then followed by the detailed takeoff and landing performance evaluation.

3.3.1 Computational Model

The flat plate WT model was not a realistic design for assessing the performance impact of CC on a full scale configuration. A scaled wing utilizing the airfoil shown in Figure 10 would have minimal wing thickness available for fuel storage and would be aerodynamically inefficient without twist or camber. Therefore, an adaptation of the wind tunnel model was generated. The original wing planform was maintained but the wing was given a linearly varying thickness-to-chord ratio with 5% at the root and 2% at the tip. Based on previous studies

performed by ASDL, the wing was twisted and cambered for a top of climb lift coefficient of 0.12. The wind tunnel model was scaled up based on a fuselage length of 326 ft. and a wing area of 8,500 ft^2. The computational model was also given a horizontal and vertical tail with dimensions based on previous studies. The original geometric properties and the full-scale values are summarized in Table 20, where the geometric locations are referenced from the nose of the vehicle. The scaled computational model is depicted in Figure 32.

TABLE 20: UNSCALED AND SCALED GEOMETRIC PARAMETERS

Geometric Parameter	Experimental Model (in)	Full Scale Computational Model (ft)
Wing		
Apex	11.26	61.29
LE x kink	35.1	179.16
LE y kink	6.388	31.61
LE x tip	43.1	218.74
TE x tip	45.0	228.15
TE y tip	12.2	60.33
TE x kink	43.1	228.15
TE y kink	6.388	31.61
TE x root	43.1	228.15
Ref. Area	1.206 (ft^2)	8,500 (ft^2)
Root t/c	0.78%	5%
Tip t/c	13.6%	2%
Horizontal Tail		
Apex	~	276.12
Span	~	36.56
Aspect Ratio	~	1.91
Taper Ratio	~	0.236
t/c	~	3%
Ref. Area	~	700 (ft^2)
Vertical Tail		
Apex	~	272.86
Span	~	29.67
Aspect Ratio	~	1.96
Taper Ratio	~	0.277
t/c	~	3%
Ref. Area	~	450 (ft^2)
Fuselage		
Length	60.0	326.0
Max Diameter	4.5	15.4

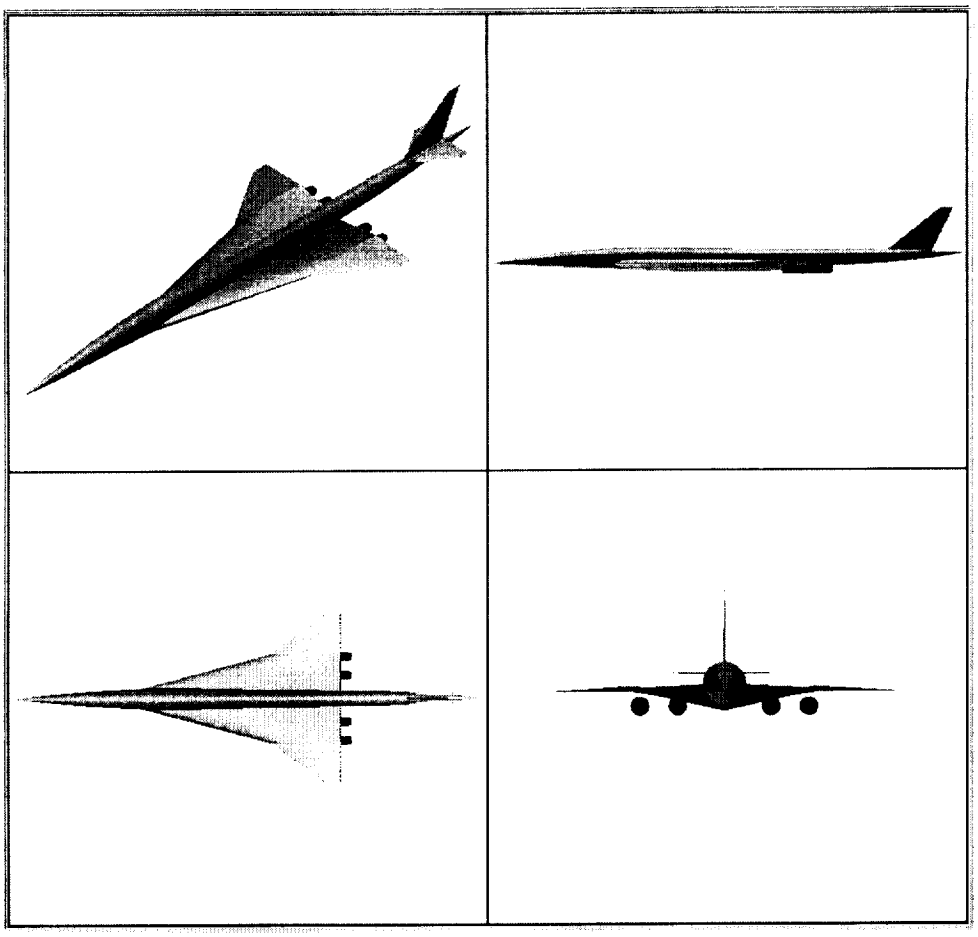

FIGURE 32: COMPUTATIONAL MODEL THREE-VIEW

3.3.2 Aerodynamics Assessment and Sizing

The conventional configuration was analyzed with a series of public domain linearized potential flow codes, Graphical User Interfaces (GUI), and in-house created shell scripts to create cruise drag polars for sizing the vehicle and low speed polars for assessing the performance. These drag polars were used by FLOPS for the system level sizing and the modified program for detailed takeoff and landing analysis. These drag polars formed the foundation upon which the effects of CC could be added in the form of ΔC_L and ΔC_D as described previously. This section describes the aerodynamic analysis tools utilized to generate cruise polars, low speed polars, and the resulting sized vehicle.

3.3.2.1 Aerodynamic Analysis

Six programs were utilized to model the geometry and generate and correlate the drag polars. These programs include BDAP [58, 59, 60], AERO2s [61], RAM [62], VORLAX [63], VORVIEW, and WINGDES [64]. A general description of these tools is contained in Appendix B and the application is described here. The geometry of computational model (Table 20) was created in RAM, which is a parametric-based geometry modeler created at NASA Ames Research Center. The geometry was fed to WINGDES to twist and camber the wing based on a top-of-climb design lift coefficient of 0.12. The new wing was incorporated to the vehicle and inspected in RAM. The

model was then fed to BDAP to calculate the skin friction and wave drag for a typical split subsonic-supersonic mission, as was shown in Figure 14. The induced drag was calculated with VORLAX utilizing VORVIEW as an interactive GUI. Note, the tools cannot predict C_{Lmax} and are limited to small disturbances. The resulting cruise aerodynamics are depicted in Figure 33 through Figure 35. In Figure 33, the lift independent drag is shown with altitude and Mach number. The induced drag is shown as a function of Mach number and lift coefficient in Figure 34 and Figure 35. For the low speed drag polars, a parametric variation of the leading edge slats and trailing edge flaps was performed. This investigation was performed to determine the best combination of deflections to minimize the low speed performance metrics (TOFL, Ldgfl, and Vapp). The low speed polars are depicted in Figure 36 through Figure 39 for the various LE flap deflections. These polars will be used with the sized vehicle characteristics in the TAKEOFF program in later sections.

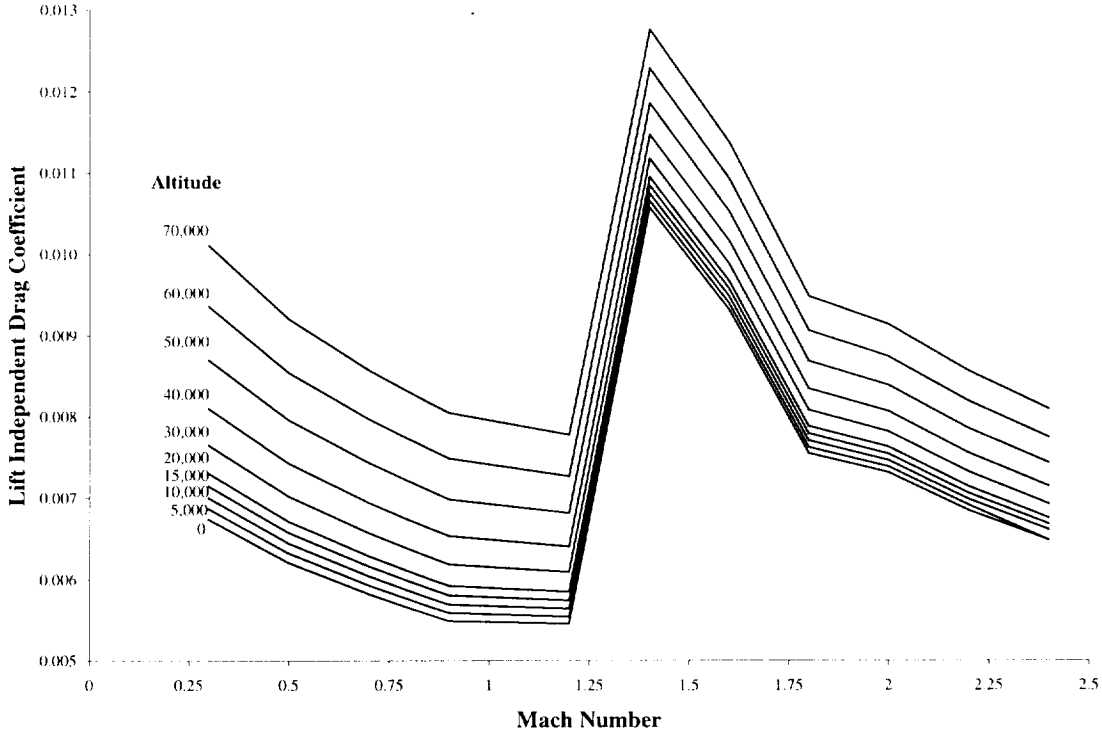

FIGURE 33: LIFT INDEPENDENT DRAG

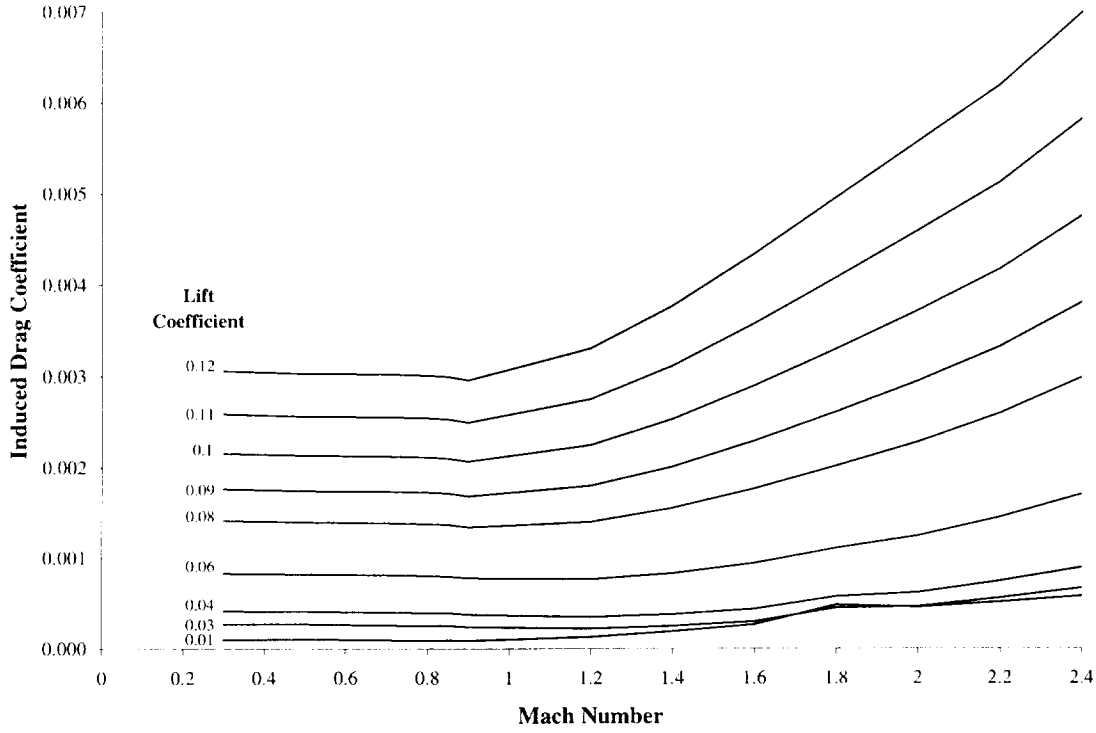

FIGURE 34: LIFT DEPENDENT DRAG (1)

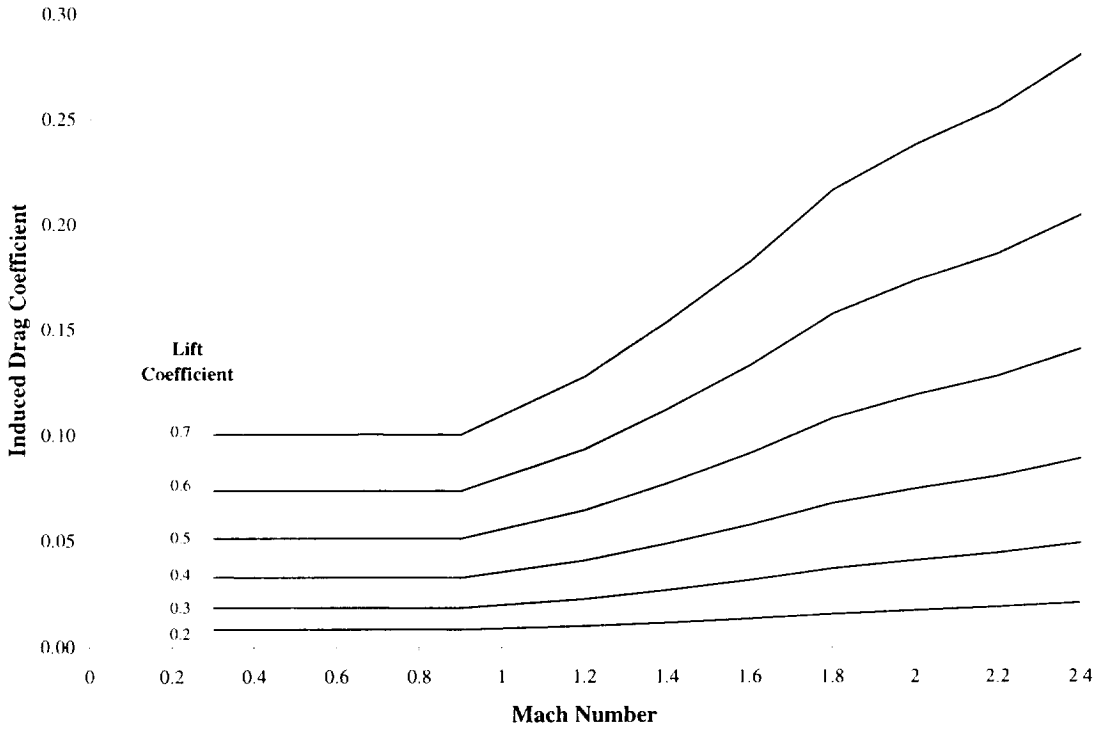

FIGURE 35: LIFT DEPENDENT DRAG (2)

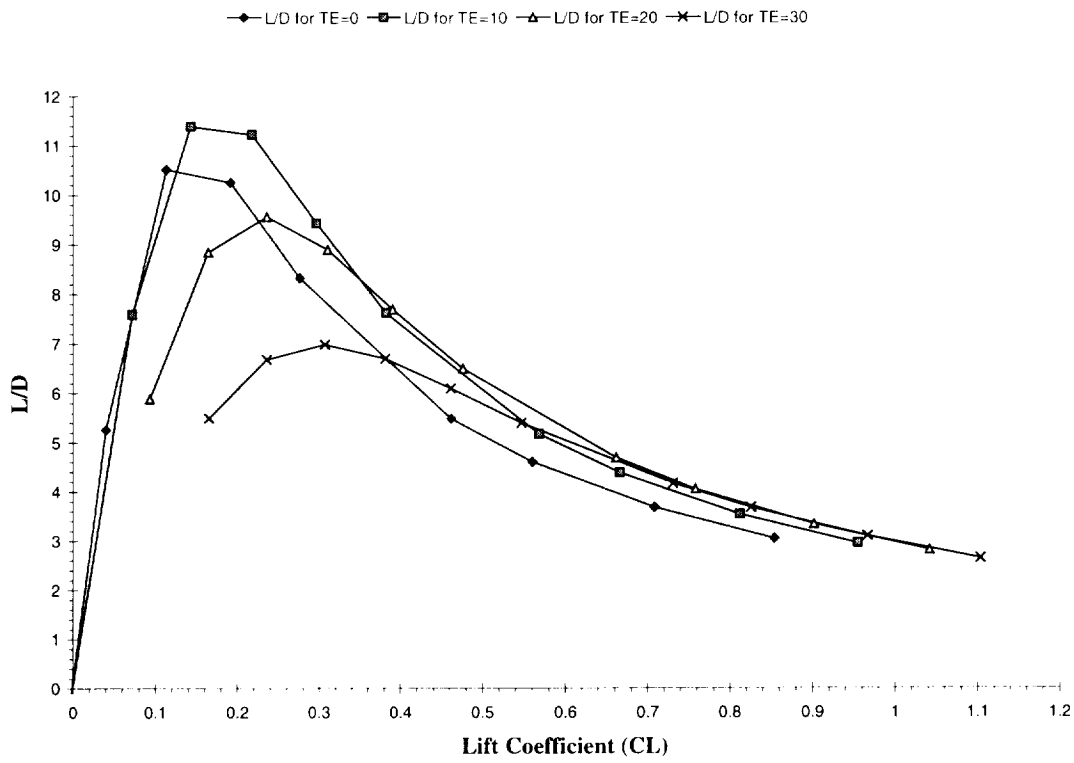

FIGURE 36: CONVENTIONAL HIGH-LIFT WITH LE δ=0°

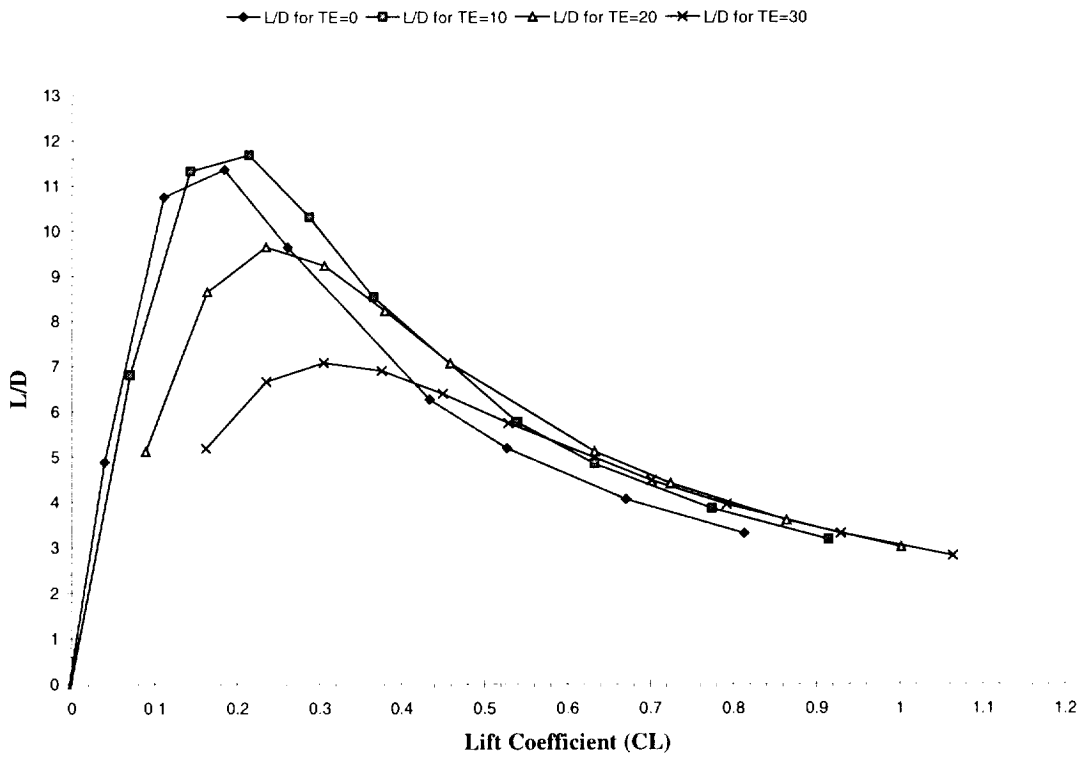

FIGURE 37: CONVENTIONAL HIGH-LIFT WITH LE δ=10°

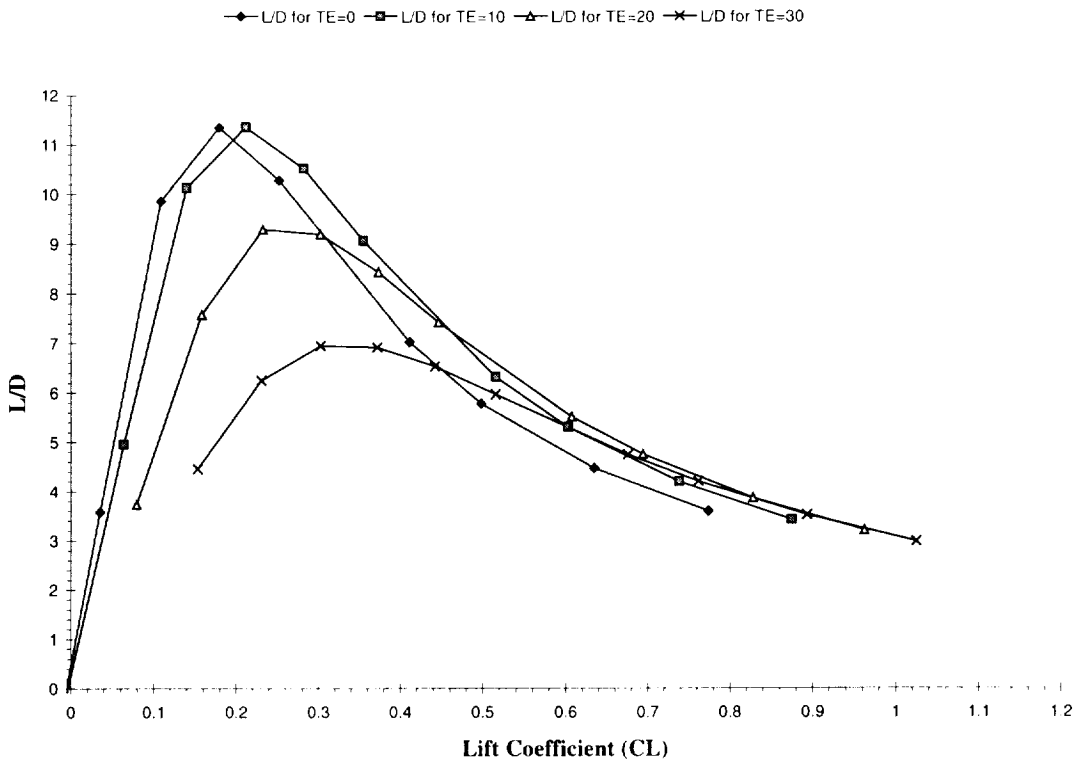

FIGURE 38: CONVENTIONAL HIGH-LIFT WITH LE δ=20°

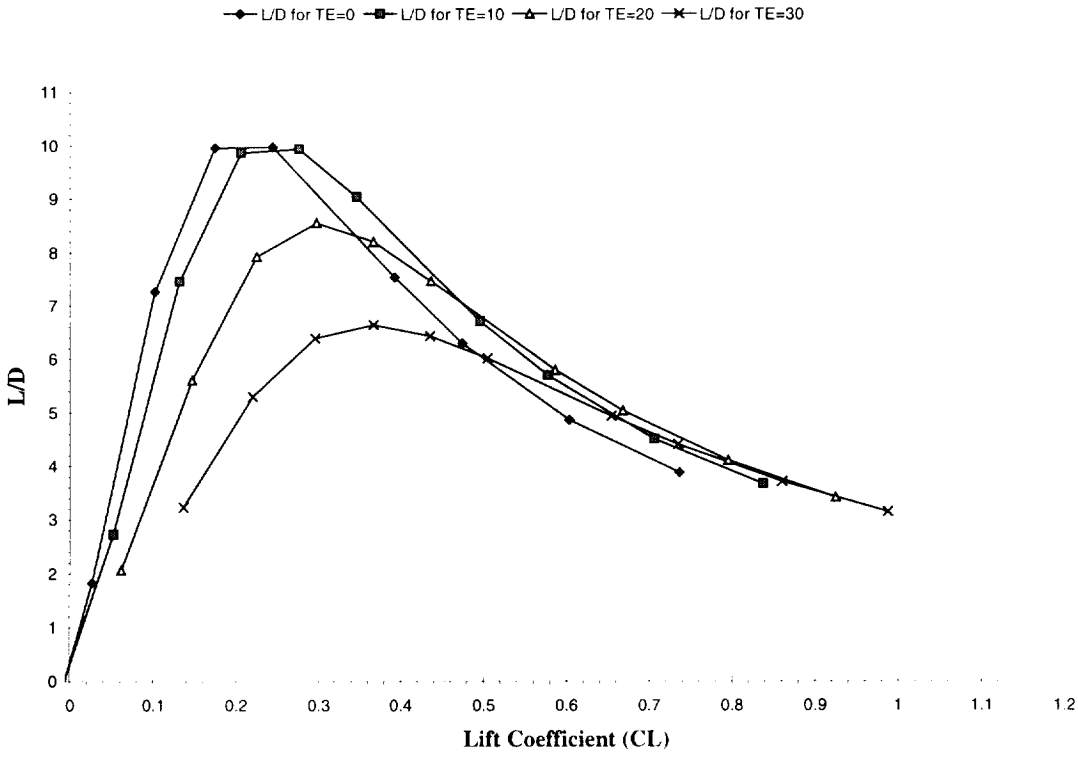

FIGURE 39: CONVENTIONAL HIGH-LIFT WITH LE δ=30°

3.3.2.2 Aircraft Sizing

Based on the cruise aerodynamics and the geometry described previously, a vehicle was sized in FLOPS for the mission defined in Figure 14 with the requirements defined in section 3.1. The sized vehicle specific characteristics needed for the TAKEOFF program are listed in Table 21. These characteristics, along with the low speed aerodynamics, and an engine deck (to be descried in subsequent sections) were the primary inputs to the TAKEOFF program.

TABLE 21: CONVENTIONAL CONFIGURATION CHARACTERISTICS

Characteristic	Value
Maximum takeoff gross weight	793807.4 lb
Landing weight	412512 lb
Taxi fuel	3031 lb
Maximum SLS thrust/engine	59535.5 lb
Wing height above ground	17 ft
Thrust incidence with ground	3°
$C_{L max}$ at takeoff	1.1
$C_{L max}$ at landing	1.2
Maximum AOA in rotation	9.8°
Maximum AOA in takeoff	20.0°
Maximum AOA at landing	9.8°

3.3.3 Propulsion

The addition of CC systems to aircraft must entail some consequences with regards to other vehicle systems, particularly with respect to the energy source used to power the CC system. This system analysis study would not be complete without due consideration of these penalties. Therefore the objective of this section is to determine what impact the extraction of engine bleed for CC use will have on engine performance, particularly takeoff thrust. In order for CC technologies to be successfully applied to a civil aircraft, they must first demonstrate the ability to deliver significant performance improvements without seriously degrading the performance of other vehicle systems, particularly the engines. Two potential sources for CC bleed flow are considered, and the penalties for two potential energy sources in terms of system Figures of Merit (FoM). This simple analysis is then used to select a baseline system configuration for further development.

There are two sources of high pressure air available on commercial aircraft: the auxiliary power unit and the engine bleed air. The decision as to which system to use as a power source rests upon five FoM:

1. Ability to provide a steady mass flow rate at a specified temperature and pressure
2. Safety
3. Cost
4. Reliability and Maintainability
5. Weight

The impact of the additional power requirements on fuel consumption is considered negligible. This fact was assumed since the CC system will only be used during takeoff and landing, during which, fuel consumption amounts to less than 1% of the total fuel burn. This section examines the merits of two concepts with respect to the aforementioned FoM and attempts to analytically quantify the advantages when possible. Based on this analysis, a decision as to which approach warrants further study is selected. This concept is then used in the TAKEOFF code.

3.3.3.1 Auxiliary Power Units Bleed

The Auxiliary Power Unit (APU) used on most commercial aircraft consists of a small gas turbine driving an electric generator and hydraulic pump. The APU is used to provide high pressure air, hydraulic system pressurization, and electrical power to the aircraft systems when the engines are not able to provide it. Typically, the APU is only used when the aircraft is on the ground and the engines are off, such as when the passengers are boarding, although it is also designed to operate as an emergency power source in-flight if necessary. The APU is a desirable source of bleed air for CC because it is under-utilized for all but the engine-start and shutdown portions of every flight and is essentially dead weight for the remainder of the mission. Additionally, if the CC system is fed by the APU, then the CC system will not influence the engine sizing, unless the engines are assigned the role of an emergency back up. Thus, using the APU as a power source is appealing because it decouples the propulsion system sizing from the CC system design. An additional advantage to using the APU air is to alleviate concerns with engine-out takeoff, though this does nothing to ameliorate concerns regarding APU failure scenarios and the associated impact on the low speed handling of the vehicle.

A survey of APU characteristics [65] indicates that existing APUs are designed primarily for electrical power generation and not mass flow. The mass flux characteristics at sea level, standard atmosphere for four types of APUs produced by Allied Signal are summarized in Table 22. APUs on the largest commercial transports provide a maximum of about 10 lbm/sec mass flow, while preliminary back-of-the-envelope estimates suggest much more is required. Although it is possible to install electrically driven compressors to supply the high power air, this would almost certainly be too expensive, heavy, and unreliable to be a viable option. The other choice is to size the APU to deliver the required mass flow rate. Additionally, it would be prudent to have two independent APUs for the sake of safety should one fail.

From a cost standpoint, it should be quite possible to develop an APU that could supply the required mass flow rate given sufficient research and development moneys. If it is assumed that the APU development cost is on the order of $50M, this would still be quite modest relative to the capital required to develop the engine and airframe. So, it is safe to say that one could develop an APU for an HSCT with the required characteristics.

If one assumes that APU weight scales linearly with the mass flow output and that the required mass flow is on the order of 100 lbm/s, it is clear based on data in Table 22 that the APU needed for CC application would be a very heavy system. To compound the problem, the additional weight would be located in the tail of the aircraft, thus exacerbating balance problems. Thus, in terms of weight (and probably cost), an APU driven CC system would be an expensive proposition.

TABLE 22: APU MASS FLUX CHARACTERISTICS

APU model	Aircraft Installation	Mass Flux (lbm/sec)	Unit Weight Dry (lb)
36-280[B]	737	2.8	350
700-4[B]	DC-10	8.8	648
331-350	A330	6.3	550
331-500	777	9.2	740.1

The final FoMs are reliability and maintainability. While it is true that APU systems have made great strides towards achieving high reliability, it is still not nearly as good as the 15,000 hr MTBF achieved by commercial aircraft engines. In addition, the increased importance of the APU would add an additional preventative maintenance burden on the vehicle maintenance crew.

To summarize, the APU approach has some advantages in terms of simplifying the coupling between the engine and CC system, but also entails significant weight and cost penalties to the total aircraft system. The APU is not deemed to have a significant safety advantage over a pure engine bleed and is probably at a disadvantage in terms of reliability.

3.3.3.2 Engine Bleed

The basic engine used for this study is a dual-spool co-rotating design with a 3x5 compression system and a 1x2 turbine system. The engine was sized for Mach 2.4 top-of-climb flight condition and the cycle is tailored for the 80-20 super/subsonic split mission. The cycle design point parameters are shown in Table 23, as are several of the relevant performance attributes.

TABLE 23: ENGINE PERFORMANCE DATA AT DESIGN POINT

Parameter	Value
Cycle	
FPR	3.7
OPR	20
T4max (°R)	3500
Thrust (SLS), lbs	65,000 lb
BPR	0.7
Size	
Mass Flow Rate (lbm/s), SLS	663
Diameter (in)	70.2
Bare Engine Weight (lb)	10,199
Bare Engine Length (in)	186
Overall Length (in)	365
Overall Weight (lb)	16,700
Performance	
Specific Thrust (lb/lb), Dry	98

It is possible to develop a simple back-of-the-envelope estimate for the impact of bleed on the engine thrust without the use of extensive analysis codes by using a bit of engineering intuition. First, consider the case of extracting bleed flow from the fan duct. Since thrust is dependent on the pressure, temperature, and mass flow at the nozzle inlet, a decrease in fan flow due to bleed will decrease the thrust via loss in mass flow rate, but will not

impact either temperature or pressure at the turbine. Therefore, the cycle specific thrust will be unaffected by fan bleed, and a good first order estimate of the loss in thrust due to bleed is to multiply the bleed flow by the cycle specific thrust at that flight condition and power setting to get the decrement in thrust. Since the dry specific thrust of the current engine is 98 lb/lb, bleeding 1 lbm/sec fan flow results in a reduction of 98 lb of net thrust. Note, this is an approximation whose accuracy becomes increasingly dubious as the fraction of flow bleed becomes large. The amount of bleed that can be extracted from the fan is limited only in as much as the thrust penalty is acceptable to the takeoff performance of the vehicle.

Next, consider the case of bleeding compressor discharge air to drive the CC system. At low power, considerable excess capacity exists in the engine. Hence, the engines should be capable of providing significant flow rates of compressor discharge air during flight idle (FI) operation. The extraction of compressor discharge air will likely require an increase in T4 to maintain minimum core speed, which will also increase the tailpipe temperature. Thus, the FI thrust might go up somewhat due to the compressor bleed. At high power settings (i.e., full throttle takeoff) compressor discharge bleed will result in a decrease of thrust, though not as much as that due to fan bleed. At first glance, this statement seems counter-intuitive, but is easily explained using a simple thought experiment. Consider an HSCT engine operating at full throttle SLS conditions with zero compressor bleed (i.e., cycle design point conditions). If one were to suddenly start bleeding the compressor discharge air with no change in fuel flow rate, the High Pressure (HP) and Low Pressure (LP) spools would slow down due to a loss in core power output. As the LP spool slows, FPR drops and the specific thrust decreases, thus resulting in a "snowballing" effect where tail pipe mass flow rate, temperature, and pressure drop. Thus, thrust and specific thrust are decreased, incurring a double penalty where takeoff net thrust is lost due to loss of specific thrust and of tailpipe mass flow rate.

Fortunately, the HSCT engine is a special case where thrust loss due to compressor bleed can be avoided if the system is properly designed. Since an HSCT engine is designed for operation at high T2 flight conditions, it will demand a high throttle ratio cycle. As a result, the core is oversized for SLS operation and the T4 required to maintain 100% corrected fan speed is less than the maximum allowable. This excess T4 capacity can be used to compensate for the CDP bleed by raising T4 to hold fan speed even at high CDP bleed rates. This will also result in increased tailpipe temperature, with an attendant increase in specific thrust. Thus, CDP bleed will be less penalizing for an HSCT engine than will fan discharge bleed, that is, until a maximum allowable T4 is reached. After this point, the penalty for CDP bleed will be very steep since specific thrust and tailpipe mass flow rate are both decreasing. This behavior is illustrated by the dashed line in Figure 40 which shows an increase in specific thrust until the T4 limit is reached. After this point, the curve breaks sharply downward and the compressor bleed penalties become increasingly intolerable.

The only way to get an aircraft estimate of thrust loss due to CDP bleed is to build an engine model and conduct cycle analysis studies. This is the focus of future and current work, but for the purposes of this study, it is conservative to assume that the compressor discharge thrust penalty behaves exactly as the fan bleed penalty until the mass flow becomes high enough that T4 max is reached.

The amount of bleed flow that can be extracted from the compressor is limited primarily by stability margin of the compression system, though it was noted earlier that the thrust penalty is excessive once the T4 limit is

reached. The core flow for this engine at FI (low flow) conditions is roughly 216 lbm/s. As a first guess, one can assume that roughly 25% of this flow can be bled from the compressor before serious operability problems arise (in terms of cooling mass flow, surge margin, and T4 limitations). This implies that approximately 50 lbm/sec could theoretically be bled from the compressor discharge at FI power settings, and this condition is taken as an upper limit for CC mass flow rate. Naturally, a much more detailed cycle analysis is warranted before development of this concept proceeds much further. For the purposes of this study, it is assume that 50 lbm/s times four engines (or 200 lbm/s) is the *practical* upper limit on allowable bleed flow for CC use.

To summarize, extracting bleed from an HSCT engine does not affect the cycle specific thrust, so the penalty due to 1 lbm/s fan bleed is 98 lb thrust for the current cycle as shown in Figure 40. Extraction of compressor discharge flow will not decrease specific thrust until the T4 limit is reached, after which, the penalties for CDP bleed become excessive. A detailed cycle analysis is required to determine the exact behavior, but one can conservatively estimate that it follows the same trend as fan bleed. The maximum allowable CC system mass flow rate is taken to be 200 lb/s.

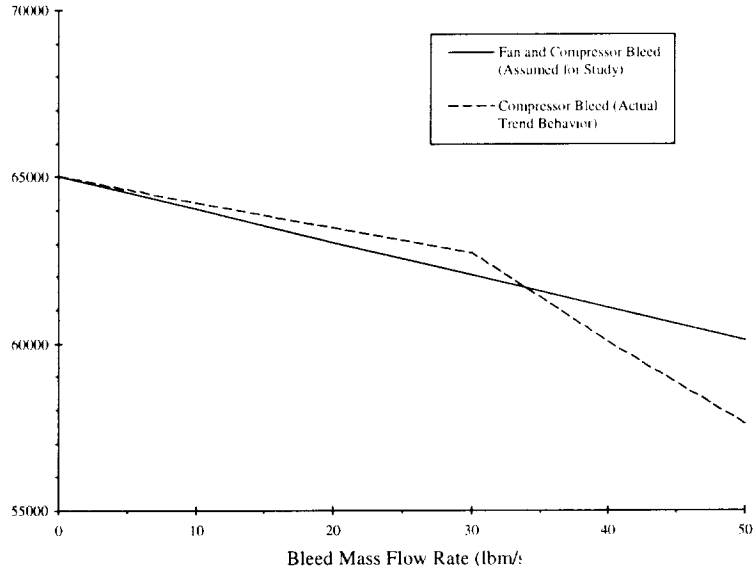

FIGURE 40: FIRST-ORDER THRUST PENALTY MODEL

The obvious sizing point for the CC system is One Engine Inoperative (OEI) flight condition. In the interest of safety, any CC system would have to be capable of maintaining adequate lift even if one engine fails. This has historically been an Achilles' heel of CC systems in that the loss of an engine not only causes a loss of thrust, but also results in a decreased wing lift capability at a safety-critical flight condition. Thus, any FAA-certifiable CC system must be capable of operating at full capacity or overcapacity using air supplied from only three engines.

An additional factor that must be considered is the CC air supply pressure and temperature from the engine. Obviously, high pressures and temperatures will allow smaller mass flow rates and smaller ducting for a given blowing effectiveness. However, the pressure and temperature delivered by the engine depends heavily on the

power setting as shown in Table 24. Unfortunately, the CC system cannot afford to have large swings in operating pressure, as these will result in a system that is drastically oversized for some flight conditions. The solution to this problem is to use fan bleed air to drive the CC system during takeoff and use CDP bleed during landing. The data of Table 24 reveals that the bleed pressures during these flight conditions are roughly equal, thus allowing a nicely tailored CC system. Additionally, compressor discharge air could conceivably be used at takeoff during an emergency, and hence increase the lift capability of the wing. Based on these considerations, one can conclude that HSCT engines have sufficient excess capacity to power a CC system.

TABLE 24: PRESSURE AND TEMPERATURE VARIATION WITH POWER SETTING

	Max Power	Flight Idle
CDP (psia)	266	47
CDT (°R)	1329	787
Fan P (psia)	51	17.1
Fan T (°R)	809	578

The next step is to evaluate the engine-fed CC system in terms of the remaining four figures of merit outlined previously. The reliability of an engine-fed CC air source could be made nearly as reliable as the engine itself since the CC system is now nothing more that a few ducts, valves, computer control systems, and a slot in the trailing edge of the wing. Since the engine will be more reliable than an APU, the engine-fed air source should have superior reliability, not to mention redundancy because there are four engines as opposed to two APUs.

The engine-fed CC system should also be easier to maintain than an APU-fed system for several reasons. First, the APU system would require two APUs with an attendant increase in the maintenance of these systems; whilst the engine-fed system simply utilizes the latent capacity of the engines during takeoff and landing. Secondly, there will be less ducting associated with the CC system because the duct going from the APU in the tail to the wing is eliminated. On the other hand, the number of valves and joints, which are required for four engines, is more than required for two APUs, thus adding complication to the total system. The addition of CC bleed air systems to the HSCT engines should not have a significant impact on the maintenance burden of the propulsive system. Overall, a well designed engine-fed CC system should be highly reliable and require little maintenance.

In terms of development cost, an engine-fed system would require close co-operation with the engine manufacturer to ensure that the high bleed flow rates required for CC do not significantly degrade engine performance or stability. However, the cost of the engineering, development, and test efforts for this concept would be small relative to the development of the propulsive system itself. Assuming that the decision to use CC was made during the early stages of engine development, the engine could be tailored to provide the required bleed flows with minimal penalty.

3.3.3.3 Propulsion Down-select

At this point, the relative merits of both an APU-fed and an engine-fed system have been examined in detail. The merits for both concepts are summarized in Table 25 for takeoff and landing using the five FoM previously mentioned. Based on this summary, it is evident that the engine-fed system is the better choice as the CC air supply source. The only major caveat is the question of OEI safety. As for the choice of whether to use fan or compressor bleed flow, both fan and compressor discharge bleed will be required to maintain a constant system pressure; the former for takeoff and later for landing. In addition, high pressure discharge air could conceivably be used for short periods during takeoff in an emergency situation. The high pressure air would greatly increase the blowing coefficient, thus enhancing lift and assisting takeoff.

TABLE 25: BLEED AIR SUPPLY CONCEPT COMPARISON SUMMARY

Figure of Merit	Engine-fed	APU-fed
1) Ability to provide a steady mass flow rate at specified temperature and pressure	Sufficient capacity at landing Excess capacity at takeoff	Requires new APU system development
2) Safety	OEI takeoff is a concern Quadruple redundant system More component parts needed (valves, joints, etc.)	Requires at least two APUs
3) Cost	Engineering, development, and test effort not significant relative to engine development cost	Must have new or derivative APU capable of required mass flow (>>10 lb/s)
4) Reliability and Maintainability	Commercial engine MTBF ~ 10-15 khrs No significant change in propulsion system maintenance burden	APU MTBF historically not good Increased maintenance burden for two APUs
5) Weight	No significant weight increase	Much heavier APU system(s)

As for OEI safety, the issue is not whether there is sufficient airflow capacity in case of an emergency because it was shown that the engine core is oversized for takeoff and has excess capacity if needed. Rather, the issue is whether this excess capacity can be utilized in time to be useful. The problem is that if an HSCT is taking off and one engine suddenly fails, this will result in a loss of thrust, but also a loss of lift. Although the other engines could make up the difference in mass flow rate, there will be a time lag in lift recovery, which could be detrimental to the safety of the vehicle. There are two possible solutions to this problem. First, a reservoir could be installed which could supply bleed air for the time lag that the operating engines would require to adjust. Secondly, a real-time monitoring control system could be installed which would immediately respond to a drop in CC pressure by opening engine bleed valves further and increasing fuel flow to the engines. This would minimize the time lag associated with engine adjustment and possibly eliminate the need for a reservoir. A control system of this nature could also schedule the fan and compressor discharge bleed to automatically maintain constant CC system pressure regardless of throttle position. Further, an automatic control system would reduce pilot workload in an emergency by automatically adjusting CC system settings, making the system transparent to the pilot.

To summarize, preliminary estimates indicate that the propulsion system is the best source of bleed air to drive the CC system. The propulsion system has sufficient excess capacity and can supply air at the right temperature and pressure to be useful. The only drawback to this approach is the coupling between the propulsive and high lift system that creates concerns for OEI safety at critical mission legs. However, with careful and creative systems design, these problems can be overcome without compromising safety or system effectiveness.

Up to this point, a simple "common sense" model has been used to estimate the thrust penalties due to engine bleed. However, this does have some shortcomings, particularly with respect to prediction of thrust loss due to compressor bleed. Therefore, current work is focused on estimation of these effects using an engine cycle model. The cycle analysis program being used for analyzing bleed effects in this study is ENGGEN [66], a simplified version of NASA's NEPP [67] cycle analysis program. ENGGEN was an obvious choice since it is already integrated into FLOPS that was used for mission analysis. In addition, ENGGEN is fast, easy-to-use, and reasonably accurate. The engine model being used for this study is a standard Mixed Flow Turbofan (MTBF) that is supplied with the ENGGEN program, albeit with modifications. A schematic representation of the model is given in Figure 41. The cycle modeled is matched to that appropriate for an HSCT mission. In addition, the model has been modified to accommodate fan bleed and compressor interstage bleed, as necessary. One additional item of note is that the model was set up to give a specified surge margin at the design point, but no additional modifications were made to the control logic to account for the migration of the operating line when bleed air is extracted. Instead, it is assumed that the engine could be set up to deliver the required mass flow rate and surge margin without an appreciable change in the cycle set-up, an assumption that warrants further consideration in future studies.

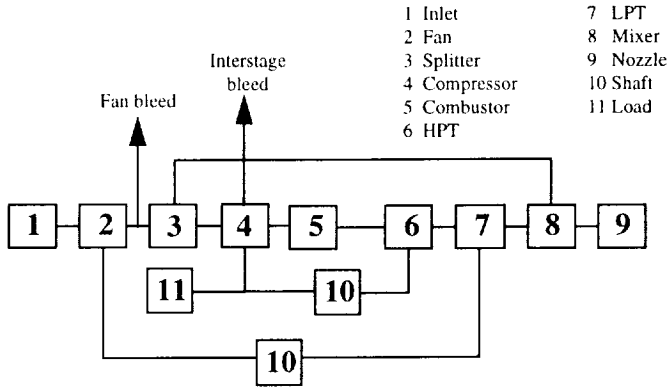

FIGURE 41: ENGGEN COMPONENT SCHEMATIC FOR HSCT MFTF MODEL

Future follow-ons to this study will include analytical estimates of thrust loss due to compressor bleed as well as thrust recovery due to increased tailpipe temperature. Additionally, it would be interesting to look at the impact of compressor bleed on compressor and fan operating line to ensure stability at these operating conditions. However, the current model is adequate to give a reasonably good estimate of thrust loss for this study, certainly enough to allow an accurate analysis of field performance.

3.3.4 CC System Configuration Development

The primary issues relevant to the design of a CC system configuration are the same as for all other aircraft systems, namely weight, cost, reliability, and volume. Any truly satisfactory CC system design must be a compromise between these conflicting requirements which achieves a good balance amongst all. Since a comprehensive systems design of a CC system is not the focus of this study, a first order analysis of two candidate system configurations will be investigated. Each system will be evaluated in terms of the factors mentioned above and a baseline configuration will be selected from these two candidates. The analysis will be quantitative in as much as is practical, but failing this, a qualitative discussion is offered.

The two systems considered are very similar in terms of ducting and layout, but differ as to their approach in achieving a safe and reliable system for commercial use. The first system uses a high pressure air reservoir to supply CC system air for the few critical seconds immediately after an engine failure but before the other engines compensate. The other approach is to use a computer control system that is coupled to the Full Authority Digital Engine Control (FADEC) systems to immediately compensate in the event of an engine failure. The basic system configuration for both concepts is shown in Figure 42. The central element of the system is an integrated duct/plenum installed near the trailing edge of the wing. This duct/plenum serves two purposes: it is a settling chamber for the engine bleed air and is a supply system for the CC slot. The advantages of having an integrated duct/plenum are that it is somewhat safer than a pure duct within plenum arrangement. The reason for this is the much higher flow capacity and lower duct Mach number of an integrated arrangement as opposed to an alternate. To illustrate this, consider the discrete arrangement whereby the duct is sized to accommodate the design mass flow rate. If a hole or puncture develops in the duct wall, the spanwise pressure distribution inside the duct will be considerably altered because the duct is sized for some design mass flow rate. A spanwise duct pressure gradient will change the spanwise distribution of CC air and therefore the spanwise lift distribution. The results will likely be a large rolling moment on the aircraft of which is a *very* undesirable proposition during takeoff and landing.

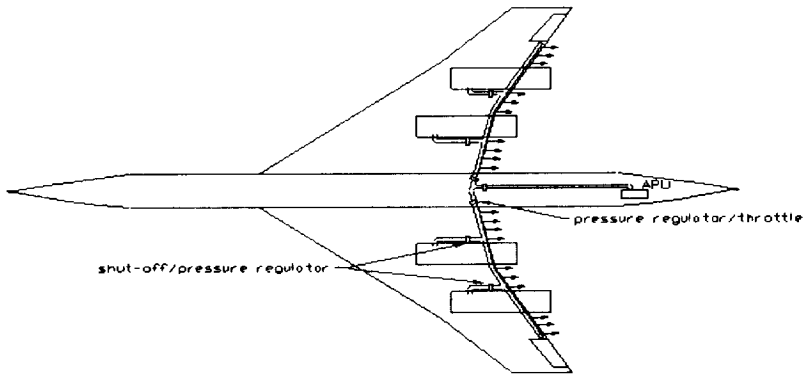

FIGURE 42: BASIC DUCT SYSTEM LAYOUT

An integrated system, on the other hand, is essentially an oversized duct with no central plenum. A hole in the CC duct system is not so likely to influence the spanwise pressure gradient within the duct because the duct is oversized. Instead, the result will be a lower overall slot mass flow rate (and an undesirable reduction in C_L) but no rolling moment. In addition, this configuration saves volume and weight because there is no need to route engine bleed air inboard to a central plenum and back out to the wing. Instead, engine bleed air is dumped directly into the duct. The disadvantage of such a configuration is that it takes up more volume in the wing and is probably going to be more difficult to manufacture. This implies that it is more expensive, especially since the air temperature is roughly 350 °F at 50 psia which implies that the duct will probably be constructed of titanium (to save weight), a notoriously expensive and difficult material with which to work. The duct/plenum is the only component that is identical for both systems. As far as the system configuration is concerned, all other aspects are different between the two approaches. These will therefore be considered separately.

A primary goal of the design of the circulation control system should be compatibility with the other aircraft systems. In particular, this requires that the ducting and associated fittings not interfere with wing structure or control surfaces. Ideally, the CC ducting would extend all the way from root to tip to maximize the effect of circulation control. Ailerons could be eliminated, and differential blowing used for roll control. However, CC technology is not presently considered mature enough to replace conventional ailerons in this flight-critical role. Also, since blowing effectiveness decreases as the square of velocity, the blown ailerons would be ineffective at high speed, thus necessitating some auxiliary means of roll control at altitude. For these reasons, conventional (no-blowing) ailerons were retained on the aircraft. To avoid a severe lift discontinuity and to increase lift, the ailerons should droop on takeoff and landing.

3.3.4.1 Emergency Reservoir Configuration

As mentioned earlier, the emergency reservoir configuration has a reservoir to supply air during those few critical seconds after engine failure. A schematic block diagram of this system is given in Figure 43. The primary elements of this system are the integrated duct/plenum, the reservoir tank, and the simple valve control system. The remainder is simply wiring, ducting, and valves required to make the system work.

First, consider the reservoir itself. In order to minimize the volume of the reservoir, the operating reservoir pressure will be much greater than that of the CC system. This necessitates the use of a throttling valve at the reservoir discharge to limit the pressure released into the CC system. Assume the reservoir is sized to supply five seconds of air to the CC system, plus a one second margin giving a total of six seconds. If one assumes the CC system operates at a minimum of 40 lbm/s and 50 psia (likely an underestimate of mass requirements), then the tank must be capable of supplying at least 240 lbm of air in six seconds.

At this point, two options are available. First, compressor discharge air could be used to fill the reservoir to 250 psia. If this is used and one assumes that at 50 psia the tank is empty, a few simple calculations reveal that the required tank volume is 283 ft^3. If the tank is assumed cylindrical with a diameter of 5 ft, then the length is 14.5 ft. Clearly, this is an unacceptably large tank. The second option is to use a tank pressure of around 600 psia and assume the tank can be filled using air supplied by an APU-driven compressor. A few calculations for this reveal that the required tank volume is 96.5 ft^3 which equates to a tank 5 ft in diameter and 5 ft long, roughly a third the

size of the previous case. These assumptions and results are summarized in Table 26 below. Clearly, the high pressure system is the better choice.

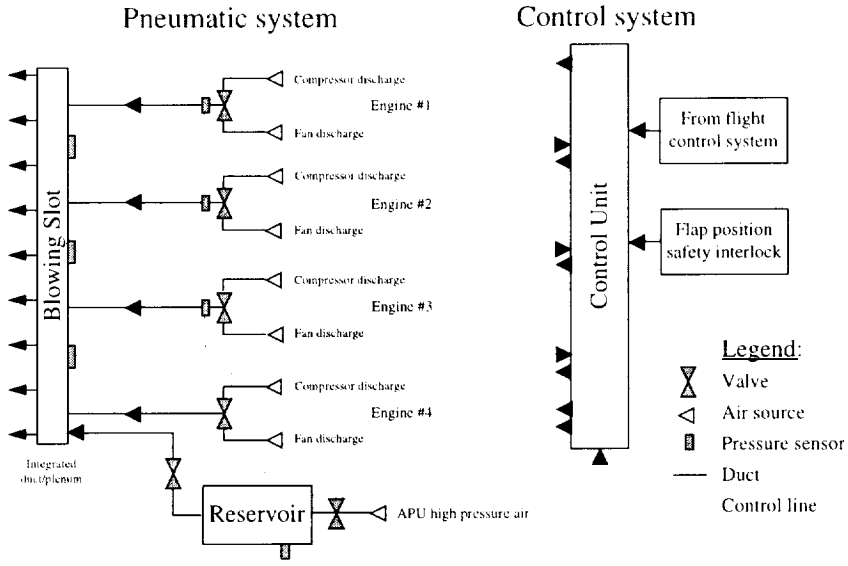

FIGURE 43: SCHEMATIC BLOCK DIAGRAM OF EMERGENCY RESERVOIR CC SYSTEM

TABLE 26: EMERGENCY RESERVOIR CONFIGURATION SUMMARY

	Initial Conditions	Final Conditions	Total Mass FlowVolume
Low Pressure	P = 250 psia	P = 50 psia	240 lb
	T = 78 °F	T = -125 °F	283 ft^3 (5x14.5 ft cylinder)
High Pressure	P = 600 psia	P = 50 psia	240 lb
	T = 78 °F	T = -199 °F	96.5 ft^3 (5x5 ft cylinder)

The control unit is a simple electronic control system with seven pressure sensor inputs and six control valve outputs. In addition, there is a control input from the flight control system and a safety interlock with flap position. The pressure sensors on the engine bleed air work with the bleed air valves to ensure constant supply air pressure. The pressure sensors in the duct are used to detect major pressure gradients within the plenum duct that would indicate system failure. This is a very simple control system, which could be implemented using simple TTL-level electronic devices. This configuration could be made quite reliable given that good systems design practices are followed. System cost is nearly impossible to accurately evaluate at this level, so it will not be attempted here. This system does take a considerable amount of volume, due to the plenum duct and the reservoir. The only remaining element is weight of which a crude estimate is given in Table 27.

TABLE 27: EMERGENCY RESERVOIR SYSTEM WEIGHT ESTIMATE

Component	Weight (lbs)
Integrated Duct/Plenum (at 3 lb/linear ft, Titanium)	240
Reservoir Tank	400
Valves (15lb each x5)	75
Control Computer	25
Misc. Ducting (Steel at 3 lb/ft)	300
Misc. Hardware	200
Total	*1240*

3.3.4.2 Computer-Control System Configuration

The second system under consideration employs a computer control system linked to the engine FADEC unit to immediately compensate in case of engine failure. A schematic block diagram is given in Figure 44. This system is similar to that shown in Figure 43, the major difference being the absence of a reservoir. Note that in this scheme, there is a direct link between the engine FADECs and the control unit. Because of the complexity of the control tasks now required, this system will be a microcontroller-based arrangement. The control system is now tasked with the job of detecting failures in both the engine and the CC system. Because there is no reservoir, the control system must react immediately upon detection of engine failure by telling the remaining FADECs to increase fuel flow rate to compensate for the increased bleed flow which is erstwhile increasing because the CC system began opening bleed valves immediately upon detection of engine failure.

The reliability of such a system should be on par with that of the previous approach since digital computer control systems can be constructed to be highly reliable. An additional benefit is the flexibility of having a software-based control system, instead of hardwired. The cost of the computer control system will increase dramatically, due to the need to debug and extensively test the control software. The system weight will drop markedly due to the elimination of the reservoir, as shown in Table 28. Note, these are only rough order-of-magnitude estimates and are not exact.

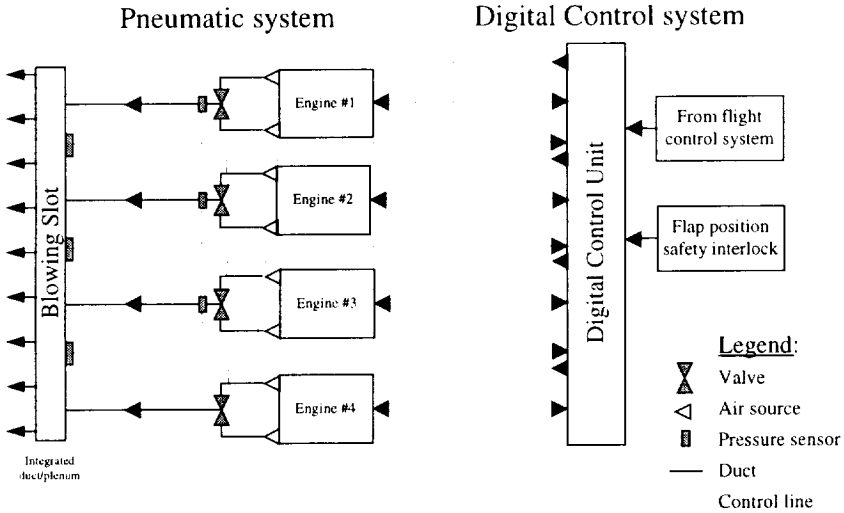

FIGURE 44: SCHEMATIC BLOCK DIAGRAM OF DIGITAL CONTROL CC SYSTEM

TABLE 28: COMPUTER CONTROL CC SYSTEM WEIGHT ESTIMATES

Component		Weight (lbs)
Integrated Duct/Plenum (at 3 lb/linear ft, Titanium)		240
Valves (25lb each x5)		125
Control Computer		25
Misc. Ducting (Steel at 3 lb/ft)		225
Misc. Hardware		220
	Total	*835*

3.3.4.3 CC System Configuration Comparison

The task of selecting a "best compromise" between the two systems discussed must ultimately depend on the final airplane configuration. For instance, if the aircraft is overweight, the systems designer would probably opt for the later configuration; while, if safety is a concern, the former might be better. The point is that the decision will depend upon the circumstances surrounding the prototype vehicle, and any selection made herein is applicable only to the aircraft studied in this report. Thus not withstanding, an attempt will be made to outline some of the merits and faults of each configuration.

These merits and faults are summarized in Table 29 for both configurations. In terms of safety and reliability, the reservoir probably has a slight advantage. Additionally, one would expect the cost of a reservoir to be less than the development cost of an electronic control system. In terms of volume and weight, the electronic control system has a decided advantage. Based on this rudimentary analysis, it appears that the electronic control system is the better option. The reason for this is that weight and volume are critical to a long-range supersonic transport. If this were a subsonic transport, weight and volume would take a back seat to cost and the reservoir system would be the better choice. Thus, the baseline CC system is an engine-fed system controlled by a digital electronic system.

TABLE 29: ADVANTAGES AND DISADVANTAGES OF PROPOSED SYSTEMS

Figure of Merit	Reservoir System	Electronic Control System
1) Safety and Reliability	Can be very high Provides air independent of engine status	High reliability in electronic components CC system operation closely linked to engines at all times Little margin for error
2) Cost	Simple reservoir tank probably not too expensive	Software creation/validation expensive High bandwidth valve controls are expensive
3) Volume	Tank occupies a great deal of volume Most of wing TE volume is consumed	Minimal TE volume consumed
4) Weight	Tank is heavy Requires extra ducting for tank 1240 lb system weight	835 lb system weight

3.3.5 DUCT SIZING

The next step in the CC system design process is to produce a first-cut design of the duct system size and layout and ensure that the system is compatible with the internal geometry of the wing. The design of the duct system is based on three premises:

1. CC system will be operating at maximum capacity whenever it is in use (i.e., system is on or off, no throttling)
2. Duct Mach numbers should not exceed 0.4 for acceptable system performance
3. The duct pressure and temperature are relatively steady and are the same for both takeoff and landing.

The first premise states that one would never want to operate the CC system at less than its rated capacity. This makes sense because the low speed characteristics of the HSCT wing are poor to begin with, and it is therefore desirable to get as much augmentation as possible. Additionally, greater augmentation allows a shallower approach angle, possibly eliminating the need for nose droop or synthetic vision. Thus, it makes sense to use the augmentation capability of the CC system to the fullest extent, and there is no reason for operating the CC system at less than its full capacity. The second premise is used to ensure that the flow never chokes in the duct during off-design operation (hot-day, high altitude, OEI, etc.). In addition, limiting the duct Mach number helps to reduce pressure losses in the duct. Furthermore, small duct Mach numbers help to maximize blowing effectiveness by delivering maximum available stagnation pressure to the slot nozzle instead of using it for mass transport in the duct. The source of the third premise is discussed in the propulsion section wherein the authors point out that a carefully designed CC system can be operated at nearly constant system pressure and temperature, regardless of engine power setting. This reduces CC system weight and volume by avoiding the need to oversize the system to meet requirements at a single critical condition.

Design of an acceptable CC duct system requires the establishment of several ground rules in order to ensure concept viability and ensure that the reader understands the design philosophy used herein. First, the CC duct system is designed for operation at two flight conditions: takeoff and landing. Furthermore, the system is designed for nominal performance at SLS day conditions. The impact of hot-day performance is to increase the duct Mach number (and losses), but the 0.4 duct Mach number design requirement ensures that the hot-day performance is not degraded beyond acceptable levels (at least not due to internal duct losses). The flight conditions used for duct sizing are detailed in Table 30 below.

TABLE 30: FLIGHT CONDITIONS USED FOR CC DUCT SIZING

Flight Condition	Altitude (ft)	Velocity (fps)	Velocity (kts)	Dynamic Pressure (psf)
Takeoff	0	336.96	199.64	135.00
Landing	0	267.37	158.42	85.00

A second ground rule used for analysis is that there is not a significant spanwise pressure gradient inside the trailing edge plenum. This is a valid assumption for several reasons: 1) the engines dump directly into the TE plenum, therefore no central reservoir exists to give rise to pressure oscillations, 2) spacing of engines along the span ensures that spanwise distance traveled by any portion of the flow will not be more than about 30% of the semi-span, and 3) 0.4 nominal duct Mach number gives rise to $\Delta P/P$ of 10% *at most*. This assumption greatly simplifies the calculation of mass flux as a function of semi-span.

The next step in the sizing process is to get a rough estimate of the duct diameter required to power the CC system. This task can be greatly simplified by observing that the duct system can be thought of conceptually as four independent CC subsystems, each providing CC for roughly 25% of the wing span and each supplied by one engine. If the ducts for each of these imaginary subsystems are independently sized, it is intuitively obvious that the largest duct size required in these systems is carrying the mass flow from the engine to the plenum. After reaching the trailing edge plenum, the flow splits into two portions and is distributed along the trailing edge nozzle. Thus, the engine-plenum duct can be taken as an upper limit on duct size, with all ducts downstream being smaller.

It has already been surmised in the propulsion section that the maximum mass flow rate one can reasonably expect from the baseline HSCT engine is on the order of 50 lbm/s. The flow function corresponding to isentropic flow of a perfect gas ($\gamma = 1.4$) at Mach 0.4 is 0.37338. If the FI condition is taken to be the duct sizing condition, then it is easily shown that the duct cross-sectional area must be 80 in^2 which equates to a 10 in diameter duct (assuming a circular cross-section). This is probably too thick to fit in the wing trailing edge, so a semi-elliptical cross-section will be required. This is the upper bound on duct size in the CC system, as the flow requirements at all other locations is less than or equal to this value.

The next step in the duct sizing process is to size the slot area of the CC trailing edge nozzle. This is done using the slot sizing code described in the methodology section and examining the results for two cases: one for takeoff, and one for landing. Note that the nozzle discharge coefficient used for these calculations is assumed to be 1.0, which should be reasonably close if the CC slot designer does a good job. Additionally, pressure losses for duct friction are accounted for, but no penalty is taken for turning losses or losses due to valves in the system.

The results for the duct sizing analysis are given in Table 31, shown below. The analysis corresponds to fan bleed at takeoff and compressor bleed at landing. Note that the results for the two cases are very similar and it is reasonable to use the average of the two as a baseline geometry for this initial study. For the 200 lbm/s bleed flow rate from the engines, a total slot throat area is roughly 275 in^2 while the total exit area is roughly 310 in^2. The converged slot height at the span station closest to the wing root is roughly 1/2 inch high and slowly tapers down to 1/10 inch slot height at the outboard-most station. Also, note that the C_μ at the flight conditions of interest is very low, resulting in degraded CC lift augmentation effectiveness.

TABLE 31: CC DUCT SIZING AND SLOT SIZING RESULTS

Parameter	Units	Take-off	Landing
Engine Bleed Point	-	Fan Discharge (Max Power)	Compressor Discharge (Flight Idle)
Total Pressure	psi	51	47
Total Temperature	°R	809	787
Converged Throat h/c	-	0.0002845	0.0002960
Converged Exit h/c	-	0.0003272	0.0003309
CC Slot Throat Area	in^2	268.9	279.7
CC Slot Exit Area	in^2	309.2	312.7
CC Duct Cross Sect. Area	in^2	82.1	88.2
Inboard Slot Exit Height	in	0.51	0.52
Outboard Slot Exit Height	in	0.08	0.08
Avail. CC Flow / Engine	lbm/sec	49.0	49.0
CC Jet Velocity	fps	1692.6	1621.6
C_μ available	-	0.0008046	0.012241

The depth of this duct sizing analysis is sufficient for the first-pass consideration studied herein. All critical dimensions have been established, and the exact dimensions of the remainder of the ducting system is somewhat flexible. Thus, these will depend on internal layout considerations (such as actuator and hinge placement, structural arrangement, etc.). However, some aspects of the analysis deserve further study at a suitable time. First, it is intuitively obvious that CC effectiveness decreases as the chord length increases. This analysis has not accounted for these effects, and instead calculates a C_μ for the entire wing based on wing area. In reality, the blowing effectiveness should be penalized for the inboard sections of the wing due to the large chord length. In addition, nonlinear effects such as upper surface vortices will play an increasingly dominant role as angle of attack increases. It is unclear if the CC will remain effective in the presence of a vortex and its attendant spanwise flow component.

Second, this study has assumed a constant h/c is maintained along the span of the wing. However, CC system effectiveness could be increased if h/c is varied as a function of span. If the blowing can be biased towards the outboard panels where the short chord lengths improve CC effectiveness, the C_L of the wing could probably be increased (though the bending stress will also increase). Additionally, it might be possible to achieve favorable interaction between the upper surface vortex and the CC blowing through prudent aerodynamic design.

3.4 Low Speed Performance Assessment

As stated previously, the performance assessment of an HSCT utilizing the CC technology was performed in three steps. First, a reference point was established for the low-speed metrics, listed in Table 5, of a configuration that utilized only conventional high-lift systems. The reference point was based on the configuration described in Table 21. A parametric investigation of the LE and TE slats and flaps of the conventional configuration was then performed to determine the optimal settings that would minimized the TOFL, LDGFL, and Vapp, the three primary metrics of interest. The corresponding low speed aerodynamics associated with each of the configurations was performed in Section 3.3.2.1 and inserted to the appropriate TAKEOFF input file. Second, the incremental changes in force coefficients (lift and drag) were applied to the 16 configurations. The results obtained from the application of CC were then compared to the conventional configurations and the improvements and degradations quantified. Both step one and two assume the vehicle was at the maximum takeoff gross weight. The final step in the performance analysis included a deviation from this point. A parametric investigation was performed for different operating conditions, that is, not fully loaded, and procedures (in the form of allowable AOA) with a comparison of the different configurations with and without CC. Furthermore, since the maximum lift coefficient for takeoff and landing could not be accurately assessed, these values were allowed to vary to determine the impact. At this point, the impact of CC was determined.

The objective of this section is to get a "first cut" estimate of the benefits from CC technology on the takeoff and landing field performance of an HSCT. As was shown in previous sections, the TOFL performance constraint was the "show-stopper" for the HSCT design space considered. In fact, feasibility of the design space can primarily be obtained through the infusion of low speed technologies, possibly CC. Hence, this section will attempt to quantitatively assess the impact of CC on both the takeoff and landing performance of an HSCT-type vehicle. Obviously, this task requires that all of the individual pieces of the problem previously discussed (aerodynamics, propulsion, CC system weight, etc.) be integrated into a coherent picture that shows the benefits and penalties of CC. This is accomplished using the modified TAKEOFF program to calculate time histories of CC-augmented aircraft. However, before proceeding, it is necessary to first establish a few ground rules for the analysis.

First, the weight penalty of the CC system is considered negligible relative to the takeoff gross weight of the vehicle. The weight of the CC system was estimated to be on the order of 800 lbs in the system configuration section. Since the baseline aircraft weighs on the order of 800,000 lbs, the CC system weight is roughly 0.1% of total vehicle weight and will have only a minor impact on the vehicle's field performance. Hence, the configuration utilized to assess the conventional performance was also used as the CC augmented configuration. Second, all of the performance calculations assumed In-Ground-Effect (IGE) and no excess drag due to OEI. The CC mass flow used in all cases was 200 lbm/s (50 lbm/s/engine). The CC is assumed to be on throughout the analysis. The reason for this is that the FAA does not allow flap deflection changes for conventional aircraft during takeoff or landing. Hence, it is unlikely that an exception for the certification of an HSCT will be made. Also, from a safety standpoint, it is fundamentally unsound design philosophy to increase the pilot workload during takeoff or landing to make CC system changes, such as flow regulation.

3.4.1 Establish Reference Point

The conventional configuration described previously was analyzed in the TAKEOFF program for various LE and TE deflections. The resulting performance metrics obtained for the different configurations are summarized in Table 32. As can be seen, a LE and TE deflection of 10° and 30°, respectively, minimized the TOFL. This outcome is consistent with current industry results. In fact, only three flap combinations could achieve the target value of 11,000 ft. All three settings required a 30° TE flap deflection to achieve enough lift. It should be noted that for the takeoff condition, performance is driven by high lift-to-drag ratios and high lift coefficients. Although other flap settings had higher L/D ratios, there was not enough lift within a reasonable field length. As for the LdgFL and Vapp (both must have the same flap settings), the setting that minimized these parameters were a LE of 20° and TE of 20° resulting in 11,890 ft and 165.97 kts. None of the cases considered could meet the imposed landing field length requirement of 11,000 ft. It should be noted that the stall speed in the takeoff condition did not change. The stall speed remained at a constant value of 158.05 kts. This result appears counter-intuitive. Yet, the internal constraints of TAKEOFF that define speeds for the iteration algorithm were driven by the limiting AOA during takeoff and landing. During the takeoff condition, a maximum AOA of 20° was assumed due passenger comfort and FAR regulations. This limiting value constrains the *allowable* AOA during the takeoff analysis, and hence, limits the stall speed as constrained by a C_{Lmax} value of 1.1. Since the corresponding lift curve slope exceeded this value, the stall speed was driven by C_{Lmax}. The TAKEOFF input files for each of the configurations were the basis upon which the incremental changes in force coefficients were added.

TABLE 32: CONVENTIONAL HIGH-LIFT CONFIGURATION METRIC VALUES

LE (deg)	TE (deg)	Case #	TOFL (ft)	LdgFl (ft)	Vapp (kts)	OEI Vrot (kts)	OEI Vlof (kts)	AEO Vrot (kts)	AEO Vlof (kts)	Vstall Landing (kts)	Vstall TO (kts)
0	0	1	16362	16735	202.58	251.35	263.92	251.35	269.64	153.57	158.05
0	10	2	12684	12637	174.01	219.14	231.87	219.14	237.21	134.92	158.05
0	20	3	11084	11258	159.54	203.16	214.83	203.16	219.68	123.11	158.05
0	30	4	10793	13617	153.84	200.00	209.47	200.00	213.69	116.05	158.05
10	0	5	17372	17228	208.44	259.55	272.07	259.55	277.78	158.32	158.05
10	10	6	13308	15762	182.02	224.88	237.64	224.88	242.95	138.29	158.05
10	20	7	11550	14678	165.83	207.92	219.59	207.92	224.38	125.74	158.05
10	30	8	**10565**	13744	155.50	196.02	206.54	196.02	211.08	118.29	158.05
20	0	9	18300	17512	213.07	265.96	278.22	265.96	283.89	162.02	158.05
20	10	10	13899	16025	185.33	229.62	242.23	229.62	247.49	140.96	158.05
20	20	11	11997	**11890**	**165.97**	212.00	223.51	212.00	228.2	127.88	158.05
20	30	12	10936	13827	157.12	199.62	209.99	199.62	214.43	120.16	158.05
30	0	13	18795	17568	217.30	265.96	278.08	265.96	283.88	165.26	158.05
30	10	14	14595	16090	188.33	234.05	246.23	234.05	251.43	143.28	158.05
30	20	15	12505	11936	165.51	215.80	226.92	215.80	231.55	129.76	158.05
30	30	16	11348	14178	160.92	202.95	212.96	202.95	217.33	121.79	158.05

3.4.2 CC Augmented Assessment

The 16 cases considered in the reference point evaluations were the foundation upon which the incremental changes in lift and drag were added. As stated previously, the TAKEOFF program was modified to take changes in lift and drag as function of speed and AOA. The incremental values in lift and drag utilized for each of the cases in Table 32 also incorporated the corresponding ΔC_L and ΔC_D listed in Table 12 through Table 19. For example, case #3 has no LE deflection and a TE deflection of 20°. The input file that was used to create this configuration was used with the additional information of the ΔC_L and ΔC_D listed in Table 14 and Table 18. That is, for each TE flap deflection, the appropriate matrix of the ΔC_L and ΔC_D were added to the input file. All other values were identical. The 16 configurations were reanalyzed and the low speed metrics that resulted are summarized in Table 33, while the relative change from the conventional high-lift systems is listed in Table 34. These results are pessimistic since the addition of CC will alter the available maximum lift coefficient. This issue will be addressed in subsequent sections.

As can be seen, the addition of CC did improve most of the configuration metrics with the exception of the 20° TE deflections impact of LdgFL and Vapp for case 11 and 15 of which degraded slightly. The most improvements in TOFL came from the 0° TE flap deflections with reductions on the order of 20%, while the largest improvements in the landing metrics varies depending upon the LE deflections and varied from 10% to 20% reductions. With the addition of CC, five cases considered could meet the TOFL requirement of 11,000 ft, while none of the cases could meet the LdgFL requirement. Although, the landing metrics were reduced, the constraints were not met. This result was again due to the convergence criteria on speeds within the TAKEOFF program. A question was then posed as to whether or not the speed convergence criteria within the program were appropriate for an HSCT-type configuration. A literature search was performed to investigate the possibility of redefining the method by which typical airfield speeds are defined. Specifically in Reference [68], a suggestion was made as to the low speed characteristics of slender wing aircraft. In particular, the flow characteristics of low aspect ratio wings differ significantly from the conventional aircraft for which the FAA regulations are written. A suggestion was made to replace the conventional stall speed with two new reference speeds: V_{min}, the minimum demonstrated flight speed in steady rectilinear flight, and V_{zrc}, the zero-rate-of-climb speed with one engine failed. From these two speeds, the remaining speeds could be defined for example, the approach speed and the second segment climb speed. This approach seemed rational, yet insufficient evidence existed to modify the convergence criteria or analysis algorithm. This decision was made since the only other existing slender wing aircraft to be certified for commercial use was the Concorde. This aircraft had to meet the existing guidelines for certification without redefinition or modification to existing FAR guidelines. Hence, to modify the program to allow for convergence seemed inappropriate since adjustments were not made for the Concorde.

The cases that contained a TE deflection of 30° could not converge on the speed requirements stipulated in Figure 11 and Figure 12. Specifically, the second segment climb speed was to be 1.2 Vstall at takeoff and the approach speed at landing was to be 1.3 Vstall as required by FAA regulations. The 30° deflection diverged on these criteria due excessive drag at takeoff and excessive lift at landing. The factors of safety placed upon the stall

speed were modified until convergence could be achieved. The values that resulted were 1.24 for landing and 1.1 for takeoff. Yet, as stated previously, the justification for these modifications could not be proved. Hence, for the remainder of this investigation, the 30° TE flap deflection was not considered.

TABLE 33: CC AUGMENTED METRIC VALUES

LE (deg)	TE (deg)	Case #	TOFL (ft)	LdgFl (ft)	Vapp (kts)	OEI Vrot (kts)	OEI Vlof (kts)	AEO Vrot (kts)	AEO Vlof (kts)	Vstall Landing (kts)	Vstall TO (kts)
0	0	1	12993	14672	199.64	219.86	231.4	219.86	236.9	153.57	158.05
0	10	2	10986	12566	175.40	199.45	209.01	199.45	213.51	134.92	158.05
0	20	3	11051	11158	160.04	199.63	204.76	199.63	207.38	123.11	158.05
0	30	4	diverged	diverged	diverged	diverged	diverged	diverged	diverged	diverged	diverged
10	0	5	13719	15390	205.81	226.20	237.63	226.20	243.1	158.32	158.05
10	10	6	10897	12881	179.77	197.14	207.36	197.14	212.13	138.29	158.05
10	20	7	10524	11660	163.46	192.54	198.73	192.54	201.84	125.74	158.05
10	30	8	diverged	diverged	diverged	diverged	diverged	diverged	diverged	diverged	diverged
20	0	9	14391	15758	210.63	231.21	242.38	231.21	247.79	162.02	158.05
20	10	10	11303	13457	183.24	200.80	210.8	200.80	215.48	140.96	158.05
20	20	11	10360	11996	166.25	189.44	196.15	189.44	199.51	127.88	158.05
20	30	12	diverged	diverged	diverged	diverged	diverged	diverged	diverged	diverged	diverged
30	0	13	15187	15761	214.84	235.77	246.4	235.77	251.78	165.26	158.05
30	10	14	11764	13505	186.26	204.17	213.77	204.17	218.38	143.28	158.05
30	20	15	10321	12091	168.69	187.24	194.25	187.24	197.86	129.76	158.05
30	30	16	diverged	diverged	diverged	diverged	diverged	diverged	diverged	diverged	diverged

TABLE 34: CC AUGMENTED COMPARISON TO CONVENTIONAL VALUES*

LE (deg)	TE (deg)	Case #	TOFL (ft)	LdgFl (ft)	Vapp (kts)	OEI Vrot (kts)	OEI Vlof (kts)	AEO Vrot (kts)	AEO Vlof (kts)	Vstall Landing (kts)	Vstall TO (kts)
0	0	1	-20.6	-12.3	-1.5	-12.5	-12.3	-12.5	-12.1	0.0	0.0
0	10	2	-13.4	-0.6	0.8	-9.0	-9.9	-9.0	-10.0	0.0	0.0
0	20	3	-0.3	-0.9	0.3	-1.7	-4.7	-1.7	-5.6	0.0	0.0
0	30	4	diverged	diverged	diverged	diverged	diverged	diverged	diverged	diverged	diverged
10	0	5	-21.0	-10.7	-1.3	-12.8	-12.7	-12.8	-12.5	0.0	0.0
10	10	6	-18.1	-18.3	-1.2	-12.3	-12.7	-12.3	-12.7	0.0	0.0
10	20	7	-8.9	-20.6	-1.4	-7.4	-9.5	-7.4	-10.0	0.0	0.0
10	30	8	diverged	diverged	diverged	diverged	diverged	diverged	diverged	diverged	diverged
20	0	9	-21.4	-10.0	-1.1	-13.1	-12.9	-13.1	-12.7	0.0	0.0
20	10	10	-18.7	-16.0	-1.1	-12.6	-13.0	-12.6	-12.9	0.0	0.0
20	20	11	-13.6	0.9	0.2	-10.6	-12.2	-10.6	-12.6	0.0	0.0
20	30	12	diverged	diverged	diverged	diverged	diverged	diverged	diverged	diverged	diverged
30	0	13	-19.2	-10.3	-1.1	-11.4	-11.4	-11.4	-11.3	0.0	0.0
30	10	14	-19.4	-16.1	-1.1	-12.8	-13.2	-12.8	-13.1	0.0	0.0
30	20	15	-17.5	1.3	1.9	-13.2	-14.4	-13.2	-14.5	0.0	0.0
30	30	16	diverged	diverged	diverged	diverged	diverged	diverged	diverged	diverged	diverged

* Values represent a relative percent change from the conventional configurations

3.4.3 Parametric Investigation

It was expected that the benefit of adding CC to an HSCT would be greater than the results shown in Table 34. At this point, the dependency of the low speed metrics on C_{Lmax} and the convergence on various speeds was evident not to mention the fact that the accurate value of C_{Lmax} was uncertain. As stated previously, a C_{Lmax} value was assumed for takeoff and landing and the corresponding stall speed calculated internal to the TAKEOFF program. Yet, one primary aspect of the CC technology is the increase in C_{Lmax} attainable. The magnitude of this increase is dependent upon the vehicle AOA and the blowing coefficient, C_μ. For a fixed jet mass flow rate and velocity, the blowing coefficient is then purely a function of the freestream velocity. This dependency creates an iterative process for the determination of C_{Lmax}. To capture this variation and uncertainty in the definition of C_{Lmax}, a range of values can be assumed and the impact of that variation quantified. Hence, the motivation for the parametric variation in C_{Lmax} and the operating AOA for the different configurations.

For each case considered in the previous section, a parametric investigation was performed through a Design of Experiments with the parameters listed in Table 35. The conventional baseline values that were originally used were a T/W of 0.3, W/S of 93.4 lb/ft^2, C_{Lmax} at TO of 1.1, C_{Lmax} at landing of 1.2, and a maximum AOA at takeoff and landing of 9.8°. These values are captured in the ranges selected for the parameters. The variation in wing loading and thrust-to-weight allows for deviations from the design point. For example, the baseline values assume a fully loaded configuration, i.e., 300 passengers, baggage, and maximum fuel. In most operating settings, this condition will not occur. Passenger load factors will be less than 100%; specific city-pair routes will not require

that the maximum fuel capacity be utilized; certain airports require steeper ascensions due to surrounding terrain; etc. The variation in W/S and T/W simulate the real world operating conditions that and HSCT could encounter. Recall the CC augmented cases involving a 30° TE flap deflection were not included in this investigation due to prior rationale.

TABLE 35: PARAMETRIC VARIABLE DEFINITIONS

Parameter	Minimum	Maximum
Thrust-to-weight ratio (T/W)	0.28	0.32
Wing Loading (W/S)	90 lb/ft^2	100 lb/ft^2
CLmax at takeoff (CLmax_TO)	1.1	1.6
CLmax at landing (CLmax_ldg)	1.2	1.6
Maximum AOA at takeoff (Max AOA TO)	9.8°	12°
Maximum AOA at landing (Max AOA Ldg)	9.8°	12°

The parametric investigation results for each case are shown in Appendix C in the form of prediction profiles but are summarized below. The best flap settings for discussion were determined by the minimum lower bound as read from the prediction profiles. Appendix C contains the 28 prediction profiles (16 cases for the conventional and 12 cases for the CC augmented). The upper and lower bounds of the primary metrics are listed on the abscissa and the influence of each parameter on the metric is evident by the corresponding slope. The difficulties encountered, with the internal constraints of speed, is evident by the extreme quadratic nature of certain parameters in the metrics. This trend is seen with the conventional configuration at TE deflections of more than 10° with the LdgFL as affected by the Max AOA Ldg. Also, the W/S had a similar influence with increase LE and TE deflections. Additionally, the influence of a given parameter on a metric changes the direction with certain flap settings when an internal algorithm constraint is met.

For the best case for the conventional and CC augmented configurations for each metric, the feasible design space which exists can be seen in a typical T/W versus W/S contour plot. For the conventional high-lift vehicle, the best range of TOFL values resulted in a 20° and 30° LE and TE deflections, respectively, which corresponds to case #12. And for the LdgFL and Vapp, an optimal configuration of a LE of 0° and a TE of 30° (case #4) was the best configuration. The feasible operating space is bounded by the active constraints of TOFL and LdgFL, as seen in Figure 45. With all other parameters held constant at the normalized baseline values shown, the operating range, which an HSCT could operate, is shown as the white space. Of the operating space considered, approximately 25% is feasible. This is a small space in which to operate in real world settings. Furthermore, in the design of any vehicle, a high W/S and low T/W are desired. Yet, the conventional configuration can achieve a wing loading of no more than 95 lb/ft^2.

For the CC augmented configuration, the best flap settings that reduced the TOFL was a LE of 20° and a TE of 20° (case #11). If one assumes that the conventional C_{Lmax} at landing can be improved by 30% from 1.2 to 1.56, the LdgFL and Vapp can be minimized with a LE of 10° and TE of 20° (case #7). The operating design space for these flap settings is shown in Figure 46. Here, the active constraints are the Vapp and TOFL with the LdgFL impact significantly reduced. This result shows the higher sensitivity of LdgFL to wing loading than the best

conventional configuration. Yet, the feasible operating space is on the order of 25%, just as in the conventional configuration.

Based on this result, a Monte Carlo simulation was performed on the flap setting configurations (conventional and CC augmented) with uniform distributions for each parameter listed in Table 35. The three metrics for the conventional and CC augmented cases were compared. The optimal flap settings, which shifted the CDF to a minimum, were identified and shown in Figure 47 through Figure 49. These CDFs represent the design space as defined by the parameters in Table 35 instead of the point comparisons shown above. For the conventional configuration, the design space spanned by case #3 instead of case #12 minimized the TOFL and case #4 remained as the optimal for LdgFL and Vapp. As for the CC augmented, case #4 minimized TOFL and case #4 minimized LdgFl and Vapp in lieu of case #7. All three CDFs shifted farther away from the appropriate constraints for the CC augmented configuration. In fact, the confidence level associated with the achievement of each metric increased with the CC augmented configuration. For the TOFL, the probability of achieving the target increased from 68% to 87%. The LdgFl and Vapp confidence levels both increased from 70% and 85%, respectively, to 100%. *Hence, the potential for improving the low speed metrics through the addition of CC exists within the assumptions and conditions stated herein.*

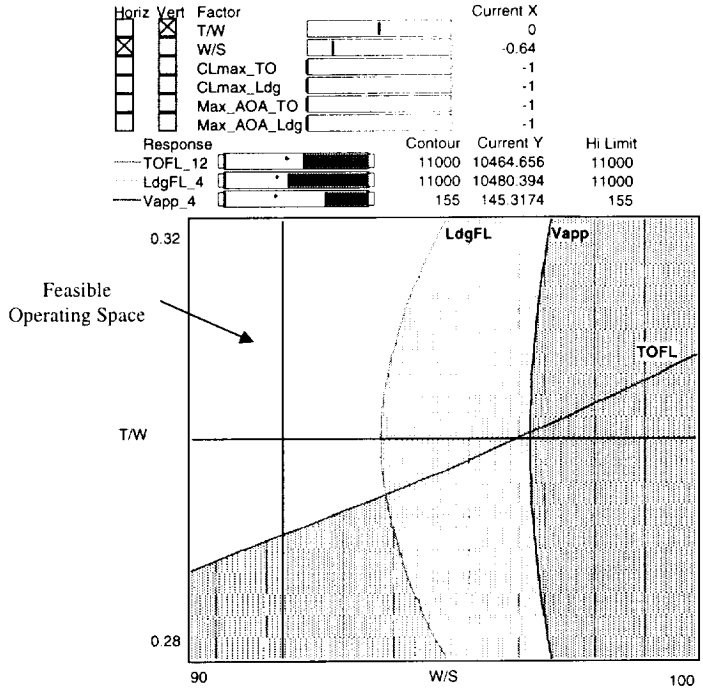

FIGURE 45: FEASIBLE OPERATING SPACE FOR CONVENTIONAL VEHICLE

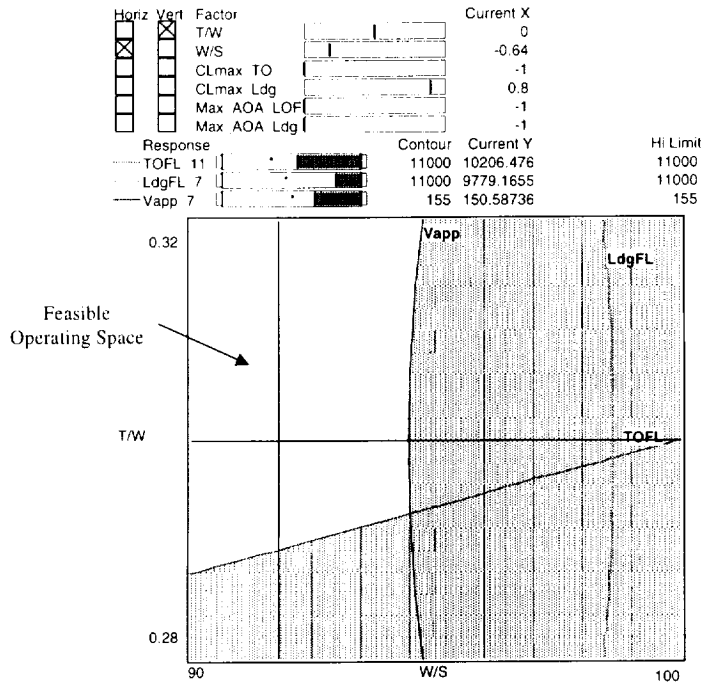

FIGURE 46: FEASIBLE OPERATING SPACE FOR CC AUGMENTED VEHICLE

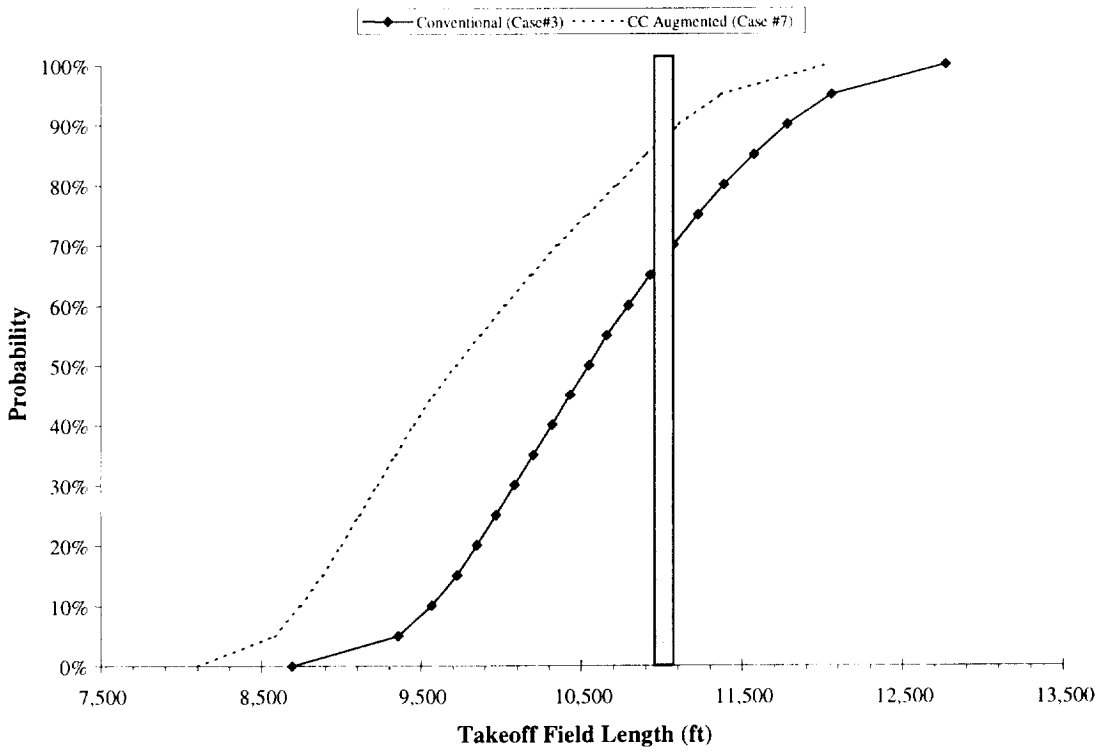

FIGURE 47: COMPARISON OF TOFL DUE TO UNCERTAINTY

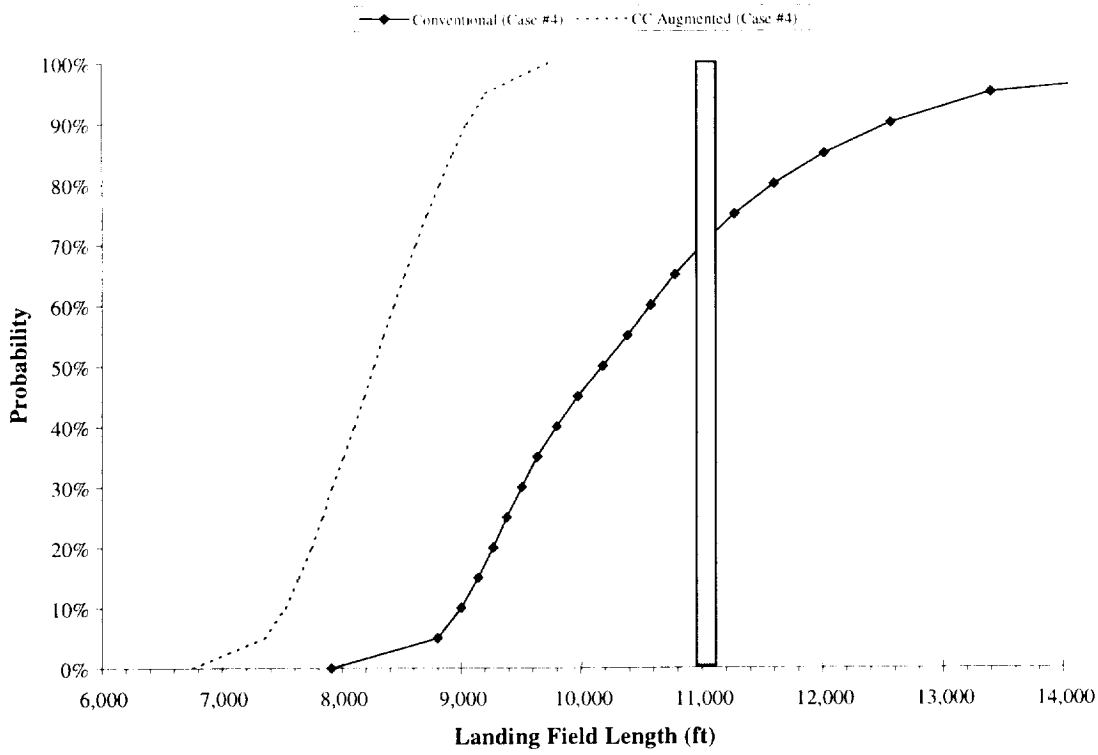

FIGURE 48: COMPARISON OF LDGFL DUE TO UNCERTAINTY

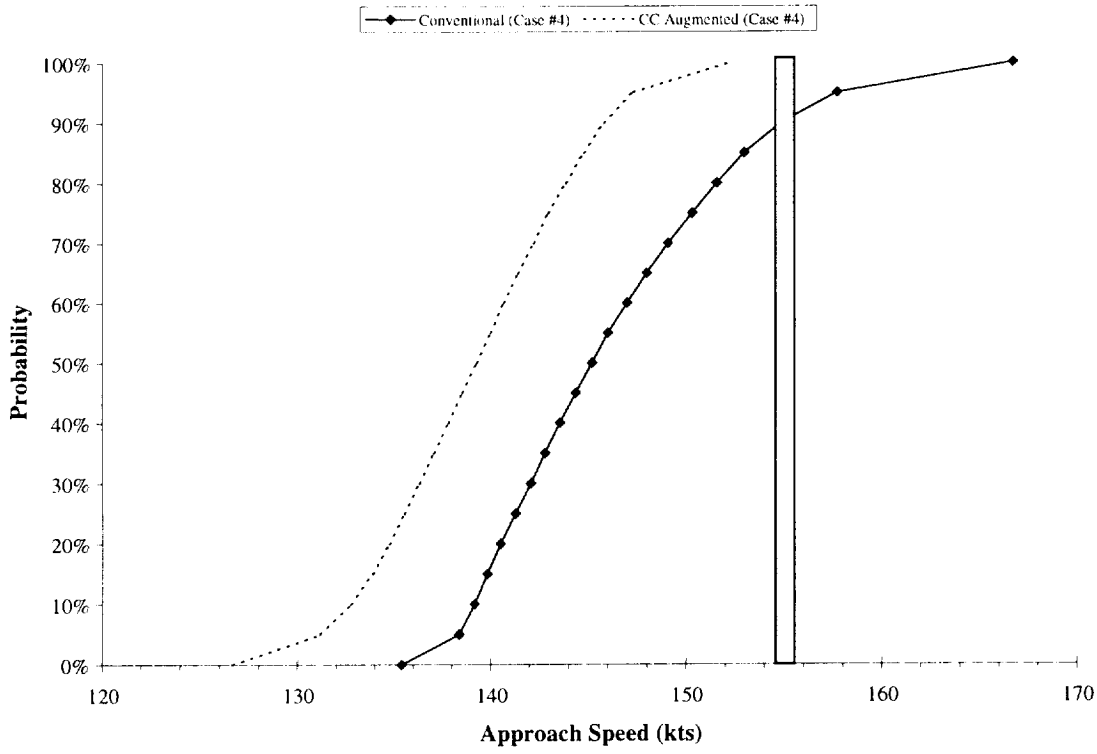

FIGURE 49: COMPARISON OF VAPP DUE TO UNCERTAINTY

3.4.4 Alternative Geometry Comparison

One final aspect of the current research is to investigate the impact of CC on an alternative geometric configuration. If one assumes that the order of magnitude and trends of the incremental changes in force coefficients could be applicable for a different geometry, the impact of the addition of CC can be investigated. In particular, previous studies at ASDL have identified an optimal aerodynamic planform that minimizes drag in the subsonic and supersonic cruise conditions. A comparison of the alternative planform to the original WT planform is shown in Figure 50. With all other configuration and mission attributes the same, the alternative geometry aerodynamics were regenerated with the identical process, as described previously. The aircraft was resized and resulted in a maximum takeoff gross weight of 781,063 lbs and a SLS thrust per engine of 58,579 lbs. If the same process of performance analysis is conducted, the impact of CC can be quantified. For each flap setting, the TAKEOFF program was executed and the results tabulated (Table 36) and compared to the conventional configuration (Table 37). A comparison between the percent reduction in the performance metrics of the alternative geometry to the scaled WT geometry shows reductions that are more significant. In fact, the TE flap deflection of 30° could converge, and the majority of the cases considered could meet the desired performance constraints. Furthermore, the improvements are also shown with the parametric investigation for operating conditions. For the T/W and W/S plot, assuming the same conditions for the previous CC augmented configurations, the amount of feasible space increases as shown in Figure 51. A higher W/S was achieved for a larger operating regime. For the landing condition, case #3 (LE 0°, TE 30°) provided the minimum LdgFL of 9,675 ft and Vapp of 147.6 kts. Case #10 provided the lowest TOFL of 9,522 ft for a LE of 20° and TE of 10°. For this point comparison to the conventional and the original CC augmented configurations, the alternative geometry was superior in performance. Yet, if the Monte Carlo simulation is considered, the alternative geometry only shows improvement in the TOFL while degrading, only sightly, the LdgFL and Vapp, as shown in Figure 52 through Figure 54. Again, high levels of probability exist for both CC augmented configurations.

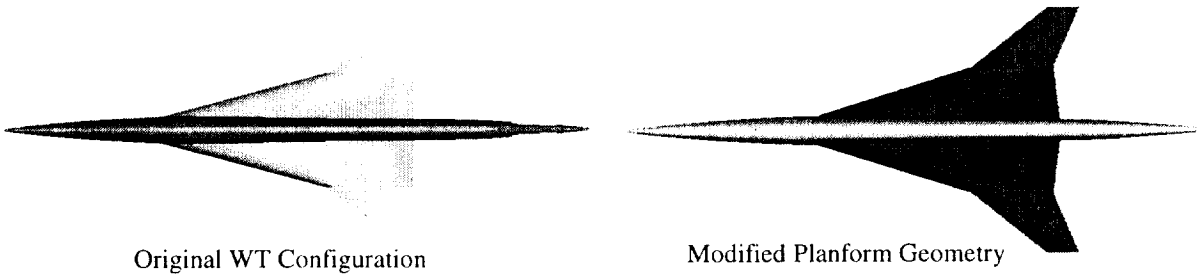

Original WT Configuration Modified Planform Geometry

FIGURE 50: ALTERNATIVE GEOMETRIC CONFIGURATION COMPARISON

TABLE 36: CC AUGMENTED METRIC VALUES (ALTERNATIVE GEOMETRY)

LE (deg)	TE (deg)	Case #	TOFL (ft)	LdgFl (ft)	Vapp (kts)	OEI Vrot (kts)	OEI Vlof (kts)	AEO Vrot (kts)	AEO Vlof (kts)	Vstall Landing (kts)	Vstall TO (kts)
0	0	1	11937	13412	188.73	210.29	221.79	210.29	227.17	145.17	156.78
0	10	2	9947	11400	165.33	188.93	198.59	188.93	203.02	127.18	156.78
0	20	3	9964	10016	150.48	189.07	194.3	189.07	196.88	115.76	156.78
0	30	4	11296	8219	141.62	195.32	196.21	195.32	196.64	108.94	156.78
10	0	5	12416	13988	193.78	214.62	226.19	214.62	231.57	149.06	156.78
10	10	6	9694	11630	168.91	184.51	195.09	184.51	199.89	129.93	156.78
10	20	7	9435	10388	153.27	181.47	187.76	181.47	190.9	117.9	156.78
10	30	8	10889	8466	143.88	191.31	192.71	191.31	193.42	110.68	156.78
20	0	9	12742	14338	198.04	216.72	228.35	216.72	233.75	152.34	156.78
20	10	10	10025	12186	171.98	187.86	198.28	187.86	202.99	132.29	156.78
20	20	11	9376	10709	155.71	179.83	186.45	179.83	189.74	119.78	156.78
20	30	12	10566	8648	145.97	187.72	189.55	187.72	190.55	112.29	156.78
30	0	13	13365	14419	201.79	220.90	232.1	220.90	237.47	155.22	156.78
30	10	14	10399	12290	174.73	191.05	201.15	191.05	205.78	134.41	156.78
30	20	15	9473	10838	157.91	179.80	186.47	179.80	189.85	121.47	156.78
30	30	16	10449	8076	147.87	185.54	187.63	185.54	188.83	113.75	156.78

TABLE 37: CC AUGMENTED COMPARISON TO CONVENTIONAL VALUES (ALTERNATIVE GEOMETRY)*

LE (deg)	TE (deg)	Case #	TOFL (ft)	LdgFl (ft)	Vapp (kts)	OEI Vrot (kts)	OEI Vlof (kts)	AEO Vrot (kts)	AEO Vlof (kts)	Vstall Landing (kts)	Vstall TO (kts)
0	0	1	-27.0	-19.9	-6.8	-16.3	-16.0	-16.3	-15.8	-5.5	-0.8
0	10	2	-21.6	-9.8	-5.0	-13.8	-14.4	-13.8	-14.4	-5.7	-0.8
0	20	3	-10.1	-11.0	-5.7	-6.9	-9.6	-6.9	-10.4	-6.0	-0.8
0	30	4	4.7	-39.6	-7.9	-2.3	-6.3	-2.3	-8.0	-6.1	-0.8
10	0	5	-28.5	-18.8	-7.0	-17.3	-16.9	-17.3	-16.6	-5.8	-0.8
10	10	6	-27.2	-26.2	-7.2	-18.0	-17.9	-18.0	-17.7	-6.0	-0.8
10	20	7	-18.3	-29.2	-7.6	-12.7	-14.5	-12.7	-14.9	-6.2	-0.8
10	30	8	3.1	-38.4	-7.5	-2.4	-6.7	-2.4	-8.4	-6.4	-0.8
20	0	9	-30.4	-18.1	-7.1	-18.5	-17.9	-18.5	-17.7	-6.0	-0.8
20	10	10	-27.9	-24.0	-7.2	-18.2	-18.1	-18.2	-18.0	-6.2	-0.8
20	20	11	-21.8	-9.9	-6.2	-15.2	-16.6	-15.2	-16.9	-6.3	-0.8
20	30	12	-3.4	-37.5	-7.1	-6.0	-9.7	-6.0	-11.1	-6.5	-0.8
30	0	13	-28.9	-17.9	-7.1	-16.9	-16.5	-16.9	-16.3	-6.1	-0.8
30	10	14	-28.7	-23.6	-7.2	-18.4	-18.3	-18.4	-18.2	-6 2	-0.8
30	20	15	-24.2	-9.2	-4.6	-16.7	-17.8	-16.7	-18.0	-6.4	-0.8
30	30	16	-7.9	-43.0	-8.1	-8.6	-11.9	-8.6	-13.1	-6.6	-0.8

* Values represent a relative percent change from the conventional configurations

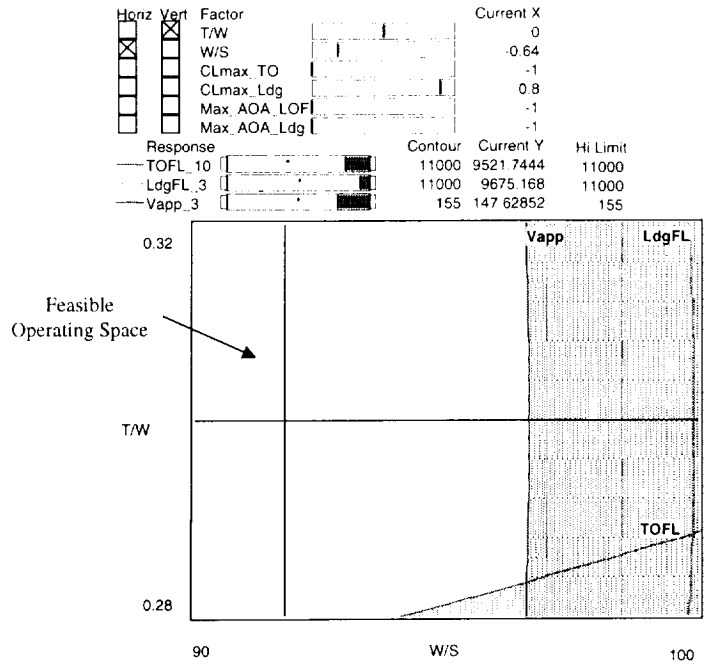

FIGURE 51: FEASIBLE OPERATING SPACE FOR CC AUGMENTED VEHICLE (ALTERNATIVE GEOMETRY)

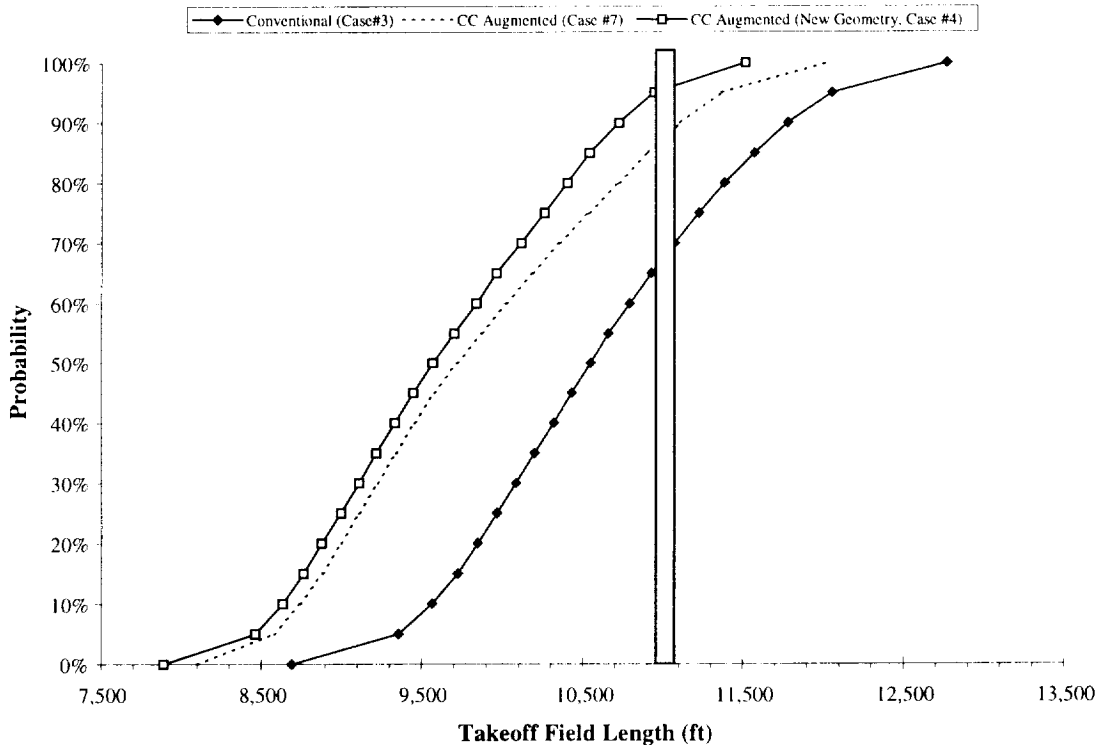

FIGURE 52: COMPARISON OF TOFL SUBJECT TO OPERATING CONDITIONS

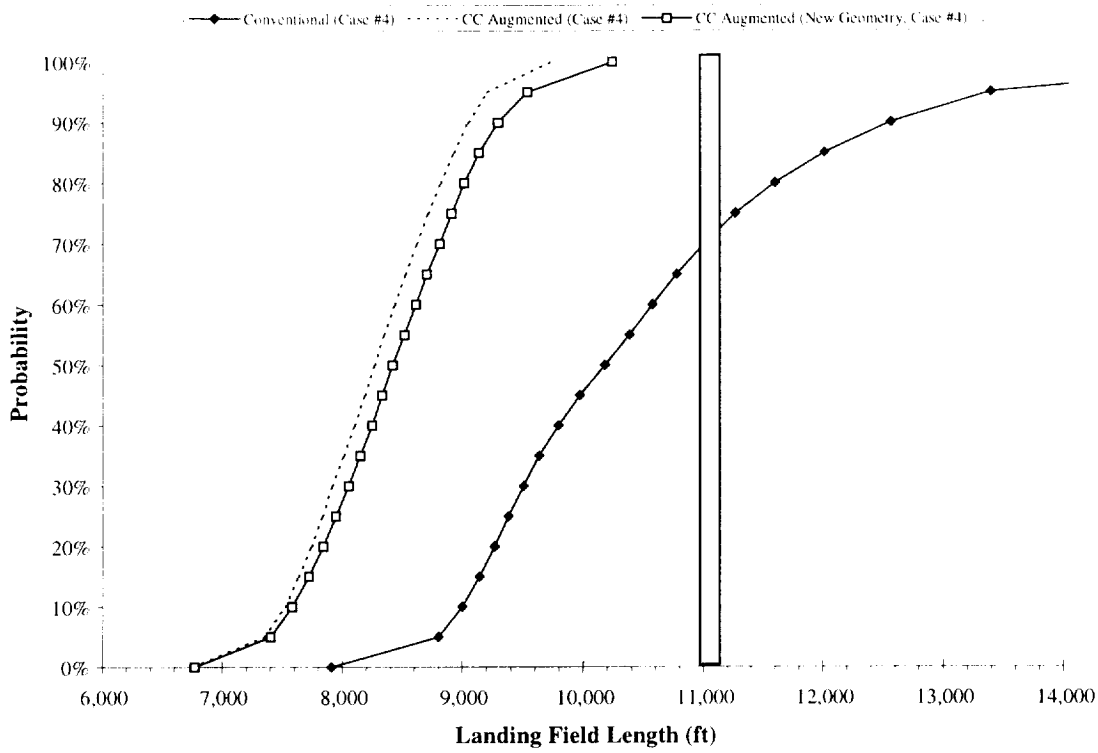

FIGURE 53: COMPARISON OF LDGFL SUBJECT TO OPERATING CONDITIONS

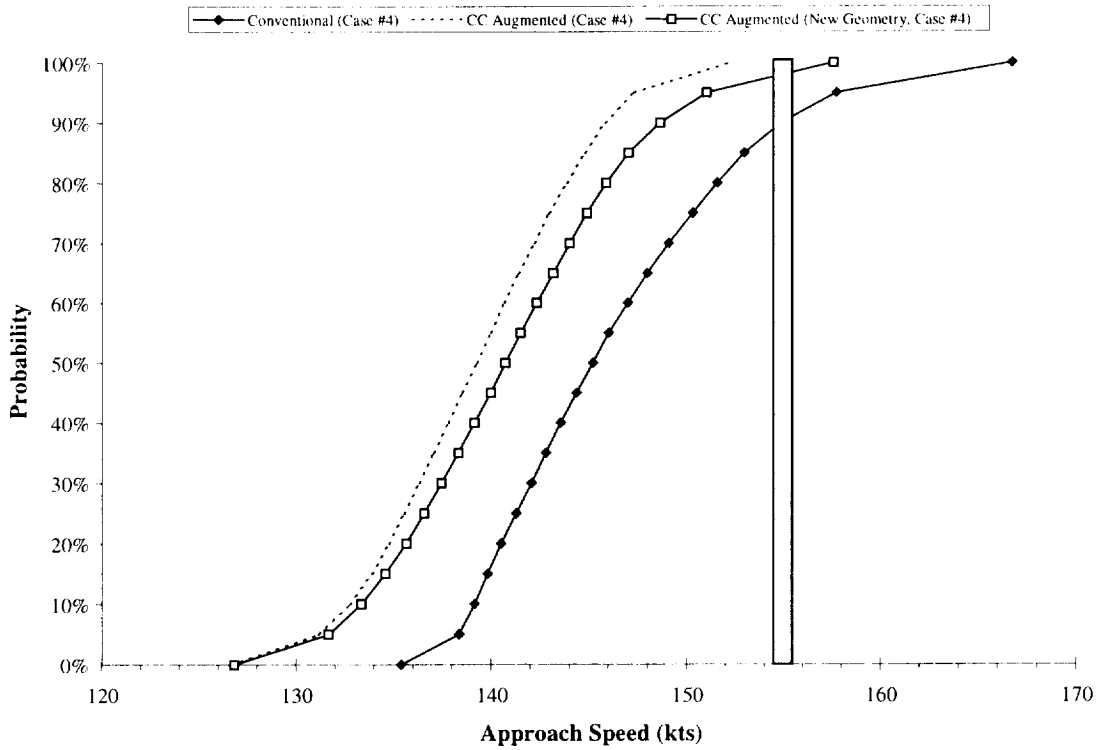

FIGURE 54: COMPARISON OF VAPP SUBJECT TO OPERATING CONDITIONS

3.4.5 Economic Comparison

Finally, a comparison of the primary economic parameters was performed for an HSCT with and without CC. The economic analysis was performed in ALCCA for the baseline configuration described previously. The economic assumptions used for the comparison are listed in Table 38. Based on these assumptions, the primary economic metrics were evaluated for the two configurations. The conventional configuration resulted in RDT&E costs of 15.259 $B, an acquisition price per unit of 208.88 $M, and a $/RPM of $0.1397. The CC configuration increased the RDT&E costs by 1.85% to 15.541 $B, the acquisition price by 3.43% to 216.04 $M, and the $/RPM by 2.48% to $0.1432. The increases economic metrics were driven by the costs associated with developing the immature technology over use of a conventional high lift system. The improved performance of an HSCT was offset slightly by reduced affordability.

TABLE 38: ECONOMIC ASSUMPTIONS

Parameter	Value	Parameter	Value
Airframe Spares (of airframe price)	6%	Fiscal Year Dollars	1996
Airline ROI	10%	Fuel Cost	$0.70/gal
Average Annual Inflation	8.00%	Hull Insurance Rate (of aircraft price)	0.35%
Residual Value (price including spares)	10%	Manufacturer LC	78.00%
Downpayment	0%	Load Factor	65%
Economic Life	20 yrs	Maintenance Burden Rate (of direct labor)	200%
Economic Range	5000 nm	Maintenance Labor Rate	$25.00/hr
Engine Spares (of engine price)	6%	Manufacturer ROI	15.0%
Engine Units Produced	4000	Production Quantity	800 units
Engineering Labor Rate	$89.68/hr	Tooling Labor Rate	$54.68/hr
Entry into Service Date	2006	Utilization	5000 hrs/yr
Financing Period	20 yrs	Years of Production	15

4. Further Study/Recommendations

There are several issues with regards to the propulsion analysis, which remain to be resolved. The most important is the stability of the engine during high compressor bleed operation. As mentioned in the propulsion section, the compressor bleed during approach at flight idle amounts to roughly 25% of the total core flow. The extraction of this much bleed could very well have an adverse impact on the surge margin of the compressor and/or the cooling flow rates to the HPT. Thus, future studies should include construction of a detailed cycle model in order to investigate the impact of compressor bleed on engine performance and stability. An additional concern warranting further study is the ability of the engines to supply the required mass flow rate during one-engine-

inoperative flight conditions without a significant degradation in engine performance. The stability issue is particularly important for this flight condition because it would be very unfortunate to have an engine failure precipitate surge in another engine due to increases CC flow requirements.

The most important unresolved issue remaining from the duct analysis is the ability of an automated CC control system to seamlessly compensate for engine failure by increasing mass flow from other engines. Up to this point, the ability of such as system to compensate for engine failure has only been postulated, but not analyzed in-depth. In order to analyze this, one would necessarily have to examine the unsteady behavior of the engines, particularly the time required to "spool-up" to compensate for engine failure. A second concern is the internal layout and clearance of the duct system inside the wing. Obviously, this problem requires the construction of a cad model for the internal wing structure, including details such as flap actuators, ribs, joints, stiffeners, duct cross-section, etc. and would be a very time-consuming task. Additional concerns include accounting for duct pressure losses due to flow turning and valves, as well as the impact of a spanwise variation of h/c.

Finally, a list of suggestions by which the short-comings of this study may be overcome are listed in Table 39. If these suggestions are followed, more realistic and accurate results may be obtained in future studies.

TABLE 39: PNEUMATIC TECHNOLOGY FUTURE STUDY RECOMMENDATIONS

Area	Difficulties
Wind Tunnel Geometric Model	*Airfoils*: moderate thickness (4%) with finite leading edge radius inboard and biconvex outboard; add twist and camber
	Secondary surfaces: More representative areas and placement
Wind Tunnel Experimental Conditions	*Dynamic Similarity*: Modify Reynolds number to match full scale
	Dynamic Pressure: Perform dynamic pressure sweeps
	Air supply: Utilize realistic bleed point parameters
Wind Tunnel Data	*Flap Setting*: Perform flap setting sweeps at more appropriate blowing levels
	Deltas: Avoid
Aerodynamic Analysis Tools	*Vortex Lift*: Add capability to aerodynamic tools
	Compressibility Effects: Add capability to current analysis tools
	CC Phenomena: Utilize more appropriate wind tunnel data
	Trim Drag: Captured
	Engine out drag: Captured
Duct Sizing	*Layout*: Optimize for actual interior of the wing; accurately assess duct weight penalties
Propulsion	*Mass Flow Requirements*: Dynamic link to aerodynamics and performance calculations
	Operational Safety: Assess impact of OEI conditions and CC system failures

5. Appendix A

Contained herein are the regression coefficients for the lift and drag coefficients as a function of flap deflection and blowing coefficient. The C_μ values that are in bold are the actual WT data regression coefficients and the other coefficients are interpolated values.

5.1 Plain Flap Interpolated Coefficients

TABLE 40: PLAIN FLAP INTERPOLATED LIFT COEFFICIENTS, δ=0°

C_μ	b_o	b_1	b_2
0	**-0.00533**	**0.0475006**	**0.0000895**
0.001	-0.003924623	0.047496489	0.000090379
0.005	0.001696885	0.047480045	0.000093895
0.007	0.004507639	0.047471823	0.000095653
0.009	0.007318393	0.047463601	0.000097411
0.01	0.00872377	0.04745949	0.00009829
0.015	0.015750655	0.047438935	0.000102685
0.02	0.02277754	0.04741838	0.00010708
0.03	0.03683131	0.04737727	0.00011587
0.04	0.05088508	0.04733616	0.00012466
0.05	0.06493885	0.04729505	0.00013345
0.1	**0.1352077**	**0.0470895**	**0.0001774**
0.2	**0.1921267**	**0.0480686**	**0.0002606**
0.3	0.242197265	0.242197265	0.242197265
0.315	**0.2455052**	**0.0532457**	**0.0001702**

TABLE 41: PLAIN FLAP INTERPOLATED LIFT COEFFICIENTS, δ=10°

C_μ	b_o	b_1	b_2
0	0.03158755	0.047824	0.00010395
0.001	0.033813962	0.047801763	0.000105103
0.005	0.042719608	0.047712815	0.000109713
0.007	0.047172431	0.047668341	0.000112018
0.009	0.051625254	0.047623867	0.000114323
0.01	0.053851665	0.04760163	0.000115475
0.015	0.064983723	0.047490445	0.000121238
0.02	0.07611578	0.04737926	0.000127
0.03	0.098379895	0.04715689	0.000138525
0.04	0.12064401	0.04693452	0.00015005
0.05	0.142908125	0.04671215	0.000161575
0.1	0.2542287	0.0456003	0.0002192
0.2	0.328817214	0.048294297	0.000221016
0.3	0.399981511	0.147563077	0.121149565

TABLE 42: PLAIN FLAP INTERPOLATED LIFT COEFFICIENTS, δ=20°

C_μ	b_o	b_1	b_2
0	**0.0685051**	**0.0481474**	**0.0001184**
0.001	0.071552546	0.048107037	0.000119826
0.005	0.08374233	0.047945585	0.00012553
0.007	0.089837222	0.047864859	0.000128382
0.009	0.095932114	0.047784133	0.000131234
0.01	0.09897956	0.04774377	0.00013266
0.015	0.11421679	0.047541955	0.00013979
0.02	0.12945402	0.04734014	0.00014692
0.03	0.15992848	0.04693651	0.00016118
0.04	0.19040294	0.04653288	0.00017544
0.05	0.2208774	0.04612925	0.0001897
0.1	**0.3732497**	**0.0441111**	**0.000261**
0.2	0.465507729	0.048519994	0.000181433
0.3	0.557765758	0.052928888	0.000101865
0.308	**0.5651464**	**0.0532816**	**0.0000955**

TABLE 43: PLAIN FLAP INTERPOLATED LIFT COEFFICIENTS, δ=30°

C_μ	b_o	b_1	b_2
0	0.10542265	0.0484708	0.00013285
0.001	0.109291131	0.048412311	0.00013455
0.005	0.124765053	0.048178355	0.000141348
0.007	0.132502014	0.048061377	0.000144747
0.009	0.140238975	0.047944399	0.000148146
0.01	0.144107455	0.04788591	0.000149845
0.015	0.163449858	0.047593465	0.000158343
0.02	0.18279226	0.04730102	0.00016684
0.03	0.221477065	0.04671613	0.000183835
0.04	0.26016187	0.04613124	0.00020083
0.05	0.298846675	0.04554635	0.000217825
0.1	0.4922707	0.0426219	0.0003028
0.2	0.602198243	0.048745691	0.000141849
0.3	0.715550004	-0.0417053	-0.120945834

TABLE 44: PLAIN FLAP INTERPOLATED DRAG COEFFICIENTS, $\delta=0°$

C_μ	b_o	b_1	b_2
0	**0.009682**	**-0.00016**	**0.000841**
0.001	0.009082	-0.00015	0.000842
0.005	0.006683	-0.00011	0.000844
0.007	0.005483	-9.5E-05	0.000845
0.009	0.004283	-7.7E-05	0.000846
0.01	0.003683	-6.7E-05	0.000847
0.015	0.000684	-2.2E-05	0.000849
0.02	-0.00232	2.43E-05	0.000852
0.03	-0.00831	0.000116	0.000858
0.04	-0.01431	0.000208	0.000863
0.05	-0.02031	0.000299	0.000869
0.1	**-0.0503**	**0.000758**	**0.000897**
0.2	**-0.12127**	**0.001015**	**0.000973**
0.3	-0.40076	-0.40076	-0.40076
0.315	**-0.19757**	**0.002166**	**0.000992**

TABLE 45: PLAIN FLAP INTERPOLATED DRAG COEFFICIENTS, $\delta=10°$

C_μ	b_o	b_1	b_2
0	0.011792	0.000419	0.000841
0.001	0.011311	0.000436	0.000841
0.005	0.009386	0.000504	0.000845
0.007	0.008423	0.000538	0.000846
0.009	0.007461	0.000573	0.000848
0.01	0.00698	0.00059	0.000848
0.015	0.004574	0.000675	0.000852
0.02	0.002167	0.000761	0.000856
0.03	-0.00264	0.000932	0.000864
0.04	-0.00746	0.001103	0.000871
0.05	-0.01227	0.001275	0.000879
0.1	-0.03633	0.002131	0.000917
0.2	-0.09809	0.003046	0.000975
0.3	-0.2641	-0.19705	-0.19987

TABLE 46: PLAIN FLAP INTERPOLATED DRAG COEFFICIENTS, δ=20°

C_μ	b_o	b_1	b_2
0	**0.013902**	**0.000996**	**0.00084**
0.001	0.01354	0.001021	0.000841
0.005	0.012089	0.001122	0.000845
0.007	0.011364	0.001172	0.000847
0.009	0.010639	0.001222	0.000849
0.01	0.010276	0.001247	0.00085
0.015	0.008463	0.001372	0.000855
0.02	0.00665	0.001498	0.00086
0.03	0.003024	0.001749	0.000869
0.04	-0.0006	0.001999	0.000879
0.05	-0.00423	0.00225	0.000889
0.1	**-0.02236**	**0.003504**	**0.000937**
0.2	-0.0749	0.005077	0.000977
0.3	-0.12744	0.006651	0.001017
0.308	**-0.13165**	**0.006777**	**0.00102**

TABLE 47: PLAIN FLAP INTERPOLATED DRAG COEFFICIENTS, δ=30°

C_μ	b_o	b_1	b_2
0	0.016012	0.001574	0.00084
0.001	0.015768	0.001607	0.000841
0.005	0.014792	0.001739	0.000846
0.007	0.014304	0.001805	0.000848
0.009	0.013816	0.001871	0.000851
0.01	0.013572	0.001904	0.000852
0.015	0.012352	0.002069	0.000858
0.02	0.011132	0.002235	0.000863
0.03	0.008692	0.002565	0.000875
0.04	0.006252	0.002895	0.000887
0.05	0.003812	0.003225	0.000899
0.1	-0.00839	0.004877	0.000957
0.2	-0.05171	0.007109	0.000979
0.3	0.009215	0.210356	0.201905

5.2 CCW Flap Interpolated Coefficients

TABLE 48: CCW FLAP INTERPOLATED LIFT COEFFICIENTS, δ=0°

C_μ	b_o	b_1	b_2
0	**0.075152**	**0.04592**	**0.00011**
0.001	0.079864	0.045893	0.000111
0.005	0.098713	0.045787	0.000116
0.007	0.108138	0.045735	0.000119
0.009	0.117563	0.045682	0.000121
0.01	0.122275	0.045655	0.000123
0.015	0.145836	0.045523	0.000129
0.02	0.169398	0.04539	0.000135
0.03	0.216521	0.045126	0.000148
0.04	0.263644	0.044861	0.00016
0.05	0.310766	0.044596	0.000173
0.1	0.485463	0.044746	0.00019
0.2	0.618257	0.050287	6.14E-05
0.3	0.751052	0.055827	-6.7E-05
0.328	**0.788234**	**0.057379**	**-0.0001**

TABLE 49: CCW FLAP INTERPOLATED LIFT COEFFICIENTS, δ=10°

C_μ	b_o	b_1	b_2
0	**0.158169**	**0.045956**	**0.000141**
0.001	0.163073	0.045931	0.000141
0.005	0.182691	0.045832	0.00014
0.007	0.1925	0.045782	0.000139
0.009	0.202309	0.045732	0.000139
0.01	0.207213	0.045707	0.000139
0.015	0.231736	0.045583	0.000138
0.02	0.256258	0.045459	0.000137
0.03	0.305303	0.04521	0.000135
0.04	0.354347	0.044962	0.000133
0.05	0.403392	0.044713	0.000131
0.1	0.589762	0.044998	9.56E-05
0.2	0.753248	0.051	-7.1E-05
0.3	0.916735	0.057001	-0.00024
0.328	**0.962511**	**0.058682**	**-0.00028**

TABLE 50: CCW FLAP INTERPOLATED LIFT COEFFICIENTS, δ=20°

C_μ	b_o	b_1	b_2
0	0.234287	0.045996	0.000143
0.001	0.24133	0.045949	0.000143
0.005	0.269502	0.045762	0.000142
0.007	0.283588	0.045669	0.000142
0.009	0.297674	0.045575	0.000141
0.01	0.304717	0.045529	0.000141
0.015	0.34651	0.045214	0.000137
0.02	0.388303	0.0449	0.000133
0.03	0.45106	0.046265	5.64E-05
0.04	0.515724	0.046155	3.63E-05
0.05	0.562541	0.046373	1.72E-05
0.1	0.75238	0.048534	-9.3E-05
0.2	0.981191	0.05514	-0.00032
0.3	1.1588	0.06017	-0.00044

TABLE 51: CCW FLAP INTERPOLATED LIFT COEFFICIENTS, δ=30°

C_μ	b_o	b_1	b_2
0	0.310405	0.046036	0.000146
0.001	0.319586	0.045968	0.000146
0.005	0.356313	0.045693	0.000145
0.007	0.374676	0.045556	0.000144
0.009	0.393039	0.045419	0.000144
0.01	0.402221	0.04535	0.000143
0.015	0.461285	0.044846	0.000136
0.02	0.520348	0.044341	0.000129
0.03	0.596817	0.04732	-2.2E-05
0.04	0.6771	0.047348	-6.1E-05
0.05	0.72169	0.048032	-9.7E-05
0.1	0.914998	0.05207	-0.00028
0.2	1.209134	0.059279	-0.00056
0.3	1.400865	0.063339	-0.00065

TABLE 52: CCW FLAP INTERPOLATED LIFT COEFFICIENTS, δ=34°

C_μ	b_o	b_1	b_2
0	**0.340852**	**0.046052**	**0.000147**
0.001	0.350889	0.045975	0.000147
0.005	0.391037	0.045666	0.000146
0.007	0.411111	0.045511	0.000145
0.009	0.431185	0.045356	0.000144
0.01	**0.441222**	**0.045279**	**0.000144**
0.015	0.507194	0.044698	0.000136
0.02	**0.573166**	**0.044117**	**0.000128**
0.03	**0.65512**	**0.047742**	**-5.4E-05**
0.04	0.741651	0.047825	-9.9E-05
0.05	0.785349	0.048696	-0.00014
0.1	0.980045	0.053484	-0.00036
0.2	1.300311	0.060935	-0.00066
0.3	1.497691	0.064606	-0.00073
0.328	**1.552958**	**0.065634**	**-0.00075**

TABLE 53: CCW FLAP INTERPOLATED DRAG COEFFICIENTS, δ=0°

C_μ	b_o	b_1	b_2
0	**0.010427**	**0.001065**	**0.000816**
0.001	0.010276	0.001109	0.000818
0.005	0.009669	0.001283	0.000824
0.007	0.009366	0.001369	0.000826
0.009	0.009063	0.001456	0.000829
0.01	0.008911	0.0015	0.000831
0.015	0.008153	0.001717	0.000838
0.02	0.007396	0.001934	0.000845
0.03	0.00588	0.002369	0.000859
0.04	0.004364	0.002803	0.000874
0.05	0.002848	0.003238	0.000888
0.1	-0.01038	0.005106	0.000938
0.2	-0.05691	0.007763	0.000961
0.3	-0.10343	0.01042	0.000984
0.328	**-0.11646**	**0.011164**	**0.000991**

TABLE 54: CCW FLAP INTERPOLATED DRAG COEFFICIENTS, δ=10°

C_μ	b_o	b_1	b_2
0	**0.020295**	**0.00167**	**0.000865**
0.001	0.020537	0.00172	0.000866
0.005	0.021505	0.001924	0.000869
0.007	0.021989	0.002026	0.00087
0.009	0.022473	0.002128	0.000871
0.01	0.022715	0.002179	0.000872
0.015	0.023925	0.002433	0.000875
0.02	0.025135	0.002688	0.000879
0.03	0.027555	0.003197	0.000885
0.04	0.029975	0.003706	0.000892
0.05	0.032395	0.004215	0.000899
0.1	0.036357	0.006514	0.000918
0.2	0.015343	0.010235	0.000906
0.3	-0.00567	0.013957	0.000894
0.328	**-0.01156**	**0.014999**	**0.000891**

TABLE 55: CCW FLAP INTERPOLATED DRAG COEFFICIENTS, δ=20°

C_μ	b_o	b_1	b_2
0	0.033117	0.002689	0.000885
0.001	0.033465	0.00277	0.000885
0.005	0.034856	0.003094	0.000887
0.007	0.035551	0.003256	0.000888
0.009	0.036246	0.003418	0.000888
0.01	0.036594	0.0035	0.000889
0.015	0.041656	0.003928	0.000892
0.02	0.046719	0.004356	0.000894
0.03	0.05491	0.005494	0.00088
0.04	0.066366	0.006118	0.000882
0.05	0.072411	0.006795	0.00088
0.1	0.094888	0.010062	0.000857
0.2	0.113252	0.015428	0.000803
0.3	0.114355	0.019625	0.000785

TABLE 56: CCW FLAP INTERPOLATED DRAG COEFFICIENTS, δ=30°

C_μ	b_o	b_1	b_2
0	0.045939	0.003708	0.000905
0.001	0.046393	0.003819	0.000905
0.005	0.048206	0.004264	0.000905
0.007	0.049113	0.004487	0.000905
0.009	0.050019	0.004709	0.000906
0.01	0.050472	0.004821	0.000906
0.015	0.059387	0.005423	0.000908
0.02	0.068302	0.006025	0.00091
0.03	0.082266	0.007792	0.000874
0.04	0.102756	0.008531	0.000872
0.05	0.112428	0.009374	0.00086
0.1	0.15342	0.01361	0.000796
0.2	0.211162	0.02062	0.000699
0.3	0.234382	0.025292	0.000675

TABLE 57: CCW FLAP INTERPOLATED DRAG COEFFICIENTS, δ=34°

C_μ	b_o	b_1	b_2
0	**0.051068**	**0.004115**	**0.000913**
0.001	0.051564	0.004239	0.000913
0.005	0.053546	0.004732	0.000913
0.007	0.054537	0.004979	0.000912
0.009	0.055528	0.005226	0.000912
0.01	**0.056024**	**0.005349**	**0.000912**
0.015	0.06648	0.006021	0.000914
0.02	**0.076936**	**0.006692**	**0.000916**
0.03	**0.093208**	**0.008711**	**0.000872**
0.04	0.117312	0.009496	0.000868
0.05	0.128434	0.010406	0.000853
0.1	0.176833	0.015029	0.000771
0.2	0.250326	0.022697	0.000658
0.3	0.282392	0.027559	0.000632
0.328	**0.291371**	**0.02892**	**0.000624**

6. Appendix B

6.1 WINGDES

WINGDES optimally twists and cambers the wing for minimum induced drag using an empirical attainable leading edge thrust and vortex forces approximation. WINGDES was developed by Harry Carlson and Christine Darden of NASA Langley in the late 1980's. It can optimize flap settings, twist, and camber of wings for minimum induced drag using a linearized-theory, attached flow method with estimated attainable leading-edge thrust and an estimation of vortex forces. It provides estimates of leading-edge thrust and vortex forces. WINGDES can evaluate wings at off-design points and its inputs include: wing geometry, airfoil thickness distribution, and design C_L and C_M at a given condition, and grid options.

However, there are several limitations to WINGDES. Although attainable leading-edge thrust plays a part in the optimization process, the vortex-lift forces do not. It is valid for subsonic and supersonic regimes, but not the transonic regime. WINGDES is not validated near drag rise or at low Reynolds #'s. It neglects interference with other bodies such as the fuselage, nacelles, and tails and can not model vertical extensions (X-Y plane only). WINGDES serves to twist and camber the wing optimally for minimum induced drag but has important limitations.

6.2 BDAP

BDAP was originally developed by the Boeing Aircraft Company and is capable of completely analyzing the aerodynamics of a three dimensional body in both subsonic and supersonic flight but not the transonic regime. BDAP primarily uses linearized potential theory to determine wave and induced drag except for the skin friction drag module which utilizes turbulent flat plate theory. No laminar flow is accounted for due to the assumptions of turbulent flat plate theory; therefore, the skin friction drag is over-estimated.

6.3 RAM

RAM, Rapid Aircraft Modeler, developed by J.R. Gloudemans, Paul Davis, and Mark Overmars of NASA Ames is a CAD type package meant to interface with flow solvers. It can quickly and parametrically model a variety of aircraft geometries and save an output file in the hermite file format needed for VORVIEW. RAM is a new program and thus has no significant documentation.

6.4 VORVIEW

VORVIEW was created to serve as a Graphical User Interface , (GUI) to VORLAX. It allows the user to slice, subdivide, and modify these divisions quickly in a mouse and keyboard graphical environment. VORVIEW offers both flat plate and cambered flat plate analysis options. VORVIEW models each wing panel as a plane that can be either modeled as a flat or cambered plate. Up to 2000 subdivisions, 50 camber points , and 175 spanwise slices can be used.

6.5 VORLAX

Developed by Luis R. Miranda, Robert D. Elliott, and William M. Baker of Lockheed in the 1970's, VORLAX uses the vortex lattice panel method to find induced forces and moments. Applicable to both subsonic and supersonic but not transonic regimes, it is capable of analyzing flat plates and bodies with thickness (wings and fusiform fuselages). Due to its linearized potential flow basis, it does not evaluate rotational terms and hence cannot evaluate vortex lift. Additionally, it assumes small disturbances and cannot model vertical displacements except for mild camber.

6.6 AERO2S

AERO2S provides pressure distributions and wing forces and moments for a given cambered surface. The code appears to be valid only for subsonic speeds and can handle leading and trailing edge flaps. Although AERO2S is a stand alone program the code is used to generate aerodynamic information needed by FLOPS.

7. Appendix C

7.1 Parametric Variation Results

The results contained herein are the prediction profiles for the impact of the variations of low speed parameters on low speed metrics. The prediction profiles allow for a visual means of identifying the influence of each parameter on a given metric. Furthermore, the best and worst possible metric values achievable with the chosen variable ranges are identified through the bounded values of the metrics on the ordinate. The figures are numbered in the identical manner of the case classification for the LE and TE deflections, see Table 32 for clarification of the numbering system.

7.2 Conventional Configuration

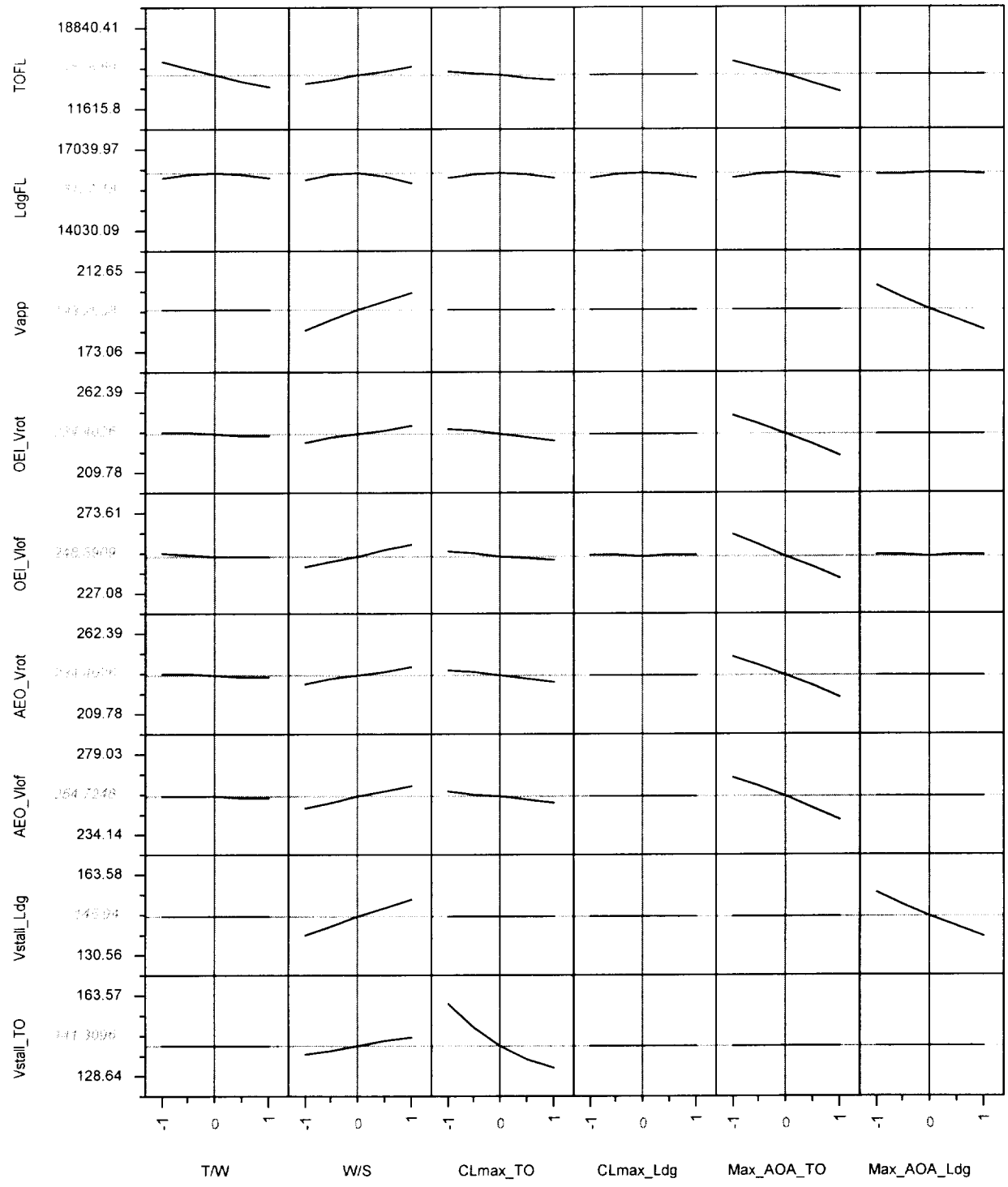

FIGURE 55: CONVENTIONAL CASE #1

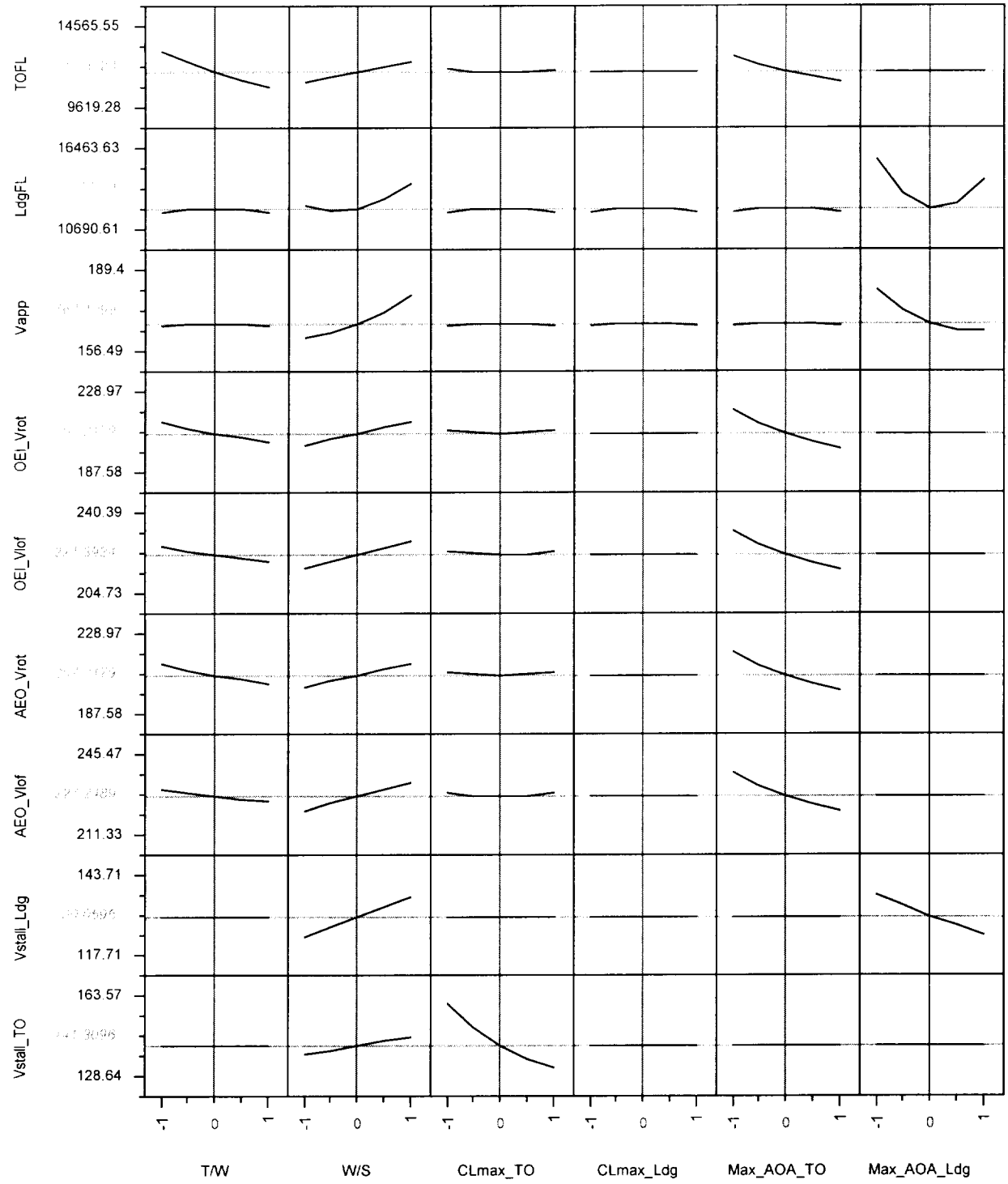

FIGURE 56: CONVENTIONAL CASE #2

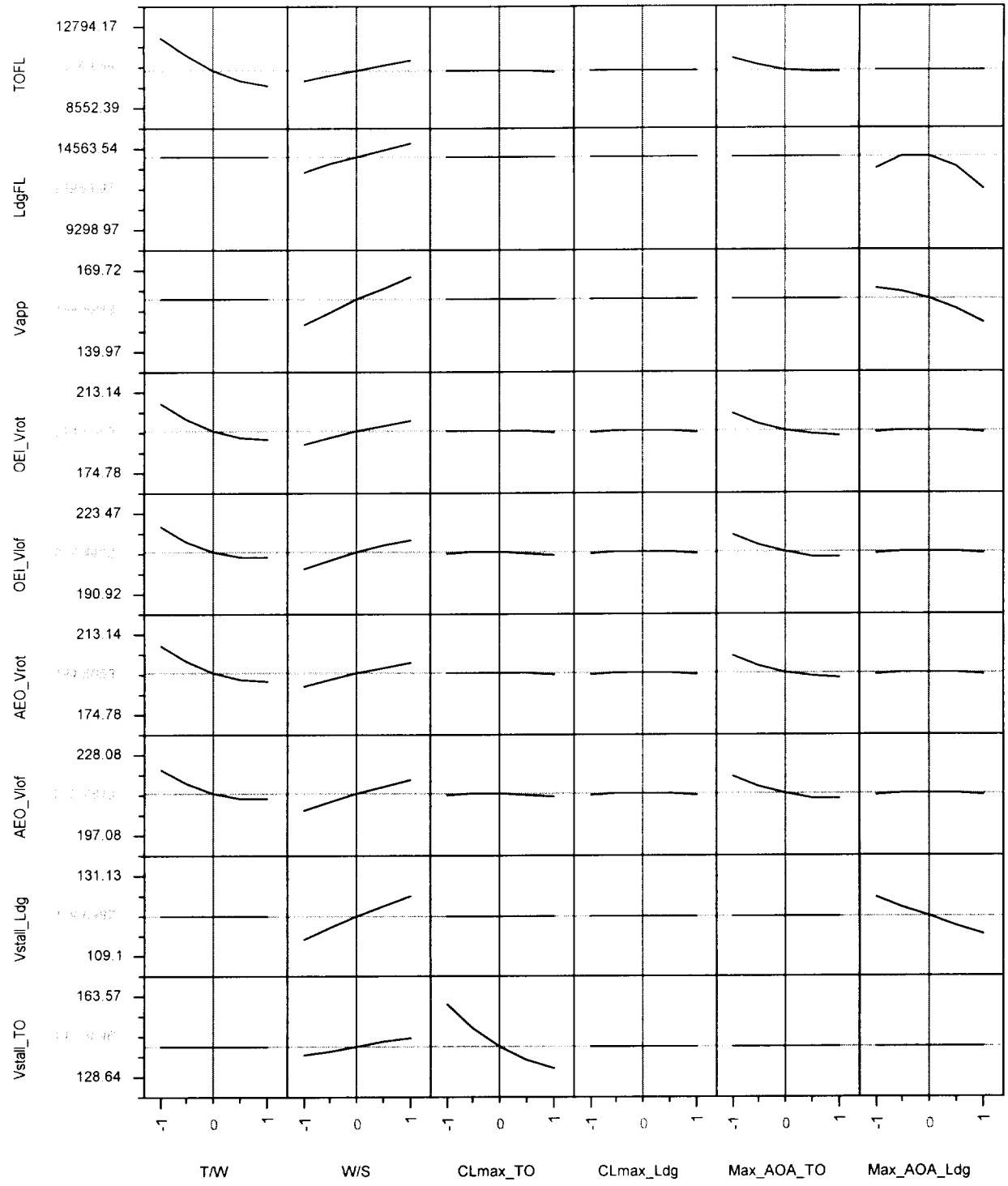

FIGURE 57: CONVENTIONAL CASE #3

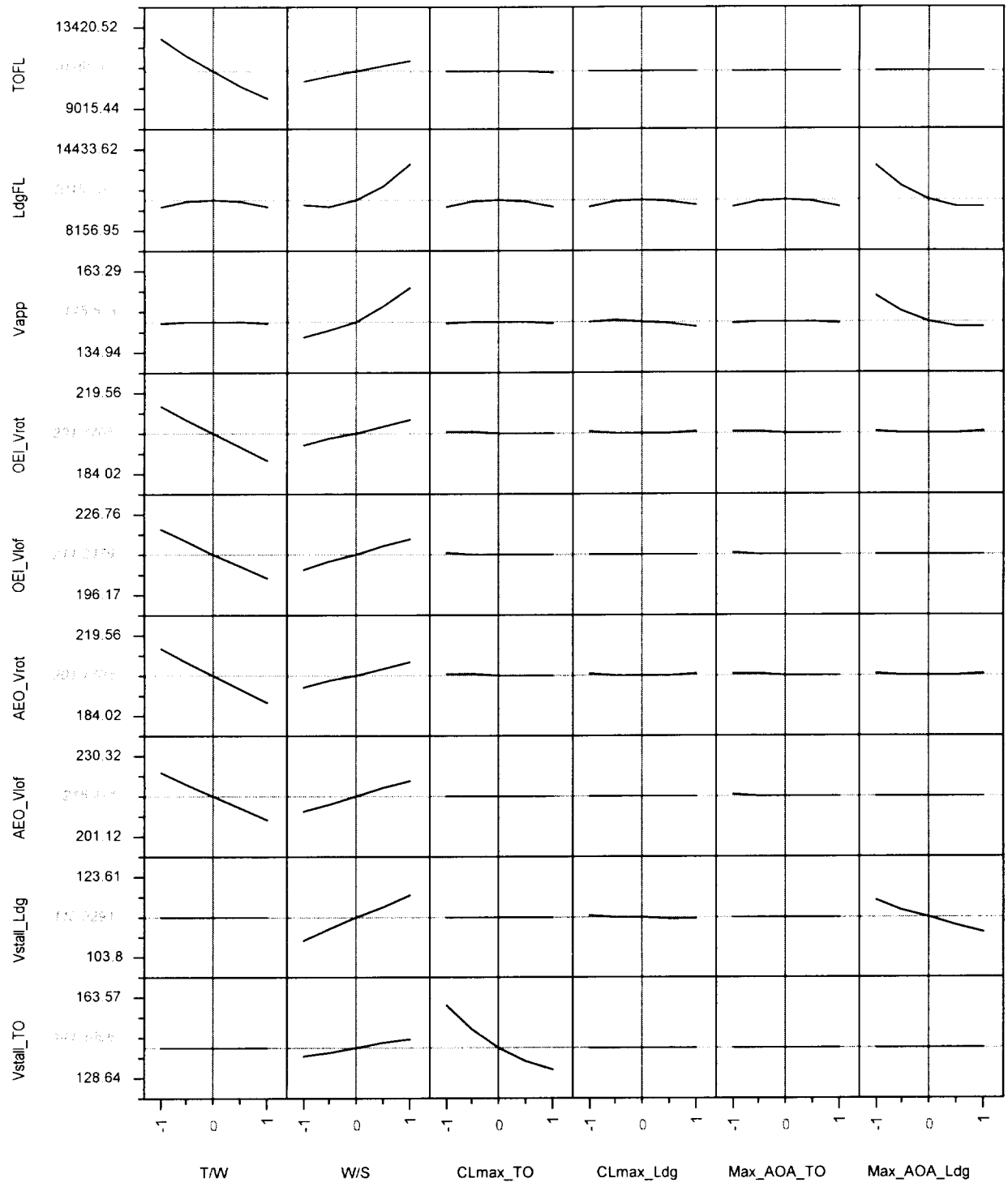

FIGURE 58: CONVENTIONAL CASE #4

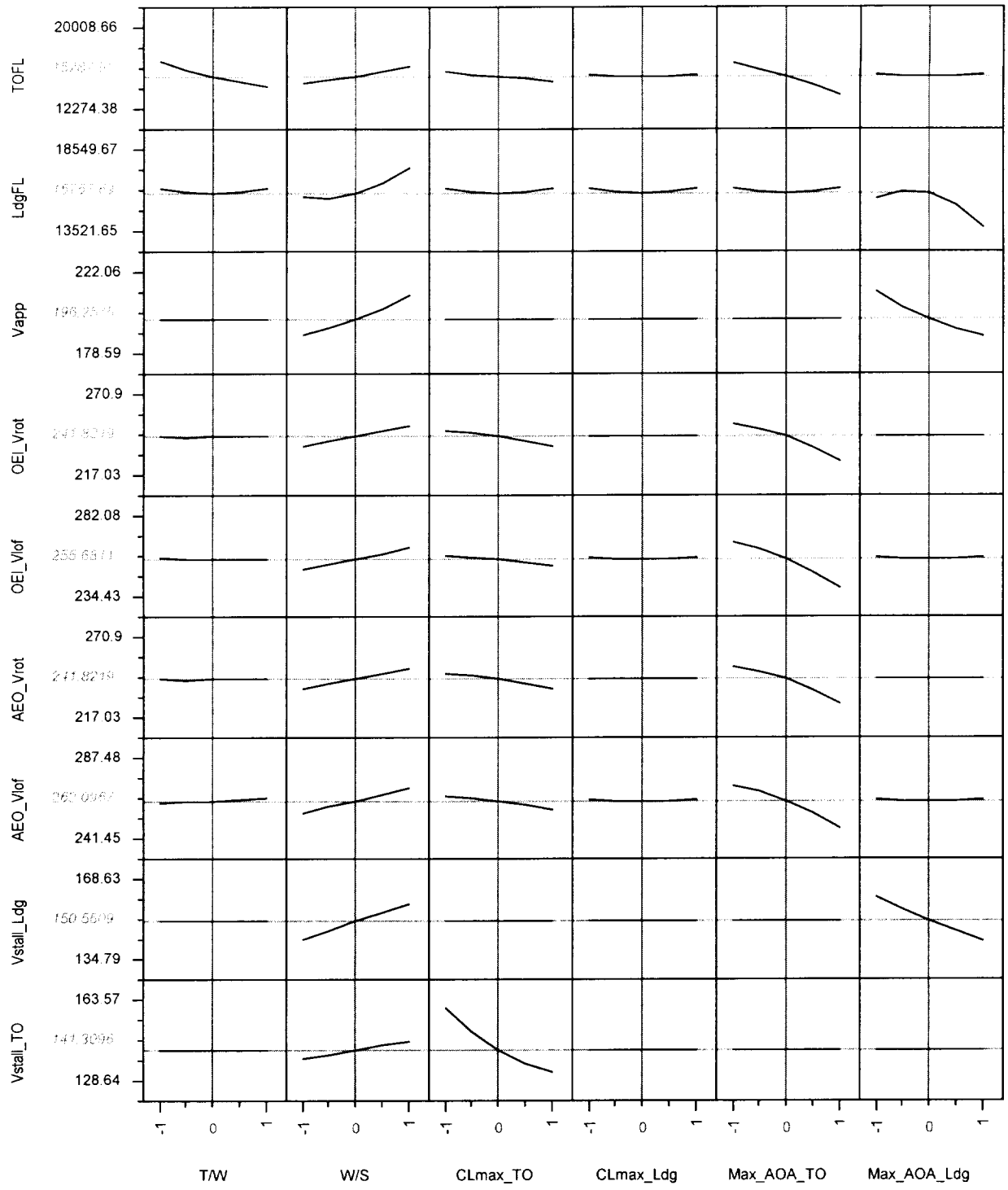

FIGURE 59: CONVENTIONAL CASE #5

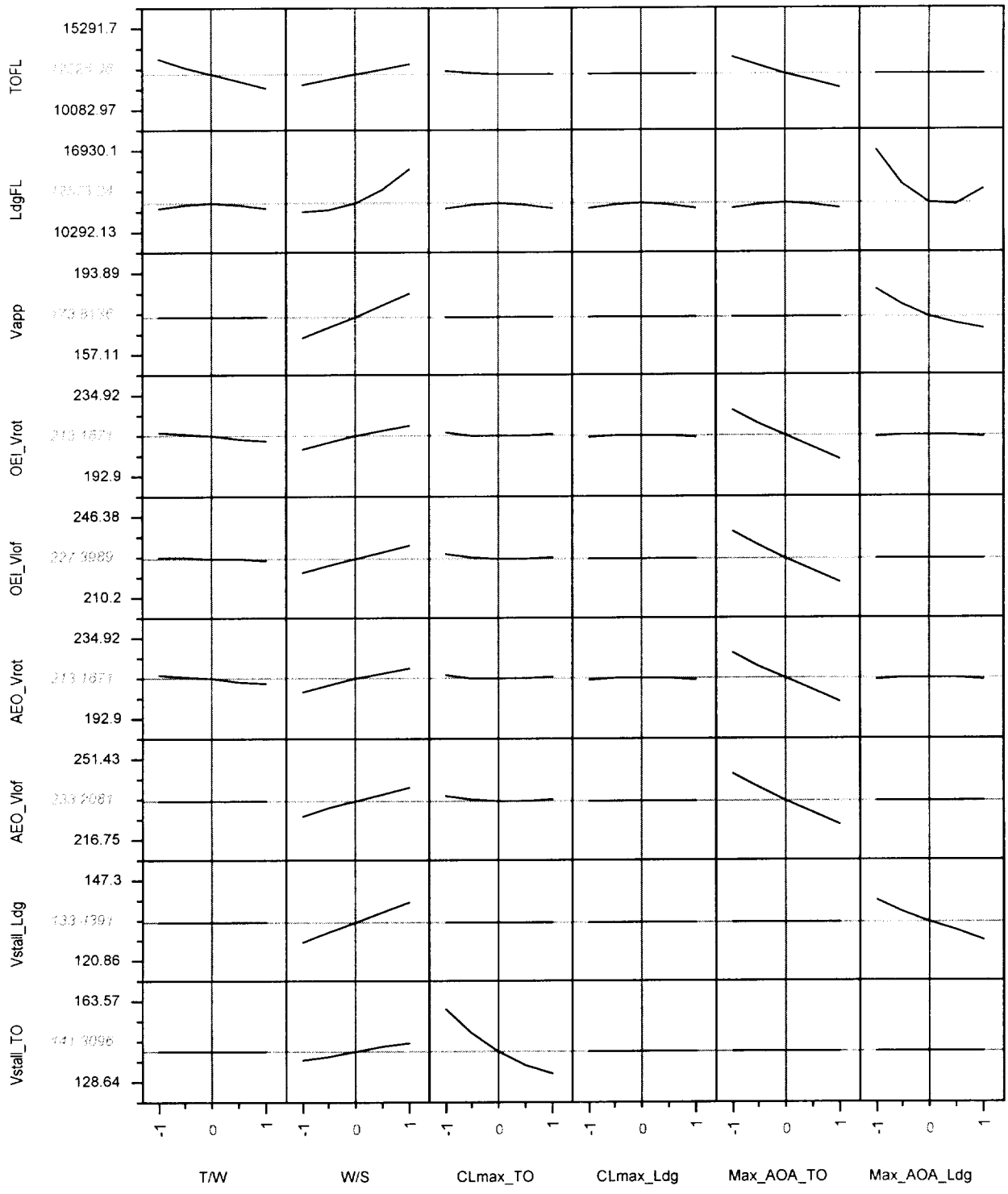

FIGURE 60: CONVENTIONAL CASE #6

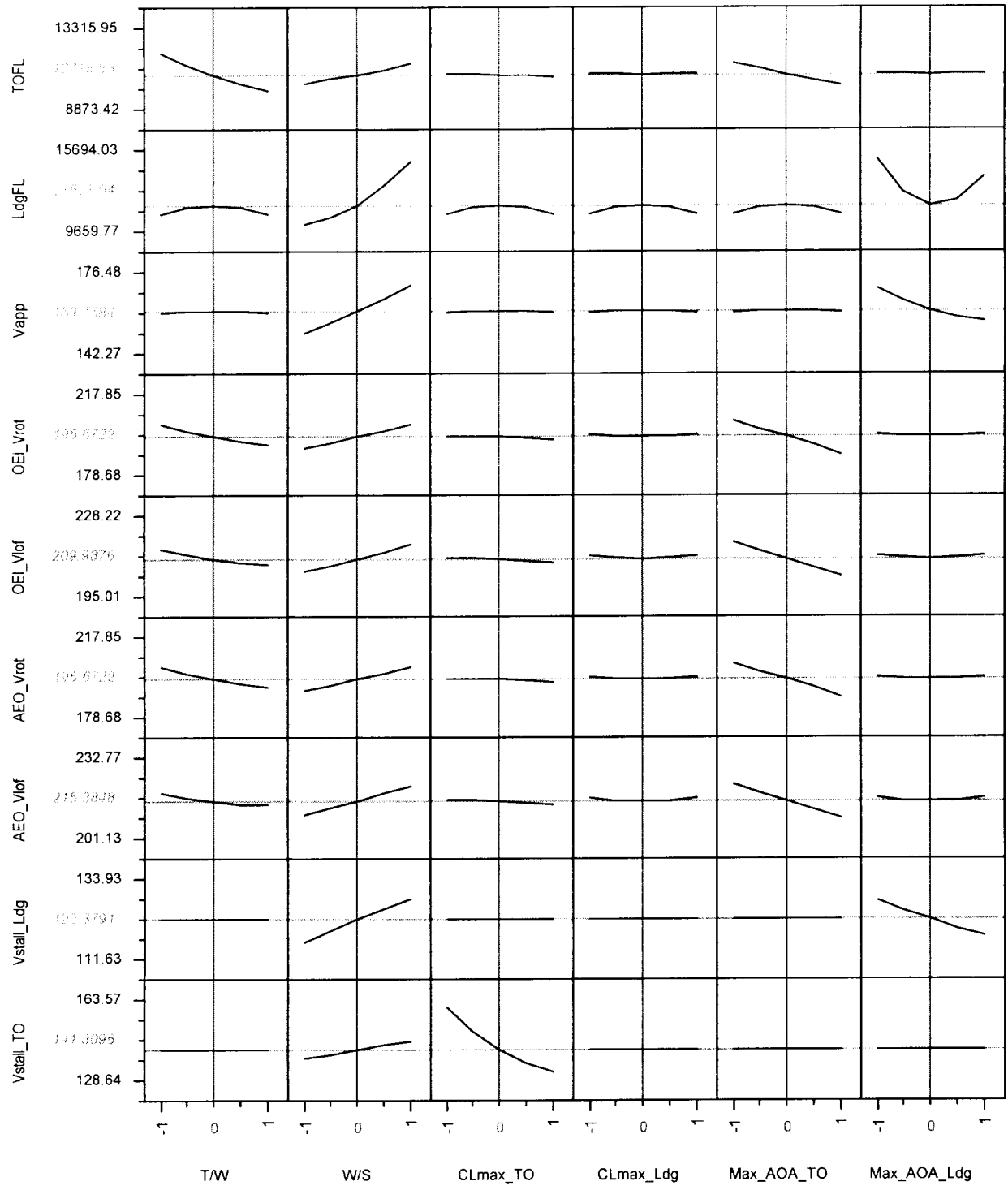

FIGURE 61: CONVENTIONAL CASE #7

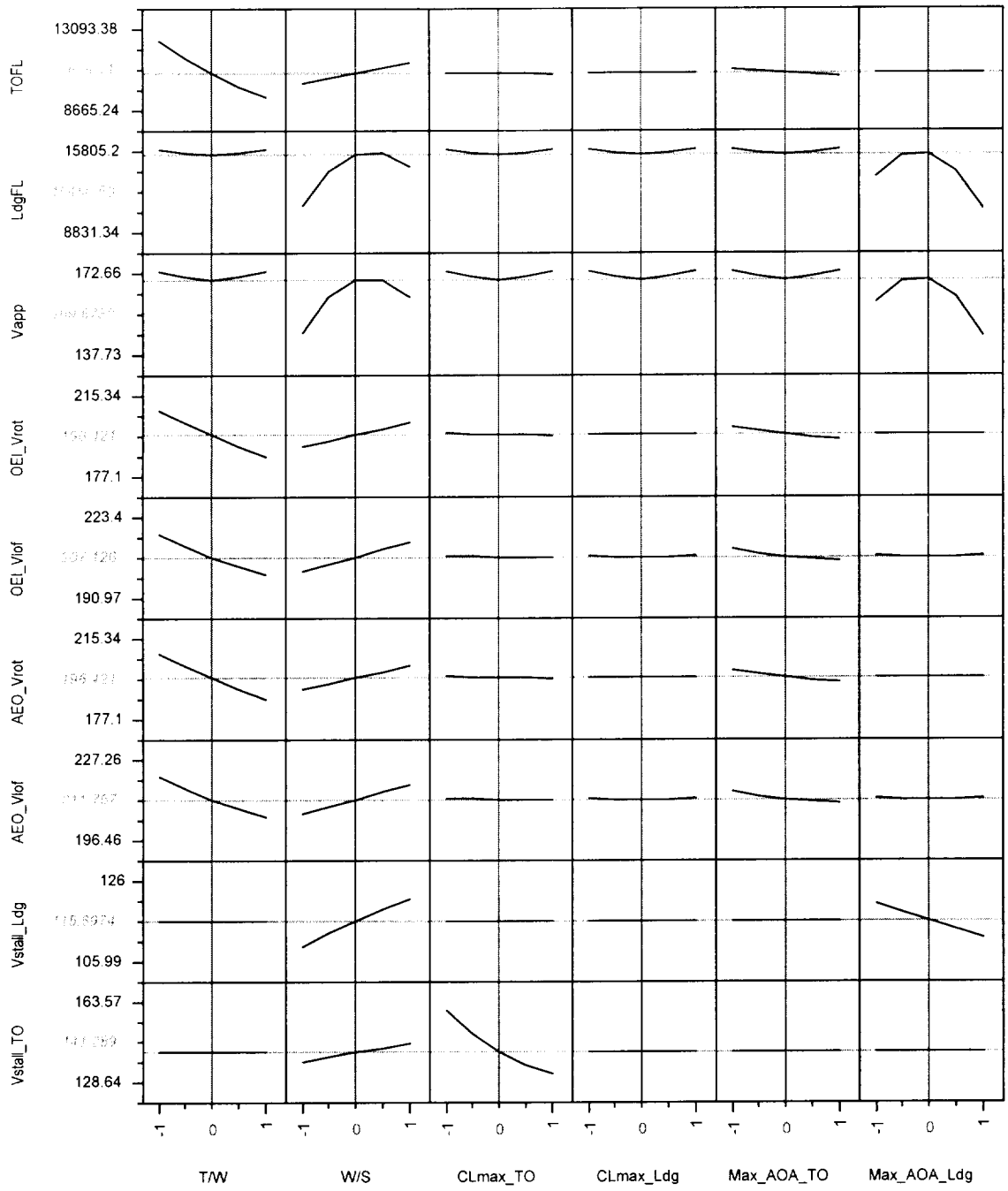

FIGURE 62: CONVENTIONAL CASE #8

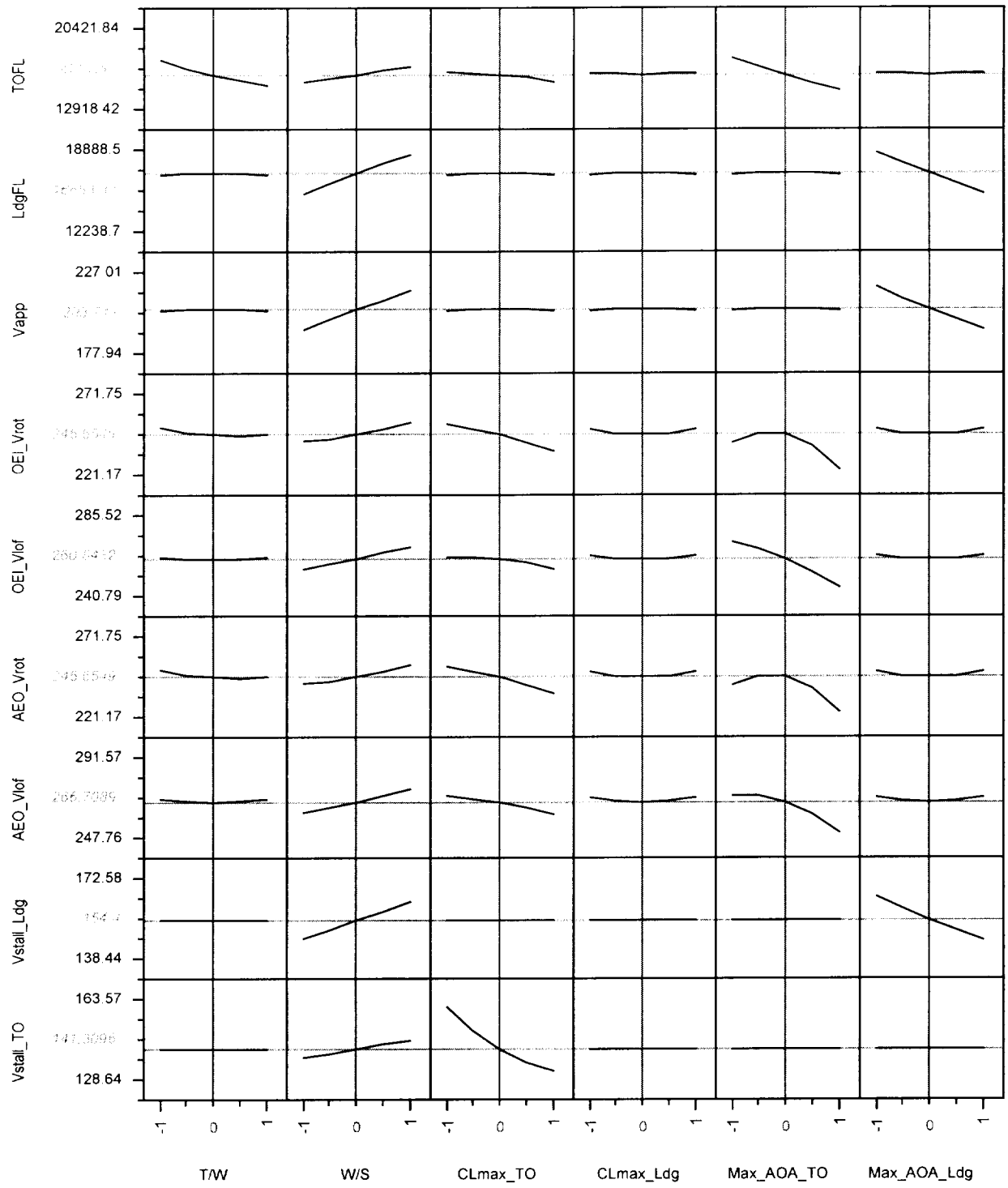

FIGURE 63: CONVENTIONAL CASE #9

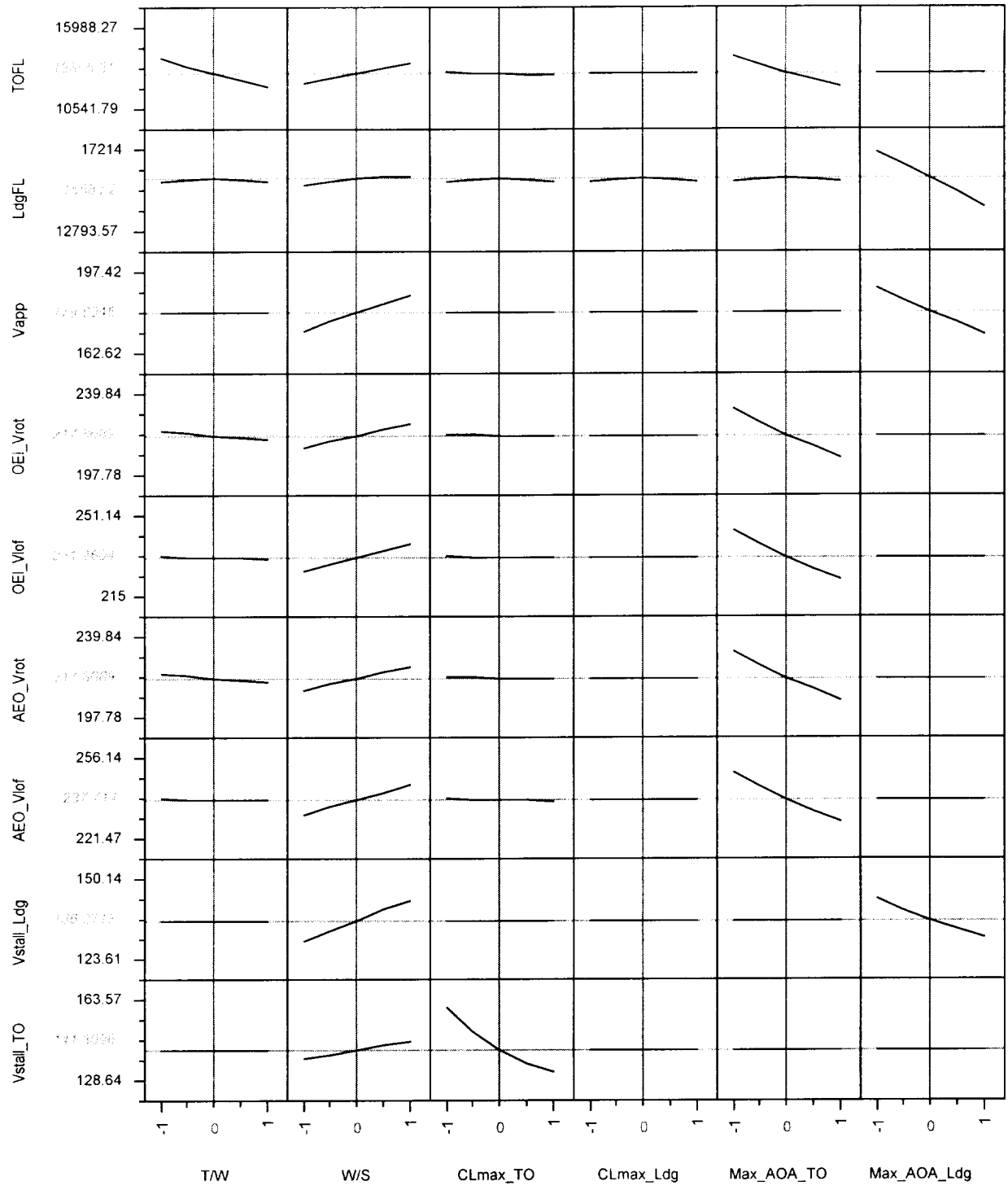

FIGURE 64: CONVENTIONAL CASE #10

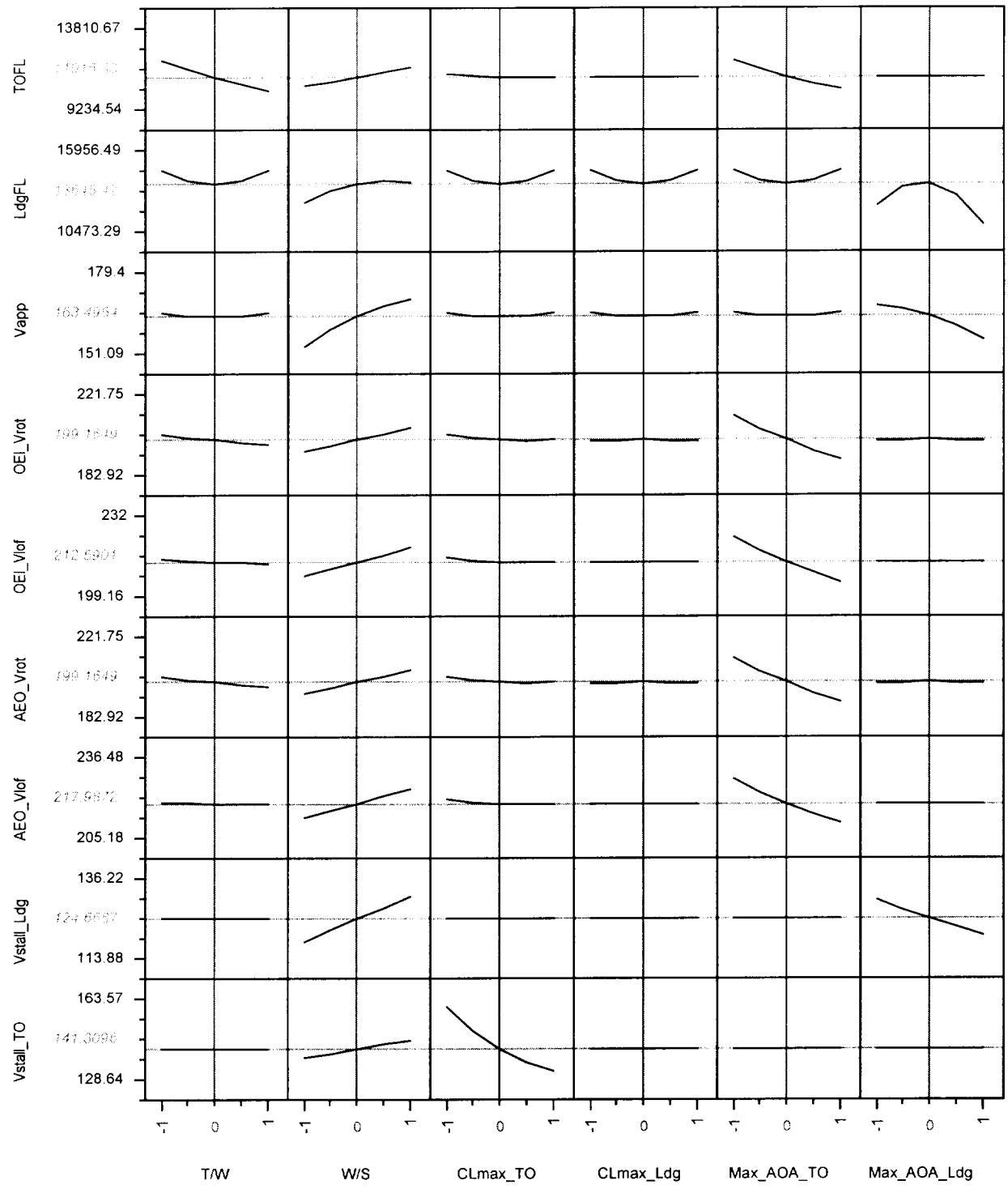

FIGURE 65: CONVENTIONAL CASE #11

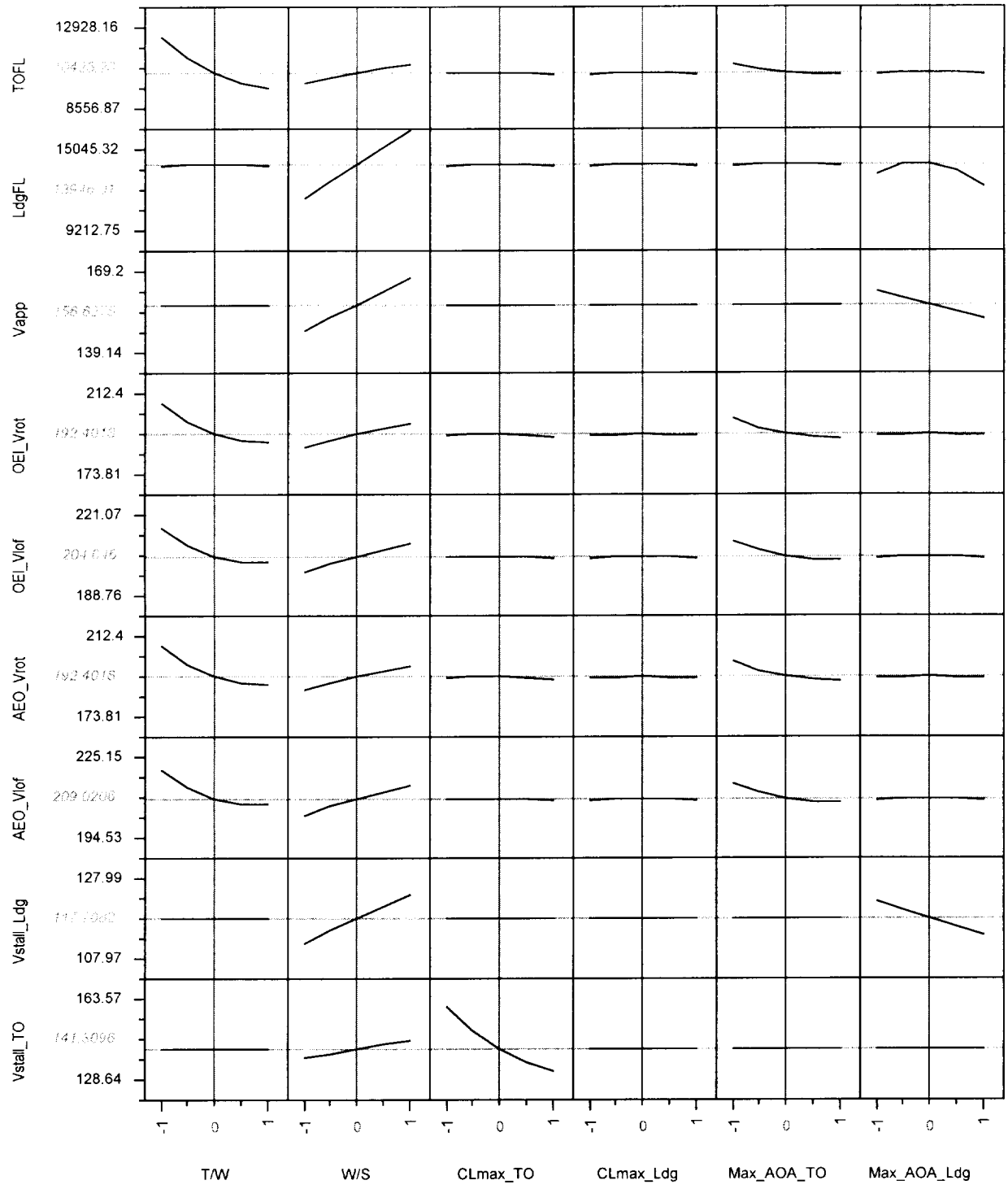

FIGURE 66: CONVENTIONAL CASE #12

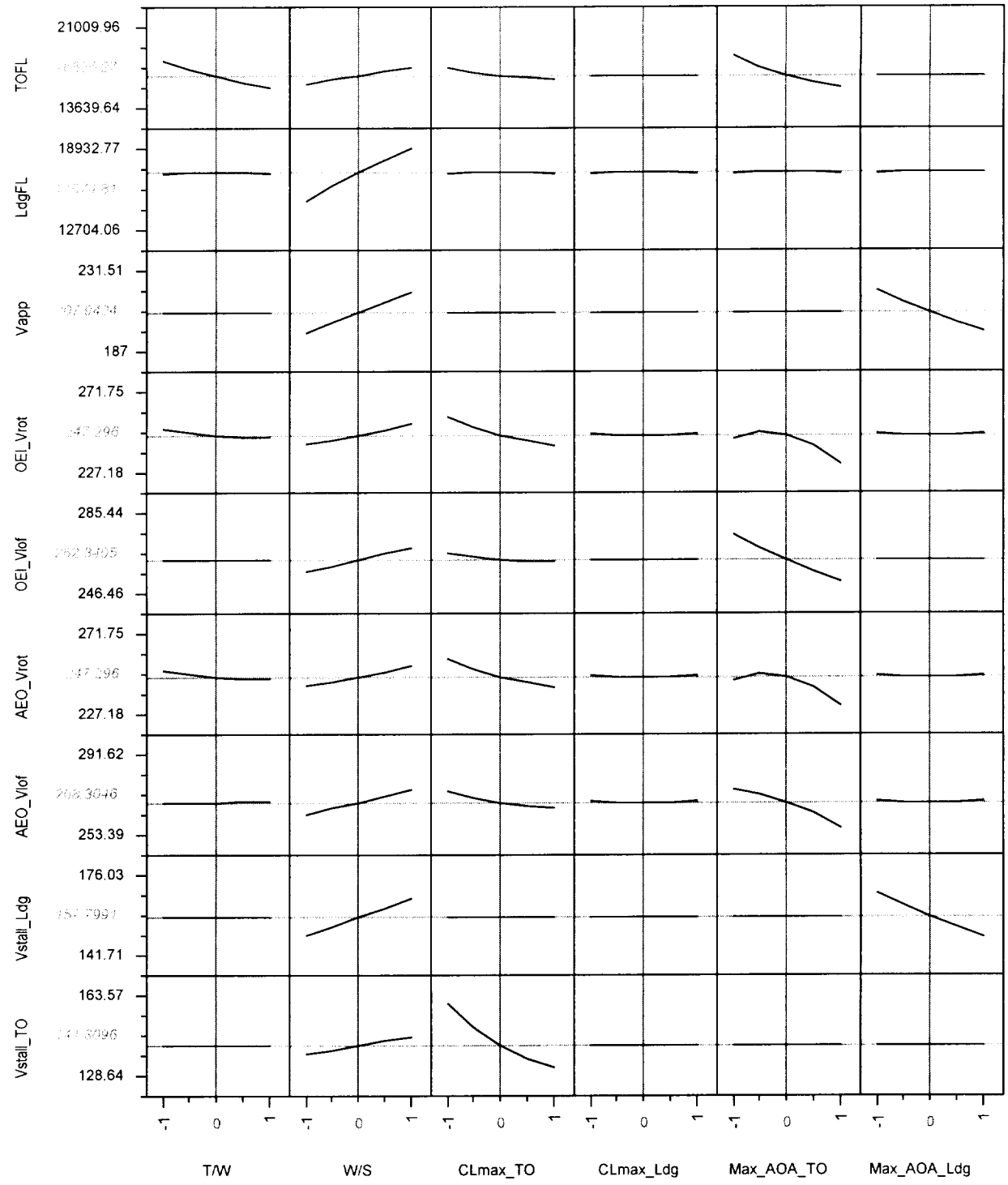

FIGURE 67: CONVENTIONAL CASE #13

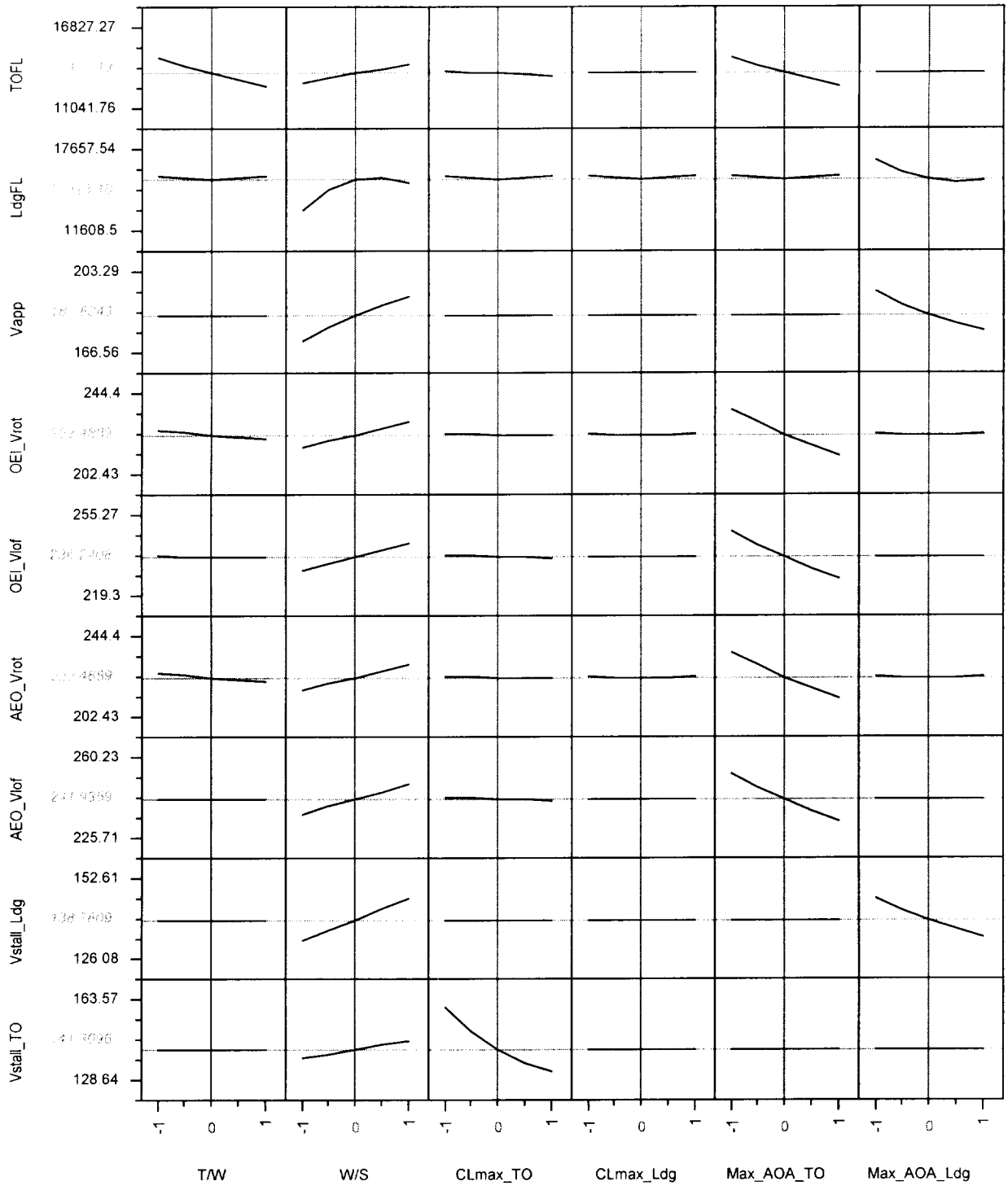

FIGURE 68: CONVENTIONAL CASE #14

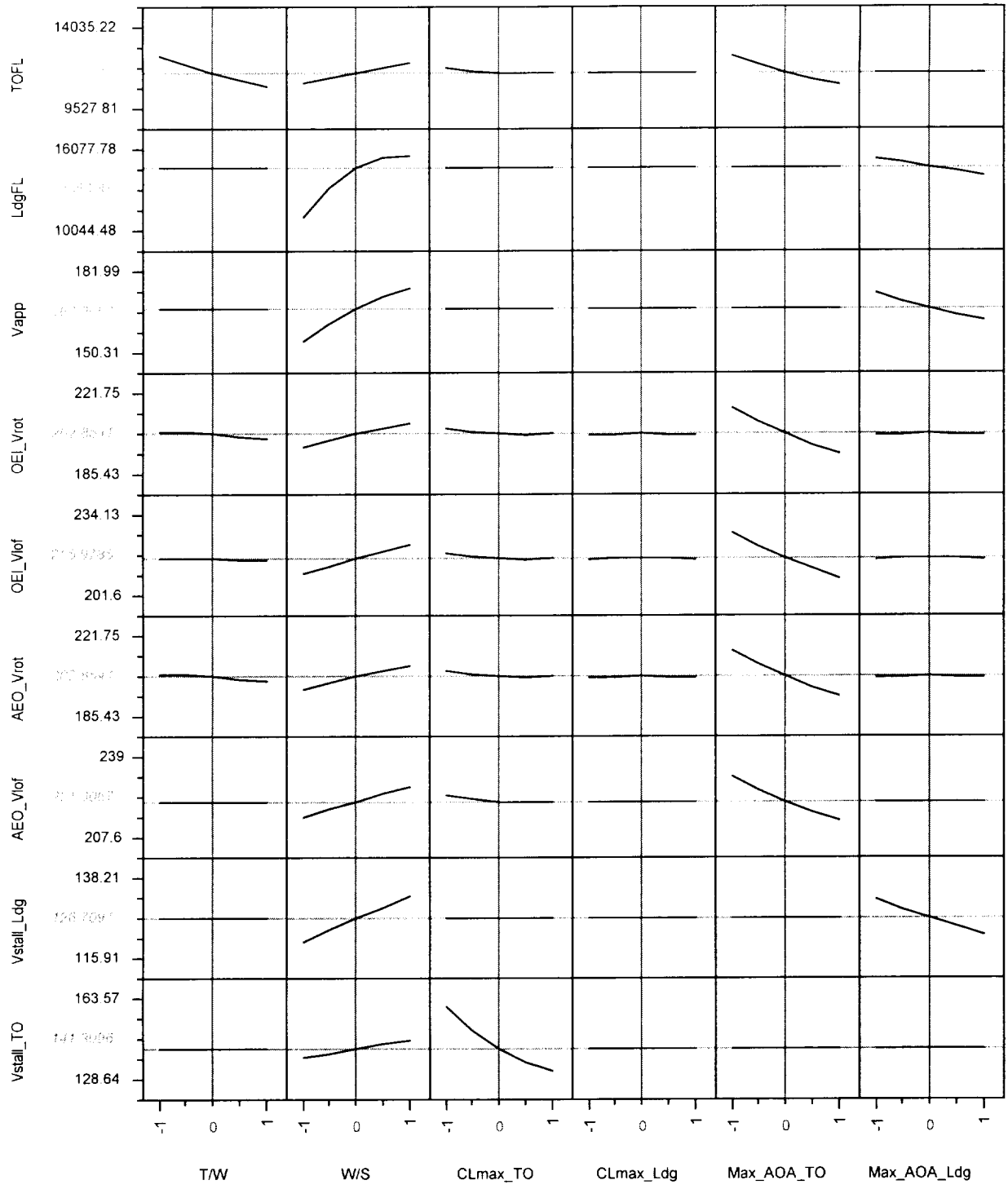

FIGURE 69: CONVENTIONAL CASE #15

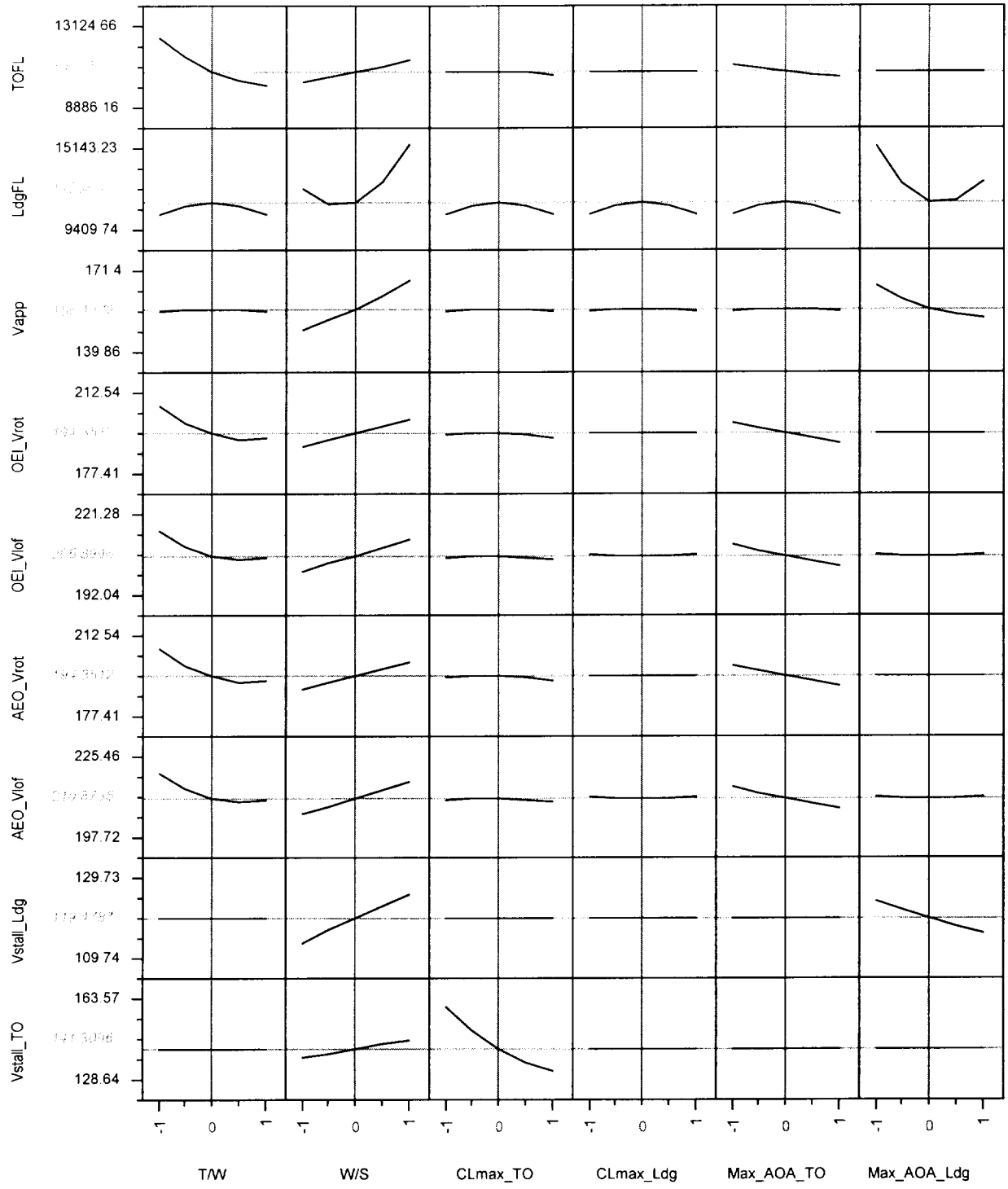

FIGURE 70: CONVENTIONAL CASE #16

7.3 CC Augmented Configuration

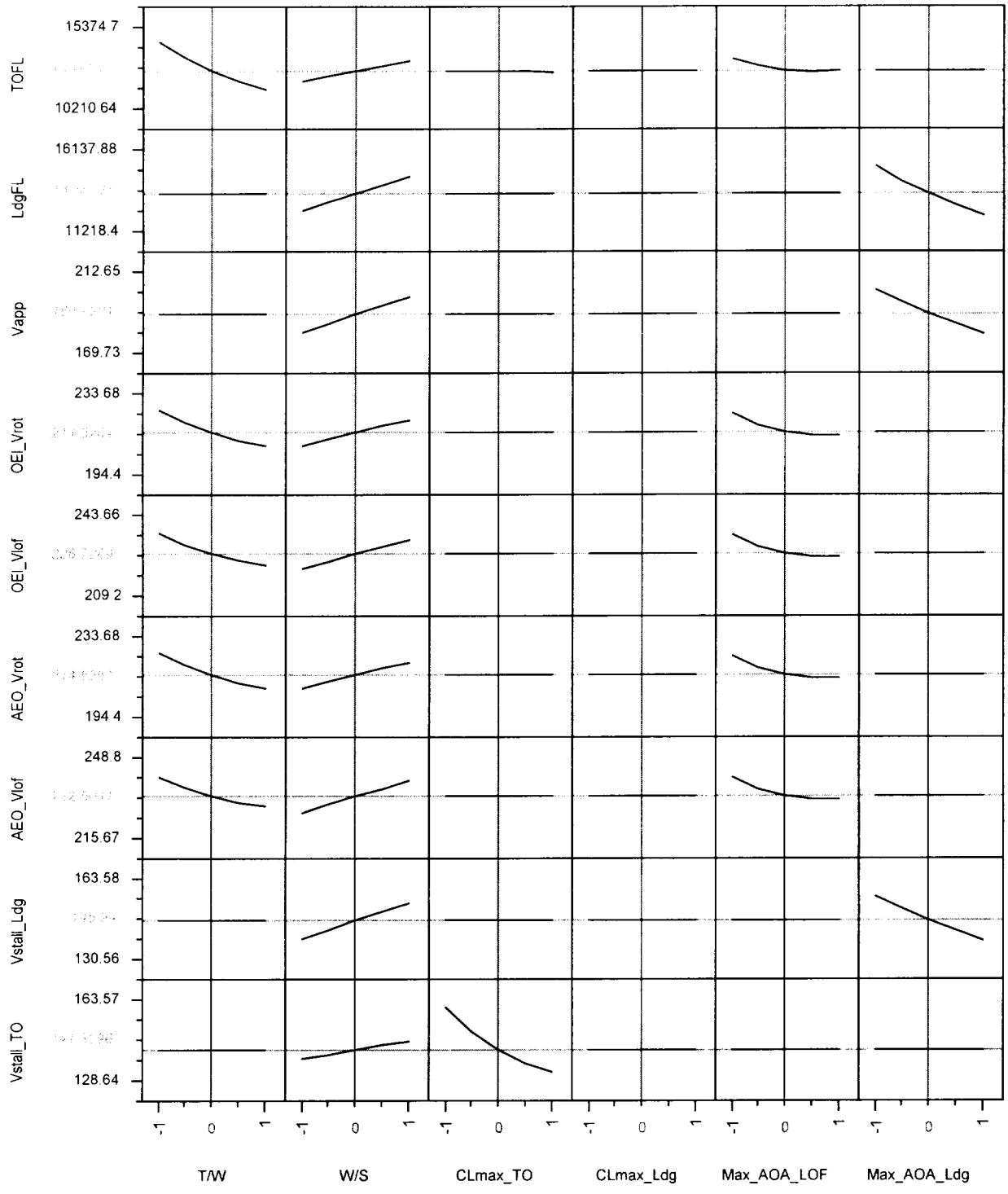

FIGURE 71: CC AUGMENTED CASE #1

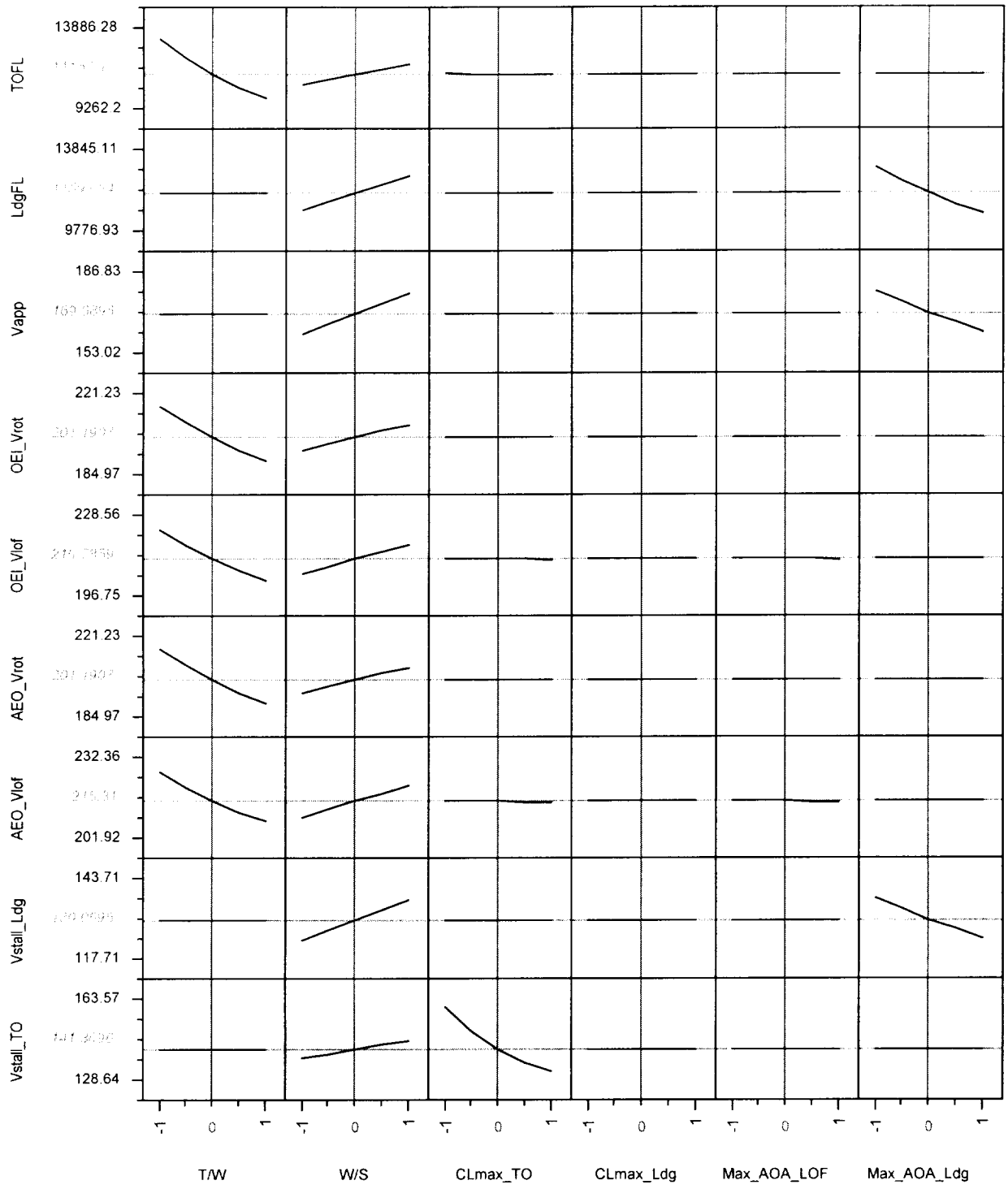

FIGURE 72: CC AUGMENTED CASE #2

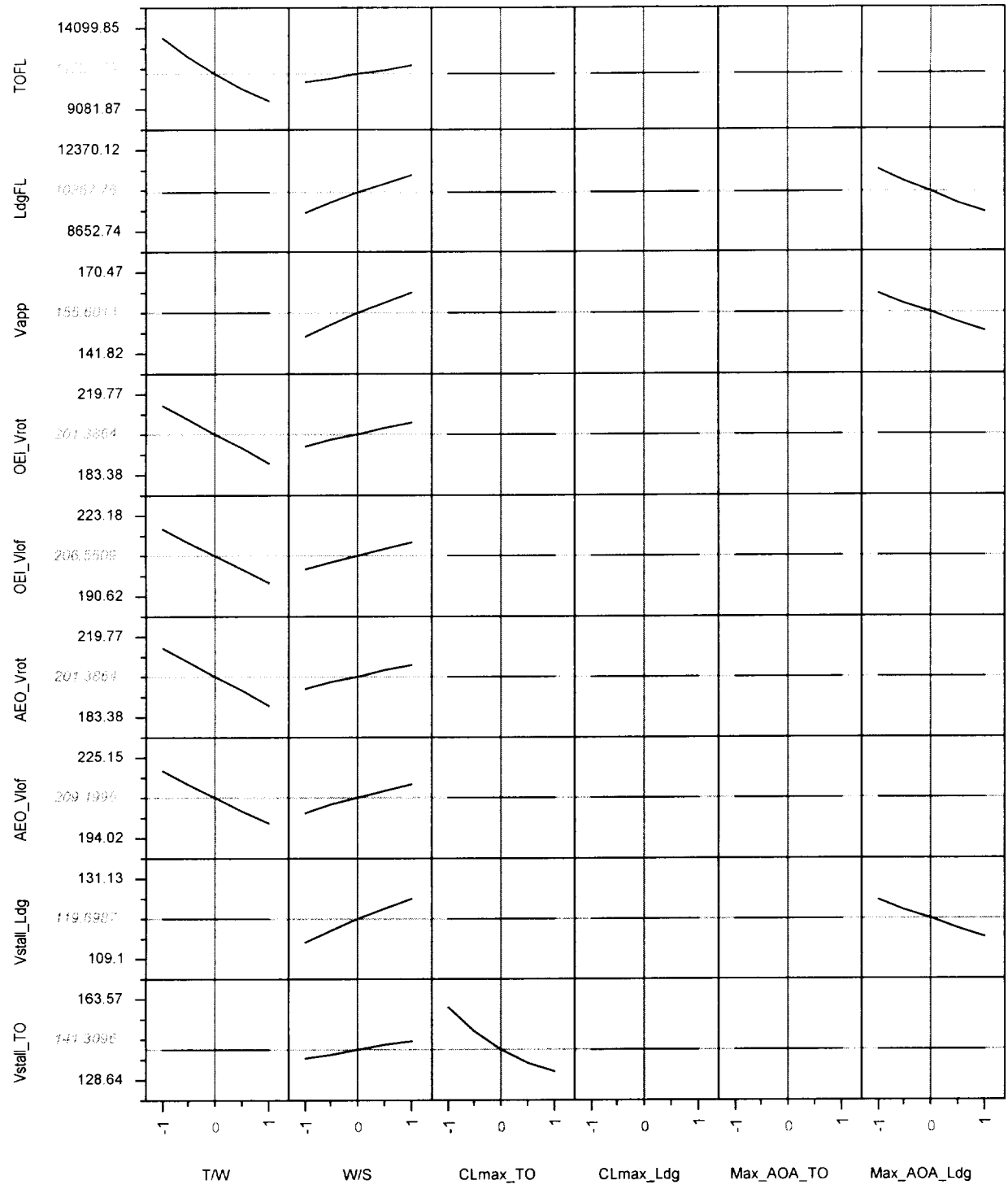

FIGURE 73: CC AUGMENTED CASE #3

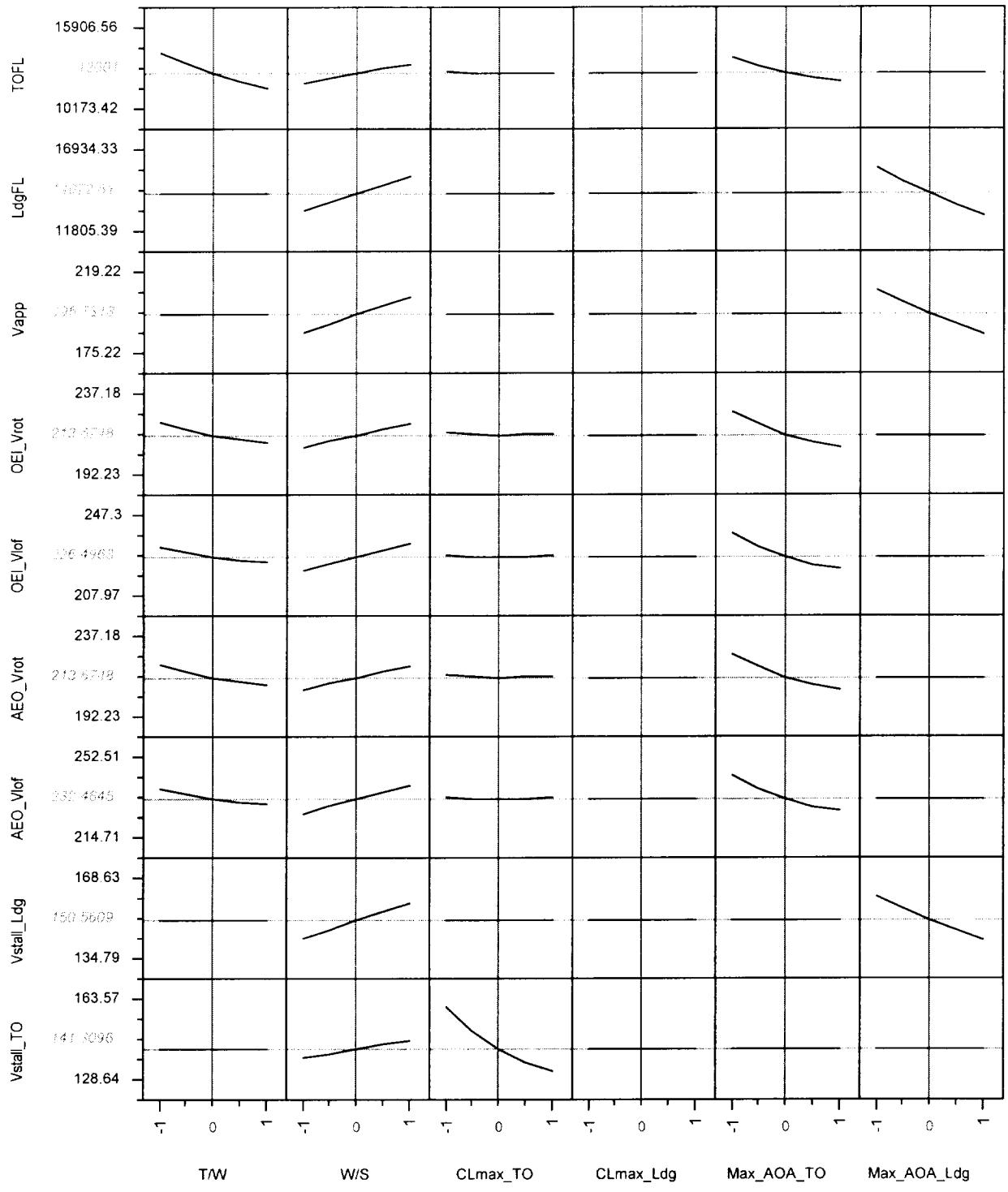

FIGURE 74: CC AUGMENTED CASE #5

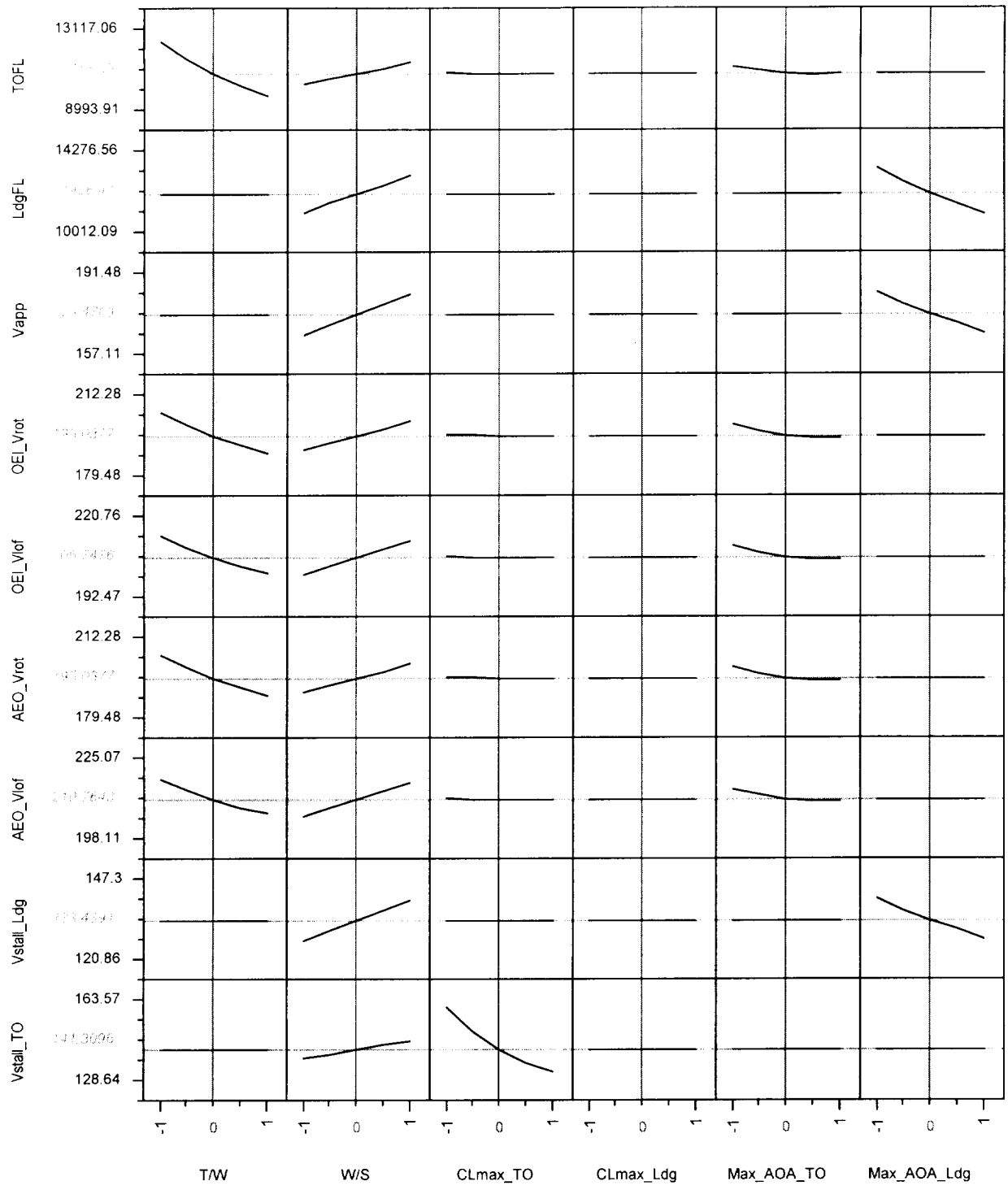

FIGURE 75: CC AUGMENTED CASE #6

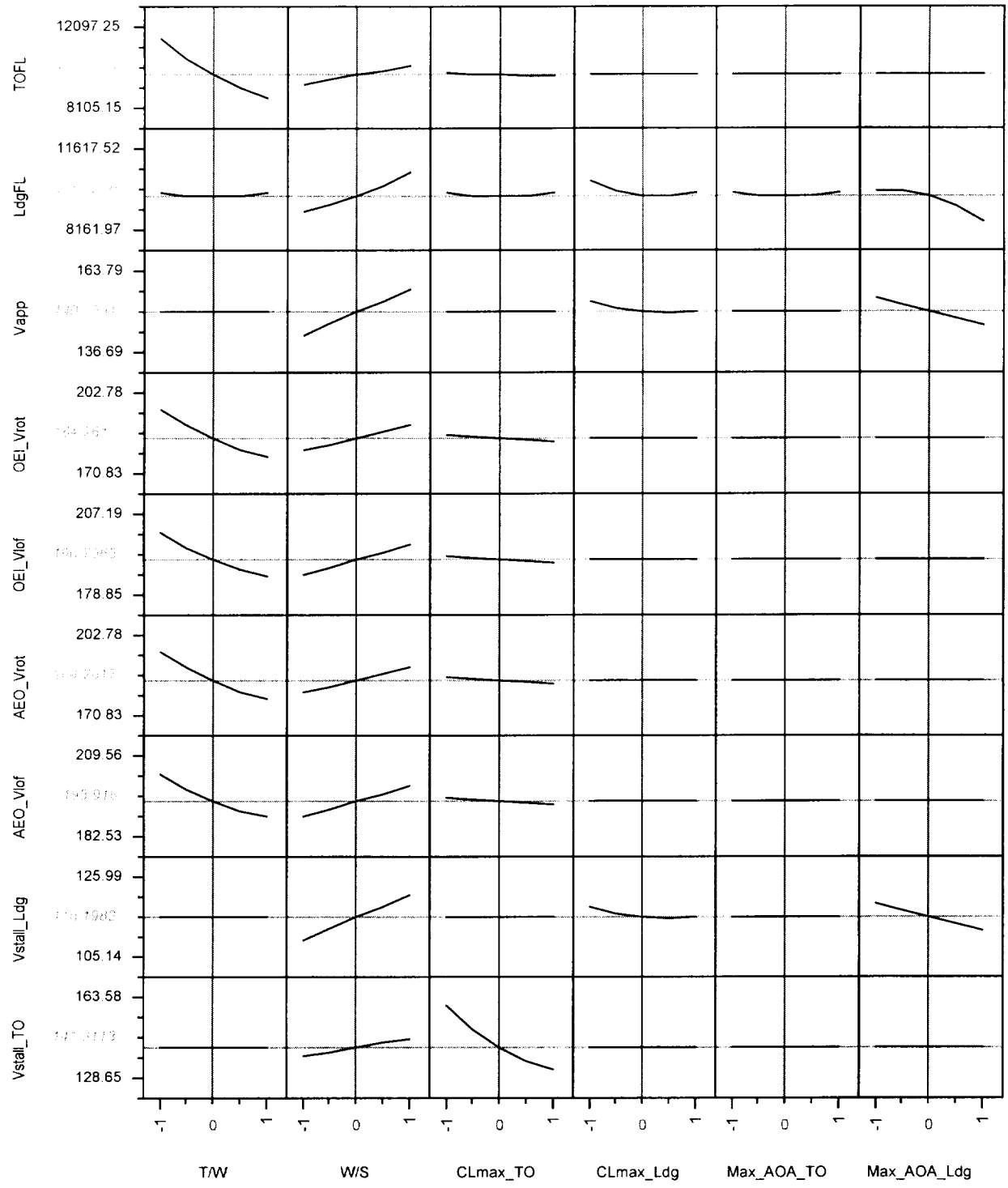

FIGURE 76: CC AUGMENTED CASE #7

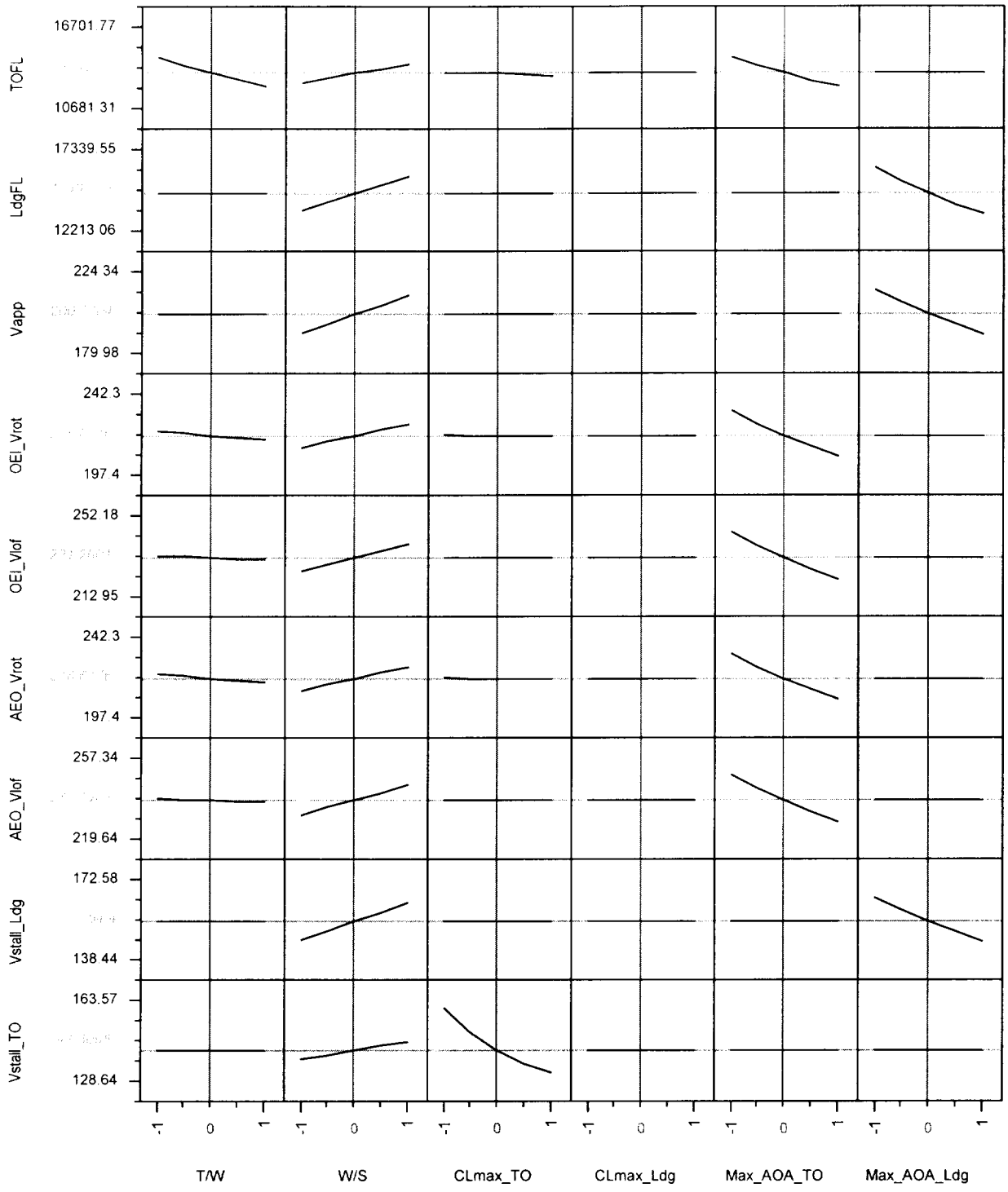

FIGURE 77: CC AUGMENTED CASE #9

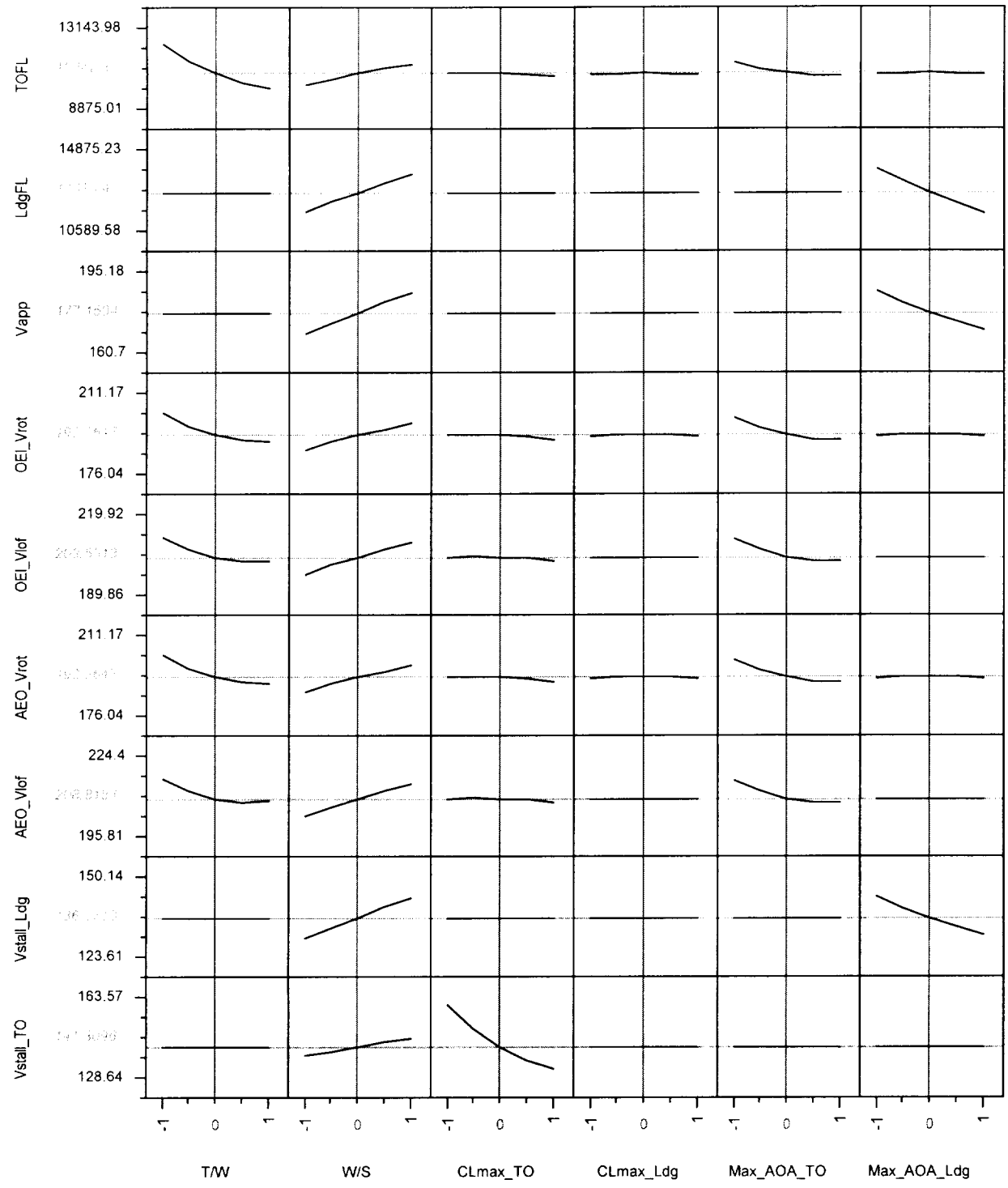

FIGURE 78: CC AUGMENTED CASE #10

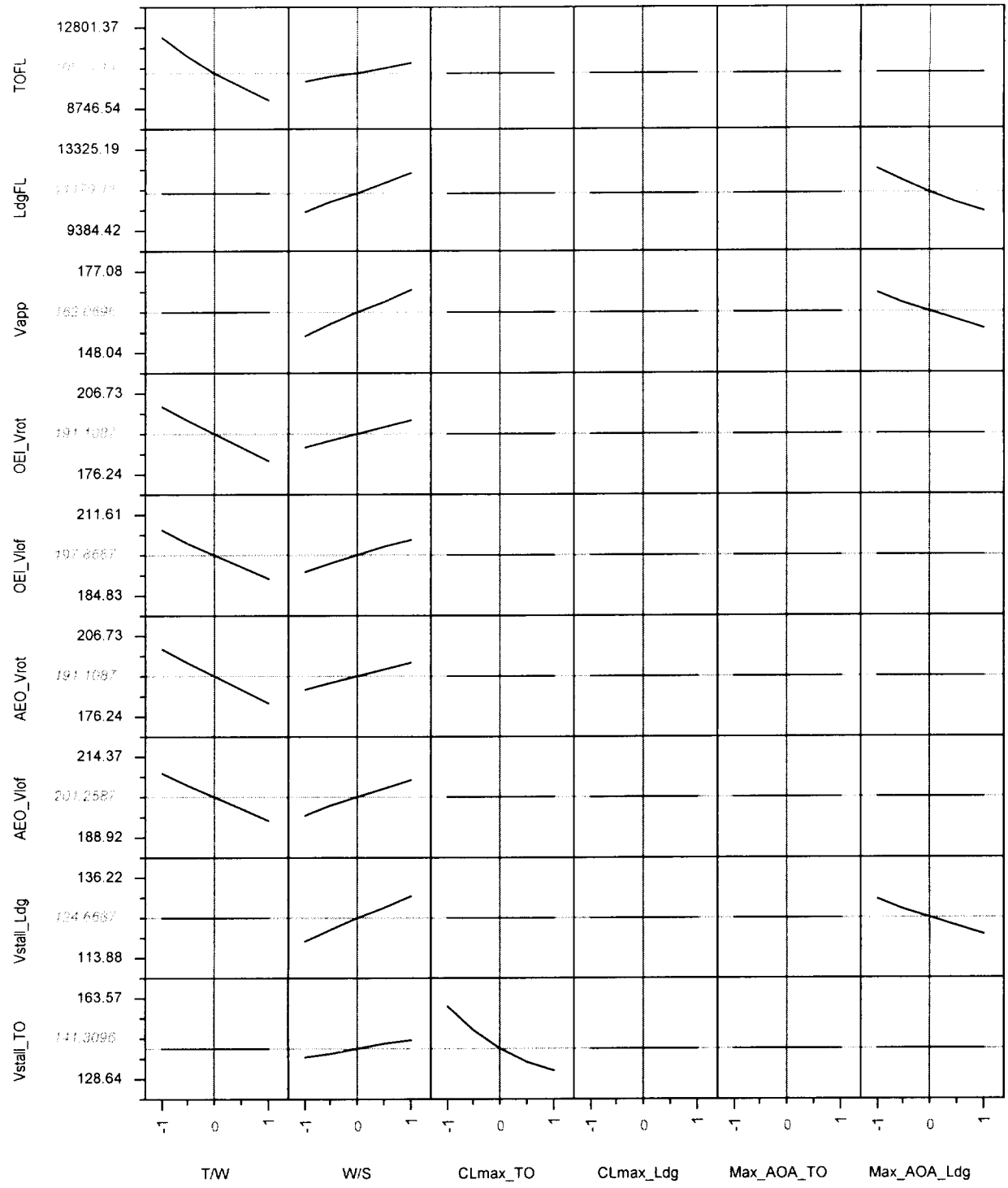

FIGURE 79: CC AUGMENTED CASE #11

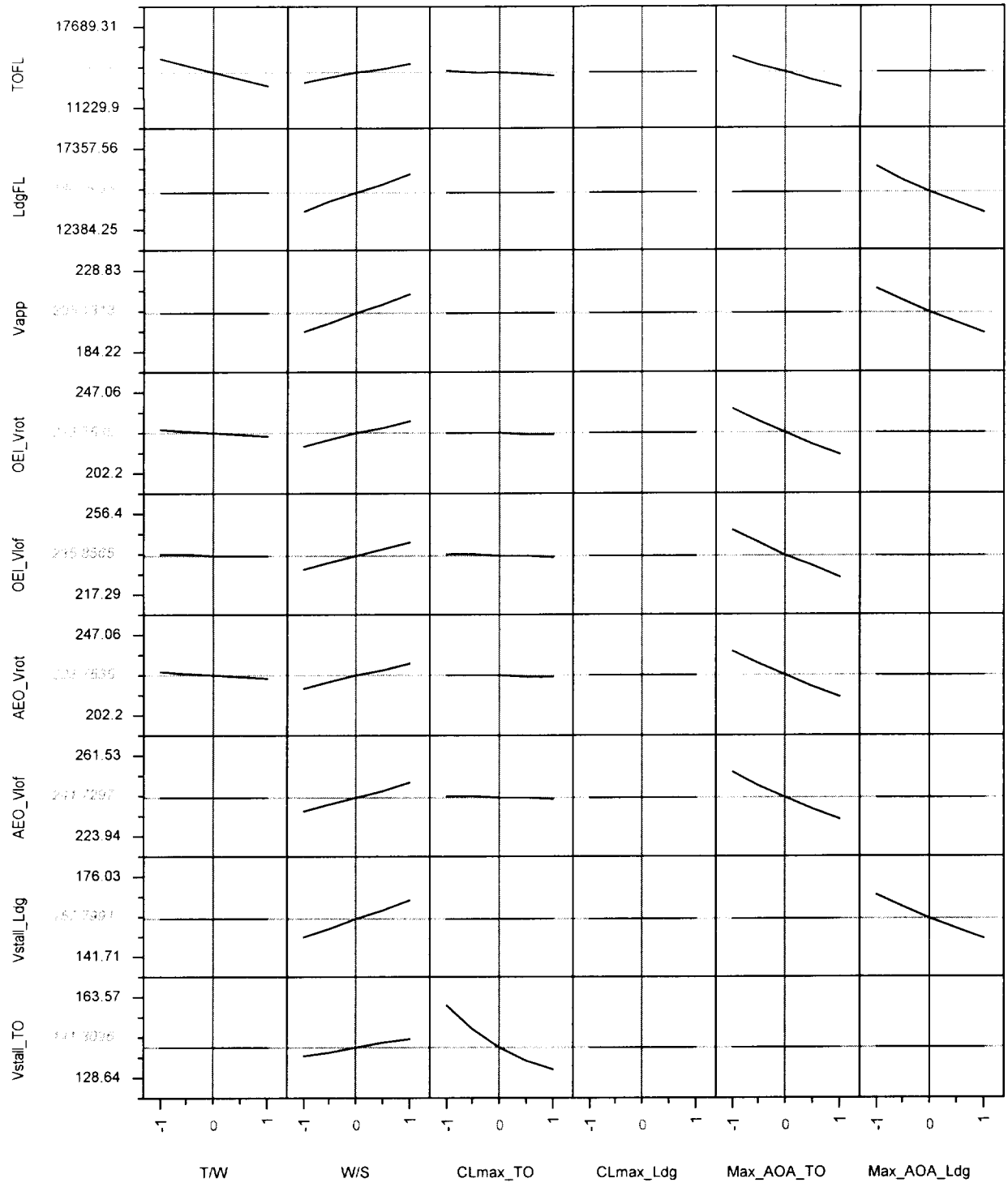

FIGURE 80: CC AUGMENTED CASE #13

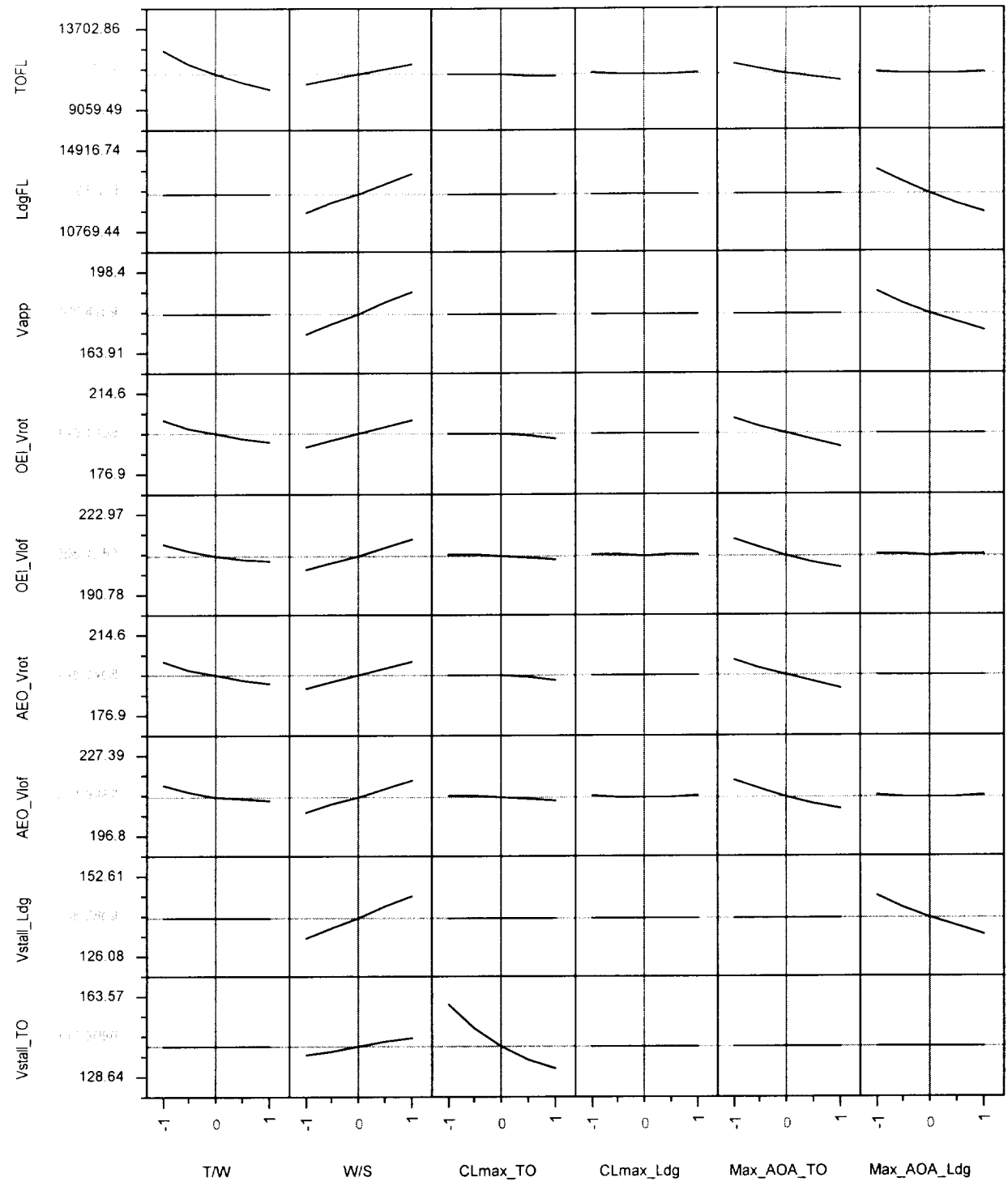

FIGURE 81: CC AUGMENTED CASE #14

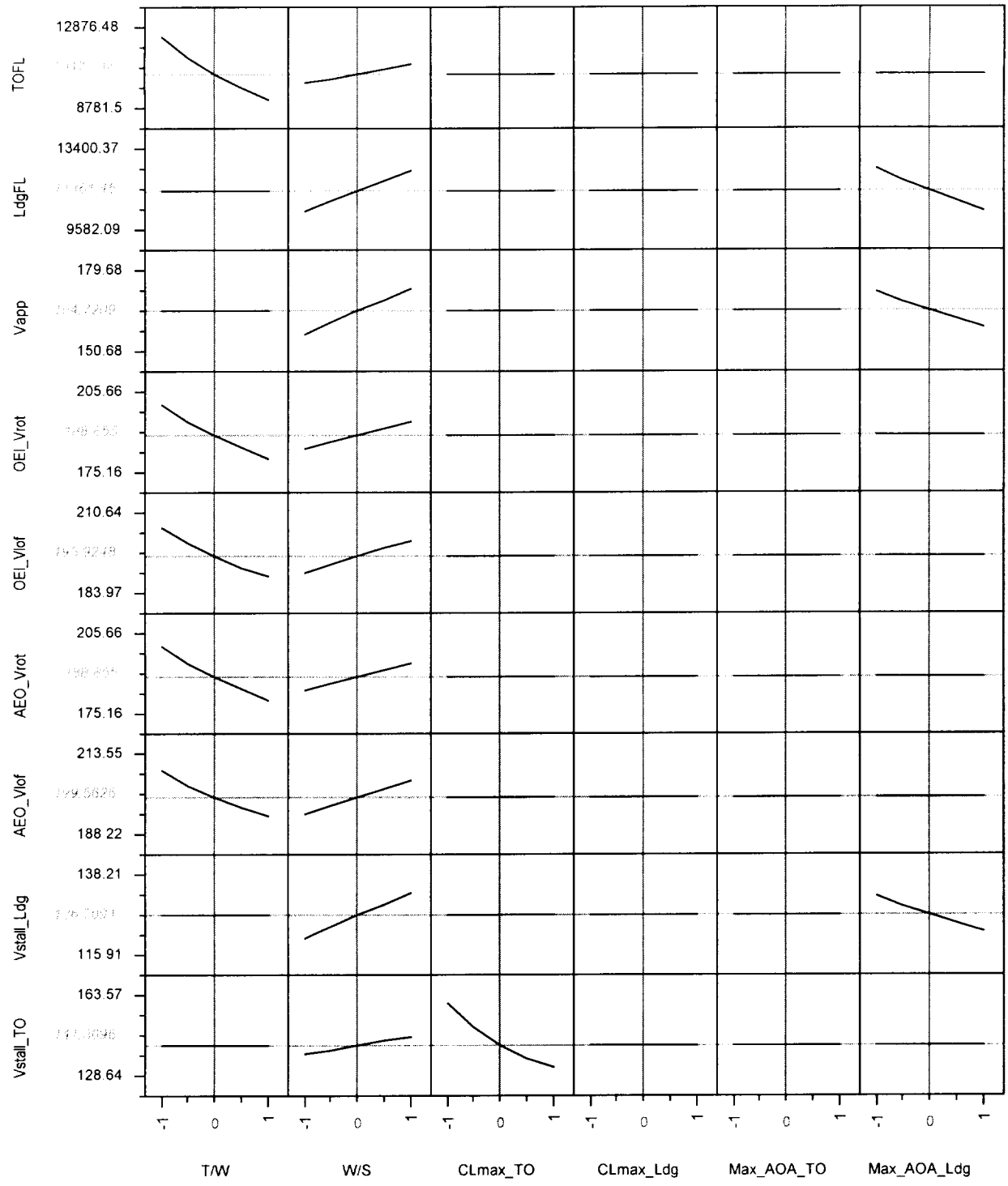

FIGURE 82: CC AUGMENTED CASE #15

8. Reference

1 Bernstein, J., "Is the World Ready for Son of Concorde"; Leary, W., "Designing an SST: Noise, Sonic Booms and the Ozone Layer", New York Times, April 10, 1990.

2 Dubois, M., "Le Transport Supersonique de Nouvelle Generation Ou un Sucesseur du Concorde Qui ne Soit pas un Nouveau Concorde", 7th European Aerospace Conference, Toulouse, France, Oct. 1994.

3 Boeing Commercial Airplens, "1997 Current Market Outlook; World Market Demand and Airplane Supply Requirements", http://www.boeing.com/cmo/les00.html, March 18, 1997.

4 Odell, T.T., "The Supersonic Transport: A Manufacturer's View", 7th European Aerospace Conference, Toulouse, France, Oct. 1994.

5 Darden,C.M., "The Importance of Sonic Boom Research in the Development of Future High Speed Aircraft", J. of the NTA, Winter 1992, pp. 54-62.

6 Rotmistrov, N.Y., Mirzoyan, A.A., "Second Generation Supersonic Transport Propulsion System Complex Study", 7th European Aerospace Conference, Toulouse, France, Oct. 1994.

7 Windisch, J.J., "Plane of Dreams - Build it and They Will Come", 17th Airport Conference, Hershey, Pa., Mar 1994.

8 Lenorvitz, J.M., "Airbus Survey Confirms Requirements for Very Large Transport Aircraft", Aviation Week & Space Technology, Oct. 28, 1991.

9 Iwaki, T., Kihara, T., "Social Impacts of SST Operation on the 21st Century", 7th European Aerospace Conference, Toulouse, France, Oct. 1994.

10 Benson, J., "Conversations with Louis J. Williams", Aerospace America, Feb, 1995.

11 Ott, J., "HSCT Computer model Takes Shape at NASA", Aviation Week & Space Technology, Oct 13, 1997, pp 68-69.

12 Goldin, D.S., "The Three Pillars of Success for Aviation and Space Transportation in the 21st Century", speech given before the Aero Club, AIAA, and NAC, March 20, 1997.

13 Kandebo, S.W., "Redefined Propulsion Tests Target HSCT Scale-up Issues", Aviation Week & Space Technology, Oct 13, 1997, pp 70-72.

14 Kulfan, R.M., "High Speed Civil Transport Opportunities, Challenges and Technology Needs", Keynote Speech, 34th National Conference on Aeronautics and Astronautics, Tainan, Taiwan, Nov 26, 1992.

15 Hirokawa, J., Sekido, T., Futatsudera, N., "Technologies Required for the Next Generation HSCT, Propulsion Systems", 7th European Aerospace Conference, Toulouse, France, Oct. 1994.

16 Bunin, B.L., Gray, I.G., Khaski, E., Olszewski, M.W., Schmitt, D., "Second Generation Supersonic: A Case for Global Cooperation", 7th European Aerospace Conference, Toulouse, France, Oct. 1994.

17 Barbaux, Y., Guedra-Degeorges, D., Lapasset, G., "The Materials Challenge for the Future SCT", 7th European Aerospace Conference, Toulouse, France, Oct. 1994.

18 Englar, R.J., "Application of Pneumatic Lift and Control Surface Technology to Advanced Transport Aircraft", presented at *Transportation Beyond 2000: Engineering Design for the Future*, Conference at NASA Langley Research Center, Hampton, Va, Sept 26-28, 1995.

19 Novak, C.J., Cornelius, K.C., Roads, R.K., "Experimental Investigations of the Circular Wall Jet on a Circulation Control Airfoil", AIAA 87-0155.

20 Englar, R.J., "Investigation into and Application of the High Velocity Circulation Control Wall Jet for High Lift and Drag Generation on STOL Aircraft", AIAA 74-502.

21 Scrugg, T.B., "Computational Investigation of Circulation Control Turbulence Modeling", Master's Thesis, School of Engineering, Air Force Institute of Technology, Dec 1990.

22 Young, T., "Outlines of Experiments and Inquiries Regarding Sound and Light", Lecture to the Royal Society, Jan 16, 1800, (see Journal Royal Aeronautical Society, Vol 61, 1957, pp. 157).

23 Kirkpatrick, D.G., Barnes, D.R., "Development and Evolution of the Circulation Control Rotor", Paper presented at the 36th Annual Forum of the AHS, Washington, D.C., May 1980.

24 Mentral, A., Zerner, F., "The Coanda Effect", Publication Scientifiques et Technique du Ministere de l'Air", No 218, 1948.

25 Dunham, J., "Circulation Control Applied to Circular Cylinder", National Gas Turbine Est (England) Report R. 287, July, 1967.

26 Cheeseman, I.C., "Circulation Control and Its Application to Stopped Rotor Aircraft", AIAA 67--747.

27 Williams, R.M., "Some Research on Rotor Circulation Control", Proc. of the 3rd Cal/AVLABS Symposium, Vol 11, June 1969.

28 Englar, R.J., "Two-Dimensional Transonic Wind Tunnel Tests of Three 15-percent Thick Circulation Control Airfoil", NSRDC Report ASED-182, Dec. 1970.

29 Roberts, S.C., "WVU Circulation Controlled STOL Aircraft Flight Tests", West Virginia University, Morgantown, WV, Aerospace TR-42, July 1974.

30 Pugliese, A.J., Englar, R.J., "Flight Testing the Circulation Controlled Wing", AIAA 79-1791, see also Aviation Week & Space Technology, Mar., 19, 1979.

31 Englar, R.J., "Development of the A-6 Circulation Control Wing Flight Demonstrator Configuration", DTNSRDC/ASED-79/01, Jan. 1979.

32 Harvell, J.K., Franke, M.E., "Aerodynamic Characteristics of a Circulation Controlled Elliptical Airfoil with Blown Jets", AIAA 83-1794.

33 Stevenson, T.A., Franke, M.E., Rhynard, Jr., W.E., Snyder, J.R., "A Wind Tunnel Investigation of a Circulation-Controlled Elliptic Airfoil", AIAA 76-933.

34 Englar, R.J., Smith, M.J., Kelley, S.M., Rover III, R.C., "Development of Circulation Control Technology for Application to Advanced Subsonic Transport Aircraft", AIAA 93-0644.

35 Englar, R.J., Niebur, C.S., Gregory, S.D., "Pneumatic Lift and Control Surface Technology Applied to High Speed Civil Transport Configurations", AIAA 97-0036.

36 Mavris, D.N., Bandte,O., "Comparison of Two Probabilistic Techniques for the Assessment of Economic Uncertainty", 19th Annual Conference of the International Society of Parametric Analysts, New Orleans, LA, May 1997.

37 Mavris, D.N., Bandte, O., "A probabilistic approach to multivariate constrained robust design simulation", SAE Technical Paper 97-5508.

38 Mavris, D.N., Mantis, G.C., Kirby, M.R., "Demonstration of a Probabilistic Technique for the Determination of Aircraft Economic Viability", SAE Technical Paper 97-5585.

39 Southwest Research Institute, FPI User's and Theoretical Manual, San Antonio, TX, 1995.

40 Twiss, B.C., Forecasting for technologists and engineers: A practical guide for better decisions, Peter Peregrinus, Ltd., London, U.K., 1992.

41 SAS Institute Inc., JMP, Computer Program and Users Manual, Cary, NC, 1994.

42 McCullers, L.A., *FLOPS User's Guide Ver. 5.94*, NASA Langley Research Center, Hampton, VA, Jan. 16, 1998.

43 Garcia, E., Marx, W., Mavris, D.N., *ALCCA User Notes*, ASDL; Atlanta, GA, Jan 4, 1999.

44 Englar, R.J., Niebur, C.S., Gregory, S.D., "Pneumatic Lift and Control Surface Technology Applied to High Speed Civil Transport Configurations", AIAA 97-0036.

45 McCullers, L.A., *Detailed Takeoff and Landing Analysis Program User's Guide, Version 2.0*, NASA Langley Research Center, Hampton, Va., June 20, 1994.

46 Mavris, D.N., Hayden, W.T., "Probabilistic Analysis of an HSCT Modeled with an Equivalent Laminated Plate Wing", SAE Technical Paper 97-5571.

47 DeLaurentis, D., Zink, P.S., Mavris, D.N., Cesnik, C.E.S., Schrage, D.P., "New Approaches to Multi-disciplinary Synthesis: An Aero-Structures-Control Application Using Statistical Techniques", AIAA 96-5501.

48 Mavris, D.N., Kirby, M.R., Qiu, S., "Technology Impact Forecasting for a High Speed Civil Transport", SAE-985547.

49 Mavris, D.N., Bandte, O., Schrage, D.P., "Economic Uncertainty Assessment of an HSCT Using a Combined Design of Experiments/Monte Carlo Simulation Approach", 17th Annual Conference of the International Society of Parametric Analysts, San Diego, Ca., May 1995.

50 Mavris, D.N., Kirby, M.R., "Preliminary Assessment of the Economic Viability of a Family of Very Large Transport Configurations", AIAA 96-5516.

51 Giles, G.L., *ELAPS User's Manual*, Feb. 1997.

52 Giles, G.L., "Design Oriented Structur e Analysis", NASA-TM 109124, June 1994.

53 Giles, G.L., "Equivalent Plate Analysis of Aircraft Wing Box Structures with General Planform Geometry", *Journal of Aircraft*, Vol 23, No. 11, Nov, 1986.

54 Mavris, D.N., Bandte, O., Schrage, D.P., "Application of Probabilistic Methods for the Determination of an Economically Robust HSCT Configuration", AIAA/USAF/NASA/ ISSMO Multidisciplinary Analysis and Optimization Conference, Bellevue, WA, Sept, 1996.

55 DeLaurentis, D.A., Mavris, D.N., and Schrage, D.P., "An IPPD Approach to the Preliminary Design Optimization of an HSCT using Design of Experiments", 20th ICAS Congress, Sorrento, Italy, Sept., 1996.

56 Loth, J.L., Boasson, M., "Circulation Controlled STOL Wing Optimization", Journal of aircraft, Vol 21, No 2, pp128-134, Feb 1984.

57 Haaland, P.D., Experimental Design in Biotechnology, Marcel Dekker, Inc., New York, NY, 1989.

58 Middleton, W.D. Landry, J.L., "A System for Aerodynamic Design and Analysis of Supersonic Aircraft, Part I: General Description and Theoretical Development", NASA CR-3351,1980.

59 Middleton, W.D., Landry, J.L., Coleman, R.L., "A system for Aerodynamic Design and Analysis of Supersonic Aircraft, Part II: User's Manual", NASA CR-3352, 1980.

60 Middleton, W.D., Landry, J.L., Coleman, R.L. "A system for Aerodynamic Design and Analysis of Supersonic Aircraft, Part III: Computer Program Description", NASA CR-2717, 1976.

61 Carlson, H.W., Chu, J., Ozoroski, L.P., McCullers, L.A., "Guide to AERO2S and WINGDES Computer Codes for Prediction and Minimization of Drag Due to Lift", NASA TP-3637, 1997.

62 "Rapid Aircraft Modeler", http://fornax.arc.nasa.gov:9999/ram.html, Oct, 1997.

63 Miranda, L.R., Elliott, R.D., Baker, W.M., "A Generalized Vortex Lattice Method for Subsonic and Supersonic Flow Applications", NASA CR-2865, 1977.

64 Carlson, H.W., Darden, C.M., "Validation of a Pair of Computer Codes for Estimation and Optimization of Subsonic Aerodynamic Performance of Simple Hinged-Flap Systems for Thin Swept Wings", NASA-TP 2828, 1988.

65 AlliedSignal Auxiliary Power Gas Turbine Power Catalog. AlliedSignal Aerospace, Phoenix, AZ, May 1993.

66 Geiselhart, K.A., Caddy, M.J., Morris, S.R. Jr., "Computer Program for Estimating Performance of Air-breathing Aircraft Engines", NASA-TM-4254, May 1991.

67 Plencner, R.M., Snyder, C.A., "The Navy/NASA Engine Program (NNEP89) - A User's Manual", NASA-TM-105186, Aug 1991.

68 Williams, J., "Airfield Performance Prediction Methods for Transport and Combat Aircraft", AGARD-LS-56, Mar 1973.